Macrophage Activation and Differentiation with Cholesterol Crystals

A thesis
submitted in partial fulfilment
of the requirements for the degree
of

Master of Science
in Biochemistry

at the
University of Canterbury
New Zealand

Hannah Burrowes

2012

Contents

List of Figures

LIST OF FIGURES

List of Tables

Acknowledgements

I would like to acknowledge my supervisor, Assoc. Prof. Steven Gieseg, and my co-supervisor, Dr Ashley Garrill, for all their help over the last two years. Steven, thank you for all your advice, and for providing copious amounts of caffeine.

To everyone in the lab, Anastasia, Laura, Raj, Alpha, Wafaa, Izani, Hanadi, Ela and Maggie, thank you for your help with my experiments and feedback on my presentations and just for generally being great people to get to know.

To Mum and Dad, thank you for supporting me both financially and emotionally throughout university.

To Freddie, thank you for being there through all the ups and downs, and the shaking. You kept me going when I felt like giving up.

Abstract

Cholesterol crystals have been linked to activation of the NLRP3 inflammasome and the formation of foreign body giant cells (FBGCs). It has been hypothesized that FBGCs have a role in advanced atherosclerotic plaque formation. This thesis examined the feasibility of producing stable cultures of FBGCs starting with human monocytes with the goal to examine pterin production by these cells in comparison to human monocyte derived macrophages (HMDMs). The study also investigated the effect of cholesterol crystals on 7,8-dihydroneopterin (7,8-NP) production and modulation of IL-1β levels in macrophages. 7,8-Dihydroneopterin is a potent antioxidant generated by macrophages which also down regulates the expression of macrophage scavenger receptor CD36. The use of alpha-tocopherol and IL-4 as FBGC fusion mediators was explored. Using these mediators, large numbers of FBGC were successfully cultured. The rates of fusion achieved in the cultures were low, and the cells had poor adhesion, which prevented pterin measurement. FBGC, which are thought to remove crystallized cholesterol from the plaque, cleared 21% of cholesterol crystal compared to 50% cleared by HMDM cells. Due to this result, the effect of cholesterol crystals on pterin production in monocytes and macrophages was explored. Cholesterol crystals cause inflammation through the activation of the NLRP3 inflammasome, however, it was unknown whether they could modulate 7,8-NP production. Cholesterol crystals caused an intracellular dose-dependent loss of 7,8-NP to its oxidized form, neopterin, in HMDM cells. Cholesterol crystals induced intracellular synthesis of 7,8-NP in HMDMs. 7,8-NP was released into the supernatant and oxidized to neopterin in media. Monocytes treated with cholesterol crystals released up to 100 nM of neopterin and 120 nM of 7,8-NP in the media after 48 hours. The combination of IFN- and cholesterol crystals appeared to inhibit the release of 7,8-NP into the media for the first 48 hours, after this time 7,8-NP release rapidly increased. The addition of exogenous 200 μM 7,8-NP showed that in the presence of monocytes, cholesterol crystals did not cause the oxidation of 7,8-NP to neopterin, as seen in HMDMs but possibly to 7,8-dihydroxanthopterin or xanthopterin. The presence of 7,8-NP increased IL-1β expression in the presence of cholesterol crystals after 24 hours incubation. FBGCs and the removal of cholesterol crystals may be a key process in the resolution of atherosclerotic plaques. It appears that cholesterol crystals are able to modulate inflammatory processes including activation of the inflammasome and balance of 7,8-dihydroneopterin to the oxidized neopterin. The infiltrating monocytes may provide antioxidant protection against the inflammation induced by cholesterol crystals and the activity of the infammasome.

Abbreviations

$(NH_4)_2HPO_4$ ammonium phosphate.

7,8-DXP 7,8-dihydroxanthopterin.

7,8-NP 7,8-dihydroneopterin.

7,8-NP-PPP 7,8-dihydroneopterin triphosphate.

ACN acetonitrile.

ASC apoptosis-associated speck-like protein.

ATP adenosine triphosphate.

BH_4 tetrahydrobiopterin.

CD36 cluster of differentiation 36.

COX cyclooxygenase.

CPDA-1 citrate-phophate-dextrose-adenine.

DAMP danger-associated molecular pattern.

DC-STAMP dentritic cell specific transmembrane protein.

DHE dihydroethidium.

EDTA ethylene-diamine-tetra-acetic acid.

ELISA enzyme-linked immunosorbent assay.

ER endoplasmic reticulum.

Abbreviations

FBGC foreign body giant cell.

FBR foreign body response.

GM-CSF granulocyte macrophage colony stimulating factor.

GSH glutathione.

GTP guanine triphosphate.

GTPCH-1 guanine triphosphate cyclohydrolase 1.

HCl hydrochloric acid.

HMDM human monocyte-derived macrophage.

HPLC high performance liquid chromatography.

HS human serum.

IFN-γ interferon-gamma.

IL-1β interleukin-1 beta.

IL-13 interleukin-13.

IL-3 interleukin-3.

IL-4 interleukin-4.

IMC integrated modulation contrast.

IRAK4 interleukin-1 receptor-associated kinase 4.

JAK1 janus kinase 1.

$KHCO_3$ potassium bicarbonate.

LDL low density lipoprotein.

LGC langhans' giant cell.

LPS lipopolysaccharide.

M-CSF macrophage colony-stimulating factor.

MCP-1 monocyte chemoattractant protein-1.

MGC multinucleated giant cell.

MMP-9 matrix metalloproteinase-9.

MR mannose receptor.

mRNA messenger ribonucleic acid.

MSU monosodium urate.

MTT 3-[4,5-dimethylthiazol-2-yl]-2,5-diphenyl-tetrazolium bromide.

MyD88 myeloid differentiation primary response protein 88.

NaCl sodium chloride.

NaH_2PO_4 sodium dihydrogen orthophosphate.

$NaHCO_3$ sodium bicarbonate.

NF-κB nuclear factor kappa-light-chain-enhancer of activated B cells.

NH_4Cl ammonium chloride.

NLR NOD-like receptor.

NLRP3 NOD-like receptor family, pyrin domain containing 3.

NO nitric oxide.

NOS nitric oxide synthase.

NSAID nonsteroidal anti-inflammatory drug.

oxLDL oxidized low density lipoprotein.

$P2X_7$ purinergic receptor.

PAMP pathogen-associated molecular pattern.

PBS phosphate buffered saline.

PS phosphatidylserine.

PTPS 6-pyruvoyl tetrahydropterin synthase.

RANKL receptor activator of nuclear factor kappa-B ligand.

ROS reactive oxygen species.

RPMI 1640 Roswell Park Memorial Institute.

SDS sodium dodecyl sulphate.

SEM standard error of the mean.

SFM serum free media.

SIRP-α signal-regulatory protein alpha.

SMC smooth muscle cells.

STAT6 signal transducer and activator of transcription 6.

TLR toll-like receptor.

α-TocH alpha-tocopherol.

TRX thioredoxin.

TXNIP thioredoxin-interacting protein.

VLDL very low density lipoprotein.

XP xanthopterin.

1

Introduction

1.1 Overview

Atherosclerosis is a complex and multifaceted disease that affects millions of people worldwide. Many aspects of the disease and its pathogenesis have been studied in detail. Recently, however, there has been growing evidence of an inflammatory role played by cholesterol crystals in atherosclerotic plaques. It is thought that the presence of cholesterol crystals initiates an inflammatory response known as the foreign body response (FBR). The FBR causes the development of infiltrating monocytes and macrophages into much larger cells called giant cells. Giant cells are thought to be able to remove chronic inflammatory stimuli such as cholesterol crystals through phagocytosis. Cholesterol crystals have also been shown to induce inflammation through the activation of the NOD-like receptor family, pyrin domain containing 3 (NLRP3) inflammasome, a protein complex which initiates the cleavage of the inactive form of interleukin-1 beta (IL-1β) to its active form. IL-1β is thought to be proinflammatory and proatherogenic in its nature.

1.2 Foreign Body Response

The FBR is an end-stage innate inflammatory response evoked when a cell encounters an object that it determines to be non-self. This response leads to the influx of macrophages at the site and the formation of giant cells (van Putten et al., 2009). Recently it has been discovered that this process initiates an inflammatory response involving the activation of the intracellular NLRP3 inflammasome (Malik et al., 2011). Endogenous crystalline material such as cholesterol crystals, as well as, exogenous material such as bioimplants have been shown to cause the foreign body response (Nair et al., 1998).

The FBR is categorized by three stages: onset, progression and resolution. The FBR occurs after an initial acute inflammatory response (Anderson et al., 2008; Kyriakides and Bornstein, 2003). If the inflammation fails to resolve because of the presence of a foreign object then a full scale FBR occurs. The onset of this response requires the cell to determine that a non-self object is present. This process is not yet fully understood. It is thought that the cell may recognize a layer of adsorbed proteins (Shen et al., 2004). Adsorbed proteins are soluble proteins that have collected on the surface of the object. The specific collection of proteins, charged ions and polarizable molecules that deposit on the surface of the object is dependent on the chemical and physical properties of the foreign body (Hu et al., 2001; Shen and Horbett, 2001; Thull, 2002). The onset of the foreign body response is characterized by the initiation of chemoattractants that cause the arrival of neutrophils, monocytes and macrophages to the site of inflammation (Luttikhuizen et al., 2006). Once the FBR begins, it progresses into a chronic inflammatory response. Foreign objects that are too large for macrophages to absorb cause the formation of giant cells. As soon

as the particle has been degraded the giant cells disappear, suggesting that their role is specifically focused on larger particles. The FBR response begins to resolve once the foreign body has been removed. At this stage the production of TGFβ is increased (Li et al., 2007). The increase in TGFβ levels suppresses the production and secretion of chemoattractants which stops the influx of inflammatory cells (Luttikhuizen et al., 2006). Finally, macrophages leave the site and progress to the draining lymph nodes (Bellingan et al., 1996).

1.3 Role of FBR in Atherosclerosis

The foreign body response is relevant to many inflammatory conditions. However, almost no research exists into how the foreign body response pertains to cholesterol crystals found in atherosclerotic plaques. Foreign body giant cells have been shown to be prevalent in mice on a high fat diet (Samokhin et al., 2010). Cholesterol containing foreign-body giant cells have been found in the aortic wall of rabbits (Bjorkerud and Bondjers, 1973).

Atherosclerosis affects a growing percentage of the world's population. Currently, 30.6% of all deaths are caused by cardiovascular disease (Roger et al., 2012). This reflects the changes in diet and lifestyle in first world nations, where obesity is becoming increasingly common. Atherosclerosis is a complex disease; its pathogenesis and causes are still largely unclear even after several decades of research. A combination of genetic and environmental risk factors influence the development of atherosclerosis. The main factors thought to be influencing the progression of atherosclerosis are: elevated low density lipoprotein (LDL) and very low density lipoprotein (VLDL) levels, smoking, and a high fat diet (Dos Santos et al., 2008).

There is much overlap between atherosclerosis and other chronic inflammatory diseases such as arthritis and type I diabetes. An interesting development is the discovery of the inflammasome complexes, which may explain the link between a number of these inflammatory conditions (De Nardo and Latz, 2011).

To date, several hypotheses have been put forward to explain the initial events that trigger the development of a healthy artery into a fatty streak, and later on, into an atherosclerotic plaque. These include the oxidative modification hypothesis and the response-to-injury hypothesis. The oxidative modification hypothesis hinges on the uptake of oxidized low density lipoprotein (oxLDL) by scavenger receptors causing foam cell formation, which are found in fatty streaks. The response-to-injury hypothesis suggests that injury of some form (mechanical or infectious) results in the infiltration of monocytes (Bobryshev, 2006), which differentiate into macrophages. These macrophages then take up lipids and become the foam cells found in fatty streaks.

It has been known for over 60 years that cholesterol crystals are present in plaques (Flory, 1945). Cholesterol crystals are most likely to cause chronic inflammation in an atherosclerotic plaque rather than triggering the initial acute inflammatory response that is seen with oxLDL. Cholesterol crystal deposits, in the form of clefts, have been found in areas near the lipid-rich core in histological plaque sections (Bocan et al., 1986). The crystal deposit is dissolved by the use of ethanol during tissue fixation. Initially, it was thought that these deposits were inert and not involved in the inflammation associated with atherosclerosis. It has only recently been discovered how these crystals induce inflammation in plaques (De Nardo and Latz, 2011; Duewell et al., 2010; Freigang et al., 2011; Rajamäki et al., 2010). Research is currently moving towards being able to selectively identify cholesterol crystals in atherosclerotic plaques

using the latest image scanning technology (Suhalim et al., 2012).

Recent research has led to the suggestion that cholesterol crystals may be involved in the weakening of the fibrous cap, which in turn can cause plaque rupture. Cholesterol crystals expand as they form and pierce through the plaque (Vedre et al., 2009). When exposed to blood, cholesterol crystals form emboli that have been shown to block blood vessels and arteries (Moolenaar and Lamers, 1996). This type of embolism is rare but most often occurs after procedures such as angiography or vascular surgery.

1.4 Giant Cells

1.4.1 Multinucleated Giant Cells

The foreign body response induces the formation of giant cells. Giant cells are formed, not by cell division, but by the fusion of many monocytes and macrophages (Murch et al., 1982), hence they are often termed multinucleated giant cells (MGCs). MGCs are found in both infectious and inflammatory conditions. These conditions include AIDS (Botticelli et al., 1989), sarcoidosis (Okamoto et al., 2003b), bone tumors (Joyner et al., 1992), giant cell arteritis (Ly et al., 2010), Crohn's disease (Liu et al., 1996) and atherosclerosis (Samokhin et al., 2010). The classification of MGC covers several different morphologies of giant cells, each with a specific phenotype and function. The most common types of giant cells are: Langhans' giant cell (LGC), Touton's giant cell, the osteoclast, and the foreign body giant cell (FBGC).

1.4.1.1 Langhans' Giant Cells

MGCs were identified by Theodor Langhans in 1868 (Pritchard et al., 2003). Langhans' giant cells are typically found in granulomas and infected tissue. They model a type I interferon-gamma (IFN-γ)-dependent immune response and primarily deal with the removal of microbial pathogens. Langhans' giant cells are particularly common in *Mycobacterium tuberculosis* granulomas, where they prevent the spread of the mycobacterium to other healthy tissue by secluding it (Lay et al., 2007). The Langhans' cells are distinctive as the nuclei form a horseshoe shape inside the cell. Okamoto et al. (2003a) found a typical cell contains between 3 and 11 nuclei.

1.4.1.2 Touton's Giant Cells

Fusion of cells to form Touton's giant cells is induced by IFN-γ (Schepetkin et al., 2001). Touton's giant cells are thought to develop from foam-like cells (Watanabe et al., 1982). Foam-like cells have a high lipid content due to the sequestering of aggregated or oxidized lipoproteins. Touton's giant cells have a much higher lipid content in their cytoplasm than other giant cells. This lipid-laden cytoplasm is encircled by the nuclei. The presence of these cells, particularly in cases of fat necrosis and xanthogranulomas, is well documented (Aterman et al., 1988; Drummond et al., 2001; Janney et al., 1991; Provenzano et al., 2010). However, very little is actually known about the formation and function of the Touton's giant cell.

1.4.1.3 Osteoclasts

Osteoclasts are specifically involved in calcium resorption, that is, the process of releasing calcium from bones into the bloodstream (Bradley and Oursler, 2008). The

osteoclast cell membrane is ruffled in order to increase surface area for calcium resorption. These cells derive specifically from bone marrow macrophages. A typical osteoclast contains around 9 nuclei which are closely associated with one another (Jaworski et al., 1981). Osteoclast formation is induced by receptor activator of nuclear factor kappa-B ligand (RANKL) and macrophage colony-stimulating factor (M-CSF) (Kreja et al., 2007).

1.4.1.4 Foreign Body Giant Cells

FBGC form in the presence of asbestos particles (Sethi et al., 1974), silica (Prieditis and Adamson, 1996), monosodium urate (MSU) crystals (Bhadani et al., 2006) and cholesterol crystals (Nair et al., 1998). FBGC are the largest of the giant cells and contain up to 100 nuclei (Enelow et al., 1992). The arrangement of nuclei in FBGCs is non-uniform. These cells are distinct from Langhans' and Touton's giant cells as they form upon stimulation with interleukin-4 (IL-4) or interleukin-13 (IL-13) (McNally and Anderson, 2011; Miyamoto et al., 2012). This giant cell phenotype is most commonly associated with the foreign body response. Historically, the process of FBGC formation was not well understood. However, recent advances in the field have provided a much clearer picture of the molecules and signalling involved in FBGC fusion.

1.4.2 Formation of Foreign Body Giant Cells

The fusion of macrophages and monocytes to form foreign body giant cells is a three stage process. The adhesion, recognition and fusion of cells requires a number of specific mediators and is tightly regulated.

1.4.2.1 Adhesion

Adhesion is a requirement for giant cell fusion. It has been found that cell membrane bound β-integrins bind to vitronectin, an adhesion glycoprotein found in serum. This binding initiates cellular attachment (Brodbeck and Anderson, 2009; Helming and Gordon, 2009). Cellular attachment requires multiple complex interactions and several other proteins have been implicated in this process. Both dentritic cell specific transmembrane protein (DC-STAMP) and E-cadherin, membrane-bound glycoproteins, are required for giant cell formation to occur (Martinez and Helming, 2009; Moreno et al., 2007). The transcription of both of these proteins is controlled through cytokine signaling. Interleukin-4 binds to the janus kinase 1 (JAK1) receptor. The cytoplasmic domain of the transmembrane receptor is then phosphorylated (Murray, 2007). This initiates the recruitment and activation of the signal transducer and activator of transcription 6 (STAT6) monomer (Gooch et al., 2002). The active monomer then dimerizes. The STAT6 dimer is a transcription factor and induces the transcription of DC-STAMP and E-cadherin. This activation of the JAK/STAT pathway also has implications in the function of giant cells.

1.4.2.2 Recognition

For fusion to occur, cellular recognition must take place. After adhering, cells begin to protrude lamellipodia (Jay et al., 2007), a cytoskeletal projection containing actin found on the leading edge of the cell (Ballestrem et al., 2000). These lamellipodia have been shown to contain high levels of intracellular and membrane bound cluster of differentiation 36 (CD36) receptors. It is thought that cellular recognition occurs through the binding of phosphatidylserine (PS) on the surface of one cell to the

scavenger receptor CD36 present on the surface of another cell (Helming et al., 2009). In order for PS to be present on the cell surface, flipping must occur. Normally, PS is located in the lipid bilayer of the cellular membrane. However, it has been shown that alpha-tocopherol (α-TocH) can induce PS flipping (Klein et al., 2006). PS flipping also occurs in apoptotic cells (Fadok et al., 1998). Additional fusion receptors such as CD44, CD47, CD54 and CD200 (Chen and Olson, 2005; Quinn and Schepetkin, 2009) indicate that the cell is not in apoptosis. Instead, a fusion process similar to, but distinct from phagocytosis is initiated (McNally and Anderson, 2005).

1.4.2.3 Fusion

Once the target cell has been identified, fusion can occur. The method of giant cell fusion is still not fully understood. It is thought that mannose receptors (MRs) are involved in giant cell fusion as they are found to be clustered at fusion interfaces (McNally and Anderson, 2011). The MR recognizes carbohydrates on glycoproteins. This recognition generally leads to the endocytosis of the proteins. However, in the case of giant cells, it is hypothesized that this recognition leads to the engulfment of an entire cell. Several other proteins and receptors are thought to be involved. The purinergic receptor ($P2X_7$) receptor which is an adenosine triphosphate (ATP) gated ion channel that forms a membrane pore, is involved in both the macrophage fusion process (Lemaire et al., 2006) and inflammasome activation (Miller et al., 2011). Blocking either CD47 or signal-regulatory protein alpha (SIRP-α), both membrane proteins that interact with one another during cell-cell adhesion (Babic et al., 2000), prevents macrophage fusion (Han et al., 2000). A chemokine, monocyte chemoattractant protein-1 (MCP-1), is also thought to be involved in the fusion process through interactions with DC-STAMP (Low et al., 2001). This chemokine has also

been implicated in both early and advanced plaque formation (Boyle, 2005).

1.5 Cholesterol Crystals

Cholesterol crystals are often surrounded by giant cells (Flory, 1945; Moolenaar and Lamers, 1996), which has lead to the suggestion that the crystals induced multinucleated cell formation. Usually, cholesterol plays an important role in maintaining the viscosity of cell membranes and is a precursor molecule to steroid hormones.

Cholesterol crystals form in aqueous solutions due the low solubility of cholesterol (De Nardo and Latz, 2011). For crystallization to occur there must be a nucleating stimulus. Crystallization most commonly occurs in areas of high free lipid content, for example, the necrotic core or in macrophage foam cells. Cholesterol crystals have been found in the necrotic core in atherosclerotic lesions of apolipoprotein E (ApoE) deficient mice (Freigang et al., 2011). Geng et al. (2003) have shown that lipid-laden macrophages produce cholesterol crystals at $37\,^{\circ}\mathrm{C}$ but raising the temperature to $40\,^{\circ}\mathrm{C}$ inhibits this ability. It has been found that cholesterol crystals can grow to 120 μM in synovial fluid (Zakharova et al., 2009).

It appears that there are two processes leading towards the formation of cholesterol crystals in the atherosclerotic plaque. The first is the formation of crystals inside a cell, e.g. a lipid-laden macrophage. The second is formation due to the death of cells and the release of free cholesterol. These crystals form acellularly, most commonly in the necrotic core of the atherosclerotic plaque. The first type of cholesterol crystal is generally needle-shaped, and if the crystals become large enough, can be released from the macrophage (Geng et al., 2003). Intracellular cholesterol crystal formation is

thought to be initiated rapidly after the oxidation of cholesterol. It appears that these macrophages are resistant to apoptosis, which is thought to add to the plaque instability. The cholesterol crystals formed in the necrotic core are much more rhomboidal and planar (Flory, 1945).

1.6 NLRP3 Inflammasome

Foreign bodies, such as cholesterol crystals, can be recognized as danger-associated molecular patterns (DAMPs) by NOD-like receptor (NLR). This leads to the activation of the NLRP3 inflammasome, a high molecular weight protein complex. NLRs are intracellular receptors that have been compared in function to the extracellular toll-like receptor (TLR), which are known to have a role in recognizing microbial pathogen-associated molecular patterns (PAMPs) (Hansson and Libby, 2006).

A basic subunit of the NLRP3 inflammasome contains NLRP3, apoptosis-associated speck-like protein (ASC), and caspase-1 (see **Figure 1.1**). Under non-inflammatory conditions, these proteins are expressed but internal auto-repression prevents their activation (Tschopp and Schroder, 2010). Currently there are three proposed models of activation of the inflammasome: the channel model, the lysosomal rupture model and the reactive oxygen species (ROS) model. The channel model suggests that the efflux of K^+ induces the formation of a $P2X_7$-pannexin 1 pore which allows the influx of extracellular factors, such as PAMPs and DAMPs that activate NLRP3 (Pétrilli et al., 2007). In the lysosomal rupture model, phagocytosis of PAMPs and DAMPs cause lysosomal damage. This in turn leads to the release of cathepsin B, a protease, which induces the activation of NLRP3 through an unknown mechanism (Hornung et al., 2008). Finally, the ROS model

proposes that the phagocytosis of PAMPs and DAMPs induces ROS production. ROS production causes the release of thioredoxin-interacting protein (TXNIP), an NLRP3 activating ligand, from its inhibitor, thioredoxin (TRX). The current view of NLRP3 inflammasome activation is that the mechanisms listed above are not necessarily mutually exclusive and that each may play a part in the activation process.

Upon activation, NLRP3 migrates from the endoplasmic reticulum (ER) and recruits ASC, which migrates from the cytoplasm (Zhou et al., 2011). Subunit oligomerization occurs in the perinuclear space through the interaction of CARD-CARD and PSY-PSY domains which are located on the ASC and NLRP3 respectively (Martinon et al., 2009). When the inflammasome is fully formed it contains 7 subunits and is approximately 2 μm in diameter (**Figure 1.2**). Based on the size of the complex, it is not surprising to find that only one NLRP3 inflammasome forms per cell. To put this in context, a whole cellular organelle such as the mitochondrion is only 1 μm in diameter.

The function of the inflammasome is to activate inflammatory caspases. The NLRP3 inflammasome activates caspase-1, a cysteine protease, which induces the cleavage of proIL-1β to IL-1β; the biologically active form. However, activation of the NLRP3 inflammasome alone is not enough to induce the production of mature IL-1β. Nuclear factor kappa-light-chain-enhancer of activated B cells (NF-κB), a DNA transcription factor, must also be activated (see **Figure 1.3**). Priming of the cell occurs by a signal cascade resulting from the recognition of PAMPs by TLRs. It has been shown that significant IL-1β production occurs in the presence of a stimuli, such as cholesterol crystals or alum, if cells have been primed with lipopolysaccharide (LPS); an known endotoxin (De Nardo and Latz, 2011; Franchi and Nuñez, 2008). However, without this priming, only a low level of IL-1β is produced.

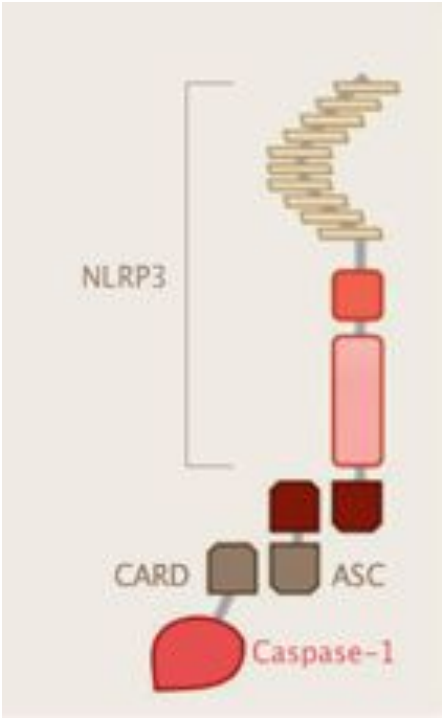

Figure 1.1: A subunit of the NLRP3 inflammasome - The basic unit of the NLRP3 inflammasome consists of a NLRP3 domain bound to the adaptor protein ASC and caspase-1. Figure adapted from Martinon et al. (2009)

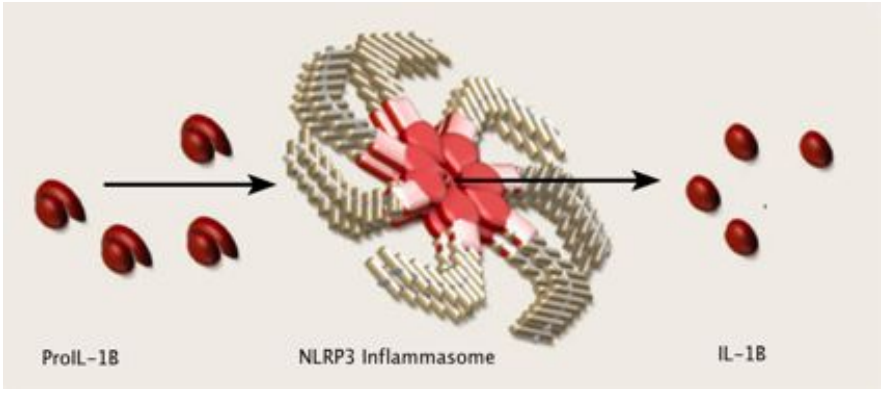

Figure 1.2: The NLRP3 inflammasome converts proIL-1β to IL-1β - Activation of caspase-1, the enzyme responsible for the cleavage of proIL-1β, requires the oligomerization of the NLRP3 subunits. IL-1β processing is thought to occur through the central pore in the inflammasome. Figure adapted from Martinon et al. (2009)

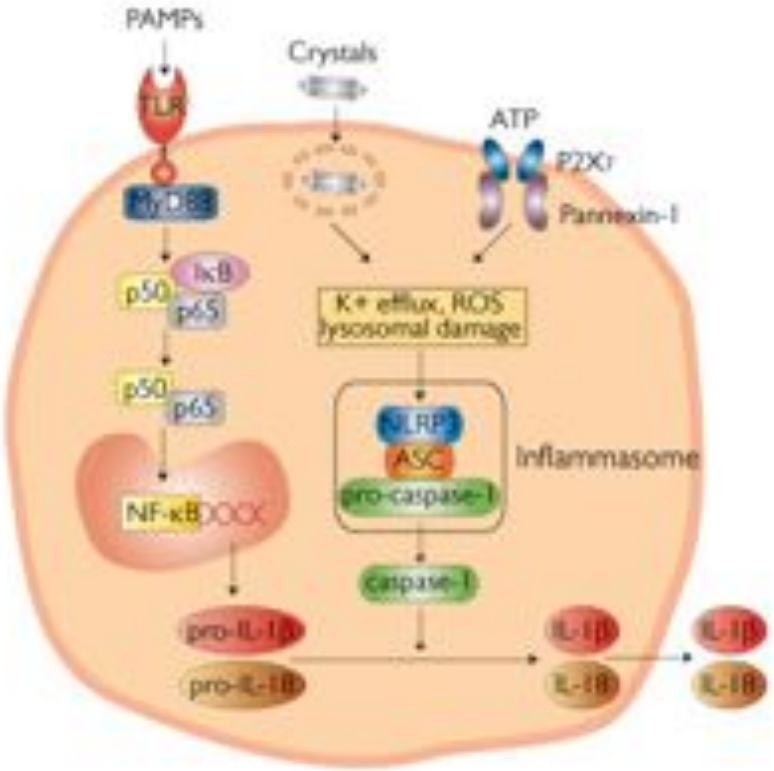

Figure 1.3: Process of NLRP3 inflammasome activation - Cholesterol crystals activate the NLRP3 inflammasome through processes including potassium efflux, lysosomal damage and production of ROS.

1.7 Interleukin-1β

Interleukin-1β is a cytokine from the interleukin-1 family. It is produced in a number of cells including monocytes, smooth muscle cells (SMC) (Wang et al., 1995), and endothelial cells (Strieter et al., 1989). Transcriptional activation of IL-1β is typically induced by the presence of LPS (Grahames et al., 1999). Monocytes are capable of producing large quantities of IL-1β messenger ribonucleic acid (mRNA), although, only a small proportion of the mRNA is translated into protein, as there is a dissociation between the transcription and the translation of IL-1β (Schindler et al., 1990). The mRNA transcript is stable for at least 24 hours after being produced. It is during this time that it can be transported to the site of translation. IL-1β is synthesized in an inactive form, proIL-1β. Monocytic cells are able to process proIL1-β and secrete it in its mature form.

Rajamäki et al. (2010) have shown that cholesterol crystals induce a dose-dependent release of IL-1β from both monocytes and macrophages. Interestingly, in primary cells this response required two stimuli, the cholesterol crystals and the additional stimulus LPS. LPS is a large molecule that is found in the outer membrane of gram-negative bacteria. As an endotoxin, it induces a strong immune response. However, in the monocyte-like cell line THP-1 the response could be achieved with out the presence of LPS. This response was found to be caspase-1 dependent, as there was found to be no IL-1β when caspase-1 was blocked.

IL-1β is thought to be proinflammatory and proatherogenic. It has been shown to upregulate cyclooxygenase (COX)-2, a key enzyme in prostaglandin synthesis (Colville-Nash and Gilroy, 2001), in smooth muscle cells (Yang et al., 2002). COX is a common target for nonsteroidal anti-inflammatory drugs (NSAIDs), such as aspirin

and ibuprofen. Patients with atherosclerosis in their coronary artery have been found to have higher levels of IL-1β that correlate with the disease severity (Galea et al., 1996).

1.8 Neopterin and 7,8-Dihydroneopterin

Neopterin is commonly used as a clinical marker of inflammation in urine and serum samples (Fuchs et al., 1993). Increased neopterin levels have been associated with increased atherosclerosis in patients (Tatzber et al., 1991; Weiss et al., 1999).

7,8-Dihydroneopterin, a precursor to neopterin, is synthesized by monocytes (Seki et al., 1996), macrophages (Sghiri et al., 2005) and giant cells (Shaskan et al., 1992), each to a different extent. 7,8-dihydroneopterin (7,8-NP) is produced by the conversion of guanine triphosphate (GTP) to 7,8-dihydroneopterin triphosphate (7,8-NP-PPP) by guanine triphosphate cyclohydrolase 1 (GTPCH-1) (see **Figure 1.4**). The phosphates are then removed by non-specific phosphatases. The 7,8-NP can then be further converted to neopterin by oxidation.

It has been proposed that 7,8-NP has an antioxidant role *in vivo* (Gieseg et al., 1995). Studies by Gieseg et al. (2001) have shown that 7,8-NP is able to protect monocyte-like U937 cells from cell death caused by oxLDL toxicity. It is thought that this protection is due to the scavenging of lipid peroxyl radicals by 7,8-NP. Interestingly, α-TocH also acts as an antioxidant and free radical scavenger (Brigelius-Flohé, 2009), as well as inducing giant cell formation. This scavenging of radicals prevents damage to the cell and the loss of glutathione (GSH), which is a key event in oxLDL triggered cell death (Baird et al., 2005). 7,8-NP has also been shown to downregulate CD36 (Gieseg et al., 2010). This downregulation limits the uptake of oxLDL which prevents foam cell formation and cell death. It is unknown whether

this downregulation of CD36 by 7,8-NP has any involvement in preventing giant cell formation.

In most cell types there is very little neopterin or 7,8-NP present as the majority of 7,8-NP-PPP is converted into tetrahydrobiopterin (BH_4) and its derivatives. BH_4 is a cofactor for nitric oxide synthase (NOS), which produces nitric oxide (NO) (Maier et al., 2000) and is also largely involved in the biosynthesis of neurotransmitters (Habecker et al., 2002). However, in monocytes and macrophages, neopterin and 7,8-NP build up due to a low level of active 6-pyruvoyl tetrahydropterin synthase (PTPS) (Leitner et al., 2003). PTPS is responsible for the downstream processing of 7,8-NP-PPP to BH_4. Transcription of the PTPS mRNA is upregulated by IL-1β. This suggests that IL-1β may have a role in determining the balance of 7,8-NP and BH_4 present in a cell.

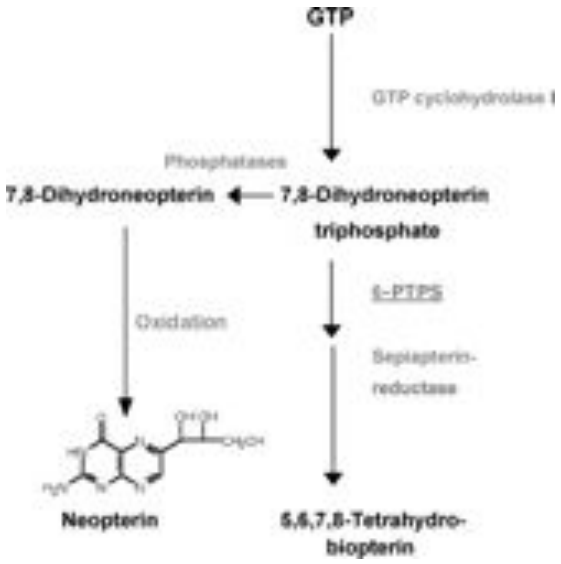

Figure 1.4: Biosynthesis of 7,8-NP and Neopterin - GTP is converted to 7,8-dihydroneopterin triphosphate (7,8-NP-PPP) by the enzyme GTP cyclohydrolase I. 7,8-NP-PPP can then either be converted to 7,8-dihydroneopterin (7,8-NP) by non-specific phosphatases, or to tetrahydrobiopterin through 6-pyruvoyl-tetrahydropterin synthase (PTPS) and sepiapterin reductase (SR). Oxidation of 7,8-NP results in the formation of neopterin.

1.9 Clinical Targets: Cholesterol Crystals and the Inflammasome in Atherosclerosis

It was thought that the formation of cholesterol crystals in the plaque was a late event in the disease progression. However, confocal microscopy techniques have shown that cholesterol crystal formation coincides with monocyte infiltration, which is an early event in plaque formation (Duewell et al., 2010). Blocking phagocytosis of cholesterol crystals prevented the activation of the NLRP3 inflammasome. Freigang et al. (2011) proposed the idea that cholesterol crystals and the NLRP3 inflammasome are linked to oxidative stress via NF-E2-related 2 (Nrf-2) signalling. Nrf-2 is known to limit the effects of oxidative stress by inducing the expression of antioxidant enzymes. Nrf-2 is required for NLRP3 activation by cholesterol crystals. It is thought that this activation of the inflammasome explains why increased Nrf-2 has been shown to aggravate atherosclerosis. Whilst there may be less oxidative stress, cholesterol crystals may promote chronic inflammation in the atherosclerotic plaque.

A key target currently is developing methods that allow for the early detection of atherosclerosis. Current technologies available are either too invasive (surgery) or of too low quality (ultrasound) to view the development of atherosclerotic plaques. Cholesterol crystals may provide a way of measuring plaque development. The crystals form in early plaques and may be visualized using multispectral CT imaging technology, though this technology is still very much in the prototype phase of development (personal communications). Early detection would allow for better prevention of atherosclerosis and intervention if necessary.

1.10 Research Programme

This thesis aims to examine the inflammatory response of giant cells to a cholesterol crystal stimulus. This will be studied by developing a giant cell culture system and then examining neopterin and 7,8-NP production after incubation with cholesterol crystals by high performance liquid chromatography (HPLC).

The interaction between giant cells and cholesterol crystals is hypothesized to result in higher 7,8-NP and neopterin production in giant cells than macrophages. In **Chapter 3** the feasibility of a giant cell culture system that is comparable to cultured HMDMs is examined. This chapter investigates the fusion mediators required for giant cell formation, attempts to quantify giant cells in culture and measure their viability using common assays.

Having established a giant cell culture, it was intended that neopterin and 7,8-NP production would be measured by HPLC. Unfortunately, experiments carried out in **Chapter 3** showed that giant cell culture is highly variable and does not produce replicable results. Instead, in **Chapter 4** the effect of cholesterol crystals on neopterin and 7,8-NP production will be investigated in monocytes and macrophages, both precursors to giant cells. This chapter will also examine the effect of cholesterol crystals on IL-1β production and possible modulation by 7,8-NP.

2

Materials & Methods

2.1 Materials

2.1.1 Reagents

All reagents used were of analytical grade or better. All solutions were prepared using ion-exchanged ultra filtered water, produced using a Milli-Q integral water purification system from Millipore (Massachusetts, USA).

α-Tocopherol (α-TocH)	Sigma Chemical Co., MO, USA
3-[4,5-Dimethylthiazol-2-yl]-2,5 -diphenyl-tetrazolium bromide (MTT)	Sigma Chemical Co., MO, USA
7,8-Dihydroneopterin (7,8-NP)	Schircks Laboratory, Switzerland
Acetic acid (glacial)	Scharlau Chemie S.A., Barcelona, Spain
Acetonitrile (ACN)	J.T. Baker, NJ, USA
Ammonium chloride (NH_4Cl)	May & Baker Ltd, Dagenham, England
Ammonium phosphate dibasic ($(NH_4)_2HPO_4$)	Sigma Chemical Co., MO, USA

Ascorbic acid	Sigma Chemical Co., MO, USA
Cholesterol	Sigma Chemical Co., MO, USA
Citrate	Sigma Chemical Co., MO, USA
Ethylene-diamine-tetra-acetic acid (EDTA)	Sigma Chemical Co., MO, USA
Ethanol	BDH Lab Supplies Ltd, Poole, England
Granulocyte-macrophage colony-stimulating factor (GM-CSF)	Bayer HealthCare Pharmaceuticals, WA, USA
Hydrochloric acid (HCl)	BDH Lab Supplies, Poole, England
IFN-γ	Boehringer Ingelheim Pty Ltd, NSW, Australia
Interleukin-4 (IL-4)	ProSpec, Ness-Ziona, Israel
Iodine (I)	BDH Lab Supplies Ltd, Poole, England
Isopropanol	BDH Lab Supplies, Poole, England
Lymphoprep	Axis-Shield PoC AS, Oslo, Norway
L-Methionine	Sigma Chemical Co., MO, USA
Methanol	Merck, Darmstadt, Germany
Neopterin	Schircks Laboratory, Switzerland
Oil Red O	Sigma Chemical Co., MO, USA
Phenol	Sigma Chemical Co., MO, USA
Phosphoric acid	Sigma Chemical Co., MO, USA
Potassium bicarbonate ($KHCO_3$)	May & Baker Ltd, Dagenham, England
Potassium Iodide (KI)	May & Baker Ltd, Dagenham, England
PrestoBlue	Invitrogen, CA, USA
Sodium bicarbonate ($NaHCO_3$)	May & Baker Ltd, Dagenham, England
Sodium chloride (NaCl)	BDH Lab Supplies Ltd, Poole, England
Sodium dihydrogen orthophosphate	Merck, Darmstadt, Germany

(NaH_2PO_4)	
Sodium dodecyl sulphate (SDS)	Sigma Chemical Co., MO, USA
Sodium hydroxide (NaOH)	Merck, Darmstadt, Germany
Sodium hypochlorite (NaOCl)	Clorogene Supplies, Petone, New Zealand
Trypan blue solution (0.4%)	Sigma Chemical Co., MO, USA

2.1.2 Media and Buffers

Penicillin/Streptomycin liquid; 1000 U of Penicillin G & 1000 μg of Streptomycin/mL	Invitrogen, CA, USA
Roswell Park Memorial Institute (RPMI 1640);	
- RPMI 1640 media, with phenol red	Sigma-Aldrich Chemical Co., MO, USA
- RPMI 1640 media, without phenol red	Sigma-Aldrich Chemical Co., MO, USA
Serum Free Media (SFM) for Macrophages	Invitrogen, CA, USA

2.1.3 General Solutions, Buffers and Media

2.1.3.1 Blood Cell Lysis Buffer

Ammonium chloride (NH_4Cl) (8.26 g) was dissolved in 1 L of nanopure water along with 1 g of potassium bicarbonate ($KHCO_3$) and 0.037 g of ethylene-diamine-tetra-acetic acid (EDTA). The solution was stored at room temperature.

2.1.3.2 7,8-Dihydroneopterin Solution

7,8-Dihydroneopterin was prepared fresh prior to each experiment. A 2 mM stock solution was prepared by sonicating 7,8-NP in ice cold RPMI 1640 until dissolved. The stock solution was filter-sterilized via a 0.22 μm membrane (Sartorius AG, Goettingen, Germany). As 7,8NP is light sensitive the solution was always kept in the dark.

2.1.3.3 HPLC Mobile Phases

All aqueous solutions for HPLC were passed through a 0.45 μm filter and degassed via sonication prior to use.

Ammonium phosphate ($(NH_4)_2HPO_4$) buffer (20 mM) was prepared by dissolving 2.64 g of $(NH_4)_2HPO_4$ in 900 mL of nanopure water. The pH was adjusted to 3.0 by the addition of 10 M phosphoric acid. Nanopure water was added until the solution reached a volume of 1 L, with a final concentration of 20 mM.

2.1.3.4 MTT assay solutions

The MTT stock solution was prepared by dissolving 5 mg/mL of 3-[4,5-dimethylthiazol-2-yl]-2,5-diphenyl-tetrazolium bromide (MTT) in phenol red free RPMI 1640. This solution is light sensitive so after filter-sterilization (0.22 μm MS®PES syringe) it was kept the dark at $-20\,^{\circ}\mathrm{C}$.

Sodium dodecyl sulphate (SDS) (10% weight to volume ratio) was dissolved in 0.01 M hydrochloric acid (HCl). This solution was stored at room temperature.

2.1.3.5 Oil Red O Stock Solutions

A 1 M concentrated citrate solution was prepared by dissolving 1.92 g of citric acid in 10 mL of deionized water. Two millilitres of the concentrated solution was diluted by the addition of 8 mL of deionized water and stored at $4\,^{\circ}\mathrm{C}$. This diluted solution is used to fix the cells prior to oil red O staining.

The oil red O stock solution was made by dissolving 300 mg of oil red O powder in 100 mL of isopropanol (99%). This solution was diluted for use at a ratio of 6 parts oil red O stock solution to 4 parts distilled water. After 10 minutes standing, this diluted solution was filtered through Whitman paper. The filtered working solution had a shelf life of 1-2 hours.

2.1.3.6 Phosphate Buffered Saline (PBS)

Phosphate buffered saline (PBS) (150 mM sodium chloride (NaCl) and 10 mM sodium dihydrogen orthophosphate (NaH_2PO_4), pH 7.4) for sterile use was autoclaved for 15 minutes at $121\,^{\circ}\mathrm{C}$, 15 psi. This solution was stored at room temperature.

2.1.3.7 Roswell Park Memorial Institute 1640 Media

Following the manufacturer's instructions, RPMI 1640 powder (with or without phenol red) was dissolved in ultrapure water. Sodium bicarbonate ($NaHCO_3$) was added and the pH adjusted to 7.4 by the addition of concentrated HCl. The media was filtered using a 0.22 μm Millex®-GP_{50} filter (Molsheim, SA) and a peristaltic pump (CP 600, Life Technologies; New York, USA). The solution was stored at $4\,^{\circ}\mathrm{C}$. RPMI 1640 for cell culture work had 1000 U/mL penicillin-G and 1000 μg/mL streptomycin added prior to use.

2.2 Methods

2.2.1 Blood Collection

The Canterbury Ethics Committee approved the use of human blood (98/07/069) for these studies. Blood was collected from consenting patients during the haemochromatosis clinic at the New Zealand Blood Bank (Riccarton Road, Christchurch). Blood from patients was collected into either Compoflex® autologous bags, containing the anticoagulant citrate-phophate-dextrose-adenine (CPDA-1) for cell preparation, or dry bags (Fresenius Kabi; Homburg, Germany) for serum preparation. Blood for cell preparation was either used within an hour of collection or refrigerated overnight before use. Blood for serum preparation was cooled to room temperature over 2 hours. The dry bag was placed at $4\,^{\circ}\mathrm{C}$ overnight to allow the blood to clot and shrink.

The following procedures were performed under sterile conditions in a Class II Laminar Flow hood (Clyde-Apex BH 200) to minimize bacterial and fungal contamination.

2.2.2 Preparation of Human Serum

Dry blood bags were refrigerated overnight in a vertical position. Plasma was collected from around the clotted blood and transferred to several 50 mL Falcon™ tubes (Thermofisher Scientific; Indiana, USA). The tubes were centrifuged at 500 g for 15 minutes (Multifuge 1 S-R, Heraeus) to remove any remaining clotted material. The serum was then transferred to new tubes for storage at $-80\,^{\circ}\mathrm{C}$.

2.2.3 Isolation of Monocytes

RPMI 1640 was warmed to $37\,^{\circ}\mathrm{C}$ prior to addition. All other solutions and media used in this procedure were warmed to room temperature before use.

The following procedure has previously been described by Yang (2009). Briefly, blood from one autologous bag was transferred to 50mL Falcon™ tubes and centrifuged for 30 minutes at 1000 g with slow deceleration. The buffy coat was transferred into fresh 50 mL tubes (up to 15 mL per tube) and PBS was then added to bring the total volume to 35 mL. Lymphoprep (15 mL), a Ficoll-Isopaque density gradient medium which causes the aggregation and sedimentation of red blood cells, was then carefully underlaid and the tubes were centrifuged for a further 30 minutes as before. The monocyte layer, located approximately in the center of the tube, was collected and transferred to new tubes (15 mL per 50 mL centrifuge tube). These tubes were topped up to 50mL with PBS and centrifuged for 15 minutes at 500 g, with the brake on to pellet the monocytes. The supernatant was discarded and the pellet was resuspended in PBS to wash away the lymphoprep. The tubes were again topped up to 50 mL and centrifuged for 10 minutes at 500 g, with the brake on. The wash step was repeated twice more to remove any remaining lymphoprep. Finally, the pellet was resuspended in serum-free RPMI 1640 ($37\,^{\circ}\mathrm{C}$) at a concentration of 5 x 10^6 cells/mL. The cells were transferred to 6 well suspension plates (Cellstar®, Greiner Bio-one; North Carolina, USA) and placed into a humidified 5% CO_2 incubator (Sanyo MCO-5AC; Osaka, Japan) at $37\,^{\circ}\mathrm{C}$.

2.2.4 Cell Culture

2.2.4.1 Monocytes

After being isolated from whole blood, monocytes were incubated for 40 hours in 6 well plates to allow for T-cell death and the adherence of platelets. The monocytes were gently removed from the 6 well plates, taking care not to disturb any adherent particles. The collected cells were centrifuged for 10 minutes at 500 g. The monocytes were then resuspended in fresh RPMI 1640 at a concentration of 10 x 10^6 cells/mL. These cells were either pipetted into 12 well suspension plates (Cellstar®) at 500 μL per well for experimentation, or diluted to 5 x 10^6 cells/mL with RPMI 1640 with 1% human serum (HS) and stored in 6 well suspension plates for use within one week.

2.2.4.2 Macrophages

As described above in **Section 2.2.4.1**, isolated monocytes were removed from the 6 well plates, centrifuged and resuspended in RPMI 1640. Cells were resuspended at a concentration of 5 x 10^6 cells/mL in RPMI 1640 with 10% HS. This solution was then supplemented with 2 μL/mL of 25 μg/mL granulocyte macrophage colony stimulating factor (GM-CSF). The cells were transferred into 12-well tissue culture plates (Nunc, Nalge Nunc International; New York, USA) at a volume of 1000 μL per well. The monocytes developed into macrophages over the course of two weeks. The media (RPMI 1640 containing 10% HS) was changed every three to four days as determined by the change in phenol red color. Phenol red is a pH indicator which turns yellow as the media becomes acidic.

2.2.4.3 Giant Cells

FBGCs are formed by the fusion of monocytes and macrophages in the presence of a foreign body. Giant cells are distinctive with their many nuclei and large surface area.

Monocytes were isolated as described in **Section 2.2.3**. Immediately after isolation the cells were seeded into 12 well tissue culture plates in RPMI 1640 with 10% HS. After 40 hours, 800 μL of medium was removed from each well and replaced with the same volume of fresh media. Five days from the initial seeding the RPMI 1640 was replaced with serum free media (SFM) for macrophages. As determined by McNally and Anderson (2003), the medium was supplemented with 50 μM α-TocH and 10 ng/mL IL-4. This media was changed every three to four days. The cells were ready for experimentation eight days after seeding.

2.2.5 Oil Red O Staining

Oil red O is a polyazo dye that is lipid-soluble (McVean et al., 1965) and has been used to stain adipose cells or areas of lipid deposits. Citrate working solution (see **Section 2.1.3.5**) was warmed to $37\,^{\circ}\mathrm{C}$ before use. Media was removed from the tissue culture plate and the cells were washed twice with PBS. A fixative solution was prepared by adding 3 parts acetone to 2 parts citrate working solution, and then 1 mL of fixative was added to each well for 30 seconds. The cells were washed with distilled water before the addition of 1 mL of oil red O staining solution. The stain was allowed to develop for 10 minutes before being removed. One millilitre of 60% isopropanol/H_2O ($^{V}/_{V}$) was added to each well to remove any remaining stain that had not been incorporated into the cells. The plate was washed thoroughly with distilled water, and then viewed under a light microscope (DM IL, Leica; Wetzlar, Germany).

2.2.6 Preparation of Cholesterol Crystals

Cholesterol crystals form *in vivo* in both bile and the necrotic core of plaques. To reproduce this *in vitro*, a method of growing crystals using cholesterol powder was adapted from Rajamäki et al. (2010). Powdered cholesterol (12.5g) was dissolved in 96% ethanol which had been heated to $65\,^{\circ}\mathrm{C}$. This solution was left overnight to cool. The ethanol was filtered through Whitman paper and the cholesterol crystals were left for several hours to dry. The dry crystals were stored in a glass container at room temperature until needed.

To prepare the crystals for addition to sterile cell culture, 100 mg of cholesterol crystals was weighed out in a small paper holder and placed into a laminar flow hood. The crystals were lightly covered in 100% ethanol to sterilize. The crystals were then dried completely by waiting for the ethanol to evaporate before being added to 10 mL of RPMI 1640 (no phenol red) in a sterile glass container as the crystals adhere to plastic. The solution was then placed in a sonicator for 20 minutes to break the crystals into smaller fragments. This solution was refrigerated at $4\,^{\circ}\mathrm{C}$ until needed and warmed to $37\,^{\circ}\mathrm{C}$ prior to use in any cell culture experiments.

2.2.7 Viability Assays

2.2.7.1 MTT Reduction Assay

The MTT reduction assay was carried out following the method adapted from Mosmann (1983). Incubation media was removed from cell culture plate wells and the cells were washed twice with PBS. RPMI 1640 (no phenol red) was mixed with 5 mg/mL MTT at a 9:1 ratio. To each well 1 mL of dilute MTT solution was added. The tissue culture plates were returned to the incubator for 2 hours to allow the

MTT to be reduced by cellular succinate dehydrogenase to form the purple formazan crystals. Plates were removed from the incubator and 1 mL of warm 10% ($^{W}/_{V}$) SDS in 0.01 M HCl was added to each well to dissolve the formazan crystals. A blank was prepared by adding all the reagents minus the cells. The blank was used to zero the spectrophotometer (Shimadzu UV-1601PC UV-visible; Kyoto, Japan) and cuvettes containing 1 mL of solution were read at 570 nm absorbance.

2.2.7.2 PrestoBlue™ Viability Assay

PrestoBlue™ (Invitrogen; New York, USA) is a resazurin-based, cell permeable solution which turns red on contact with the reducing environment inside a viable cell.

For adherent cultures, treatment solutions were removed from the wells and the cells were gently washed twice with PBS. PrestoBlue™ was diluted in RPMI 1640 (no phenol red) at a 1:9 ratio and 400 μL of this dilute solution was added to each well. Triplicate blanks containing only RPMI 1640 and PrestoBlue™ were also prepared. Cells were incubated until control wells produced a pink color which occurred after approximately 30 minutes. Two hundred microliters from each well was transferred to a black Nunc Maxisorp 96-well plate. Fluorescence intensity was measured on a POLARstar Galaxy microplate reader (BMG LABTECH; Ortenberg, Germany) using an excitation wavelength of 544 nm and emission wavelength of 590 nm.

For non-adherent cultures, cells were collected from the wells and transferred to 1.7mL microtubes (Axygen; California, USA). The tubes were centrifuged for 5 minutes at 500 g to pellet the cells. The supernatant was removed via aspiration. After this, 200 μL of warm RPMI 1640/PrestoBlue™ (9:1) was added to each microtube. Cells were incubated with the solution as described above and then transferred into a 96-well plate. Fluorescence intensity was measured as described above.

2.2.7.3 Trypan Blue Exclusion Assay

The trypan blue exclusion assay was adapted from the method of Moldeus et al. (1978). For non-adherent cells, the solution in each well was gently pipetted up and down to mix before 50 μL was transferred to a microtube. Next, 50 μL of trypan blue stain (0.4%) was added to the tube and gently mixed with the cell solution. Tubes were left for 2 minutes to allow the dye to permeate any non-viable cells. A haemocytometer (Marienfeld, Germany) was used to count the proportion of dead (blue-stained) cells compared to viable (non-stained cells). For adherent cells, the incubation media was first aspirated and then 50 μL of trypan blue stain (0.4%) was added directly to the cell culture plate. After 2 minutes the Trypan blue was aspirated from the wells. The cells were washed twice with PBS to remove any remaining stain that had not been taken up. The adherent cells were viewed under an inverted light microscope. Dead and live cells were counted in 5 fields of view for each well.

2.2.8 HPLC Pterin Analysis

2.2.8.1 Cell Preparation

Non-adherent cells were pipetted into microtubes and centrifuged at 500 g for 5 minutes to pellet the cells. To prepare the extracellular samples, 200 μL of supernatant from each tube was transferred into two microtubes (100 μL into each). These samples were then processed following the methods described in **Sections 2.2.8.2** and **2.2.8.3**. To prepare the intracellular samples, the rest of the supernatant from the original microtube was aspirated off. The remaining cell pellet was washed twice with PBS. Finally, the pellet was resuspended in 200 μL of PBS, ready to be processed for neopterin analysis (see **Section 2.2.8.2**). Half of this sample was transferred to another

microtube for total pterin analysis (see **Section 2.2.8.3**).

For adherent cells, extracellular supernatant samples were collected directly from the cell culture plates. From each well, 200 μL of supernatant was transferred into two microtubes (100 μL into each). One tube was prepared for neopterin analysis, the other for total pterin analysis. For the intracellular samples, first all the remaining supernatant was aspirated off and then 200 μL of PBS was added to each well. Using the tip of the pipette as a scraper, adherent cells were lifted off the plate and transferred into microtubes. The cells were gently pipetted up and down to resuspend in the PBS. The solution was transferred into two microtubes (100 μL into each) for neopterin and total pterin analysis.

2.2.8.2 Neopterin Sample Preparation

All tubes had 100 μL of 100% acetonitrile (ACN) added to induce protein precipitation. ACN is ideal as it is able to precipitate protein without causing the loss of 7,8-NP which can occur with acidic protein precipitation (Flavall et al., 2008). The tubes were vortexed before being centrifuged for 10 minutes (20,300 g, $4\,^{\circ}\mathrm{C}$) to pellet the precipitated material. Fifty microliters from each tube was transferred into HPLC vials ready for injection.

2.2.8.3 Total Pterin Sample Preparation

As described in **Section 2.2.8.2**, 100 μL of ACN was added to each tube to induce protein precipitation. This material was then pelleted by centrifugation. After this, 40 μL of acidic iodide (5.4% ($^{W}/_{V}$) iodine and 10.8% ($^{W}/_{V}$) potassium iodide in 1 M HCl) was added. Acidic iodide converts any 7,8-NP into neopterin by oxidation. The tubes were briefly vortexed and then incubated in the dark for 15 minutes. After the

incubation, 20 μL of 0.6 M ascorbic acid was added to reduce any remaining iodide and the tubes were briefly vortexed again. Finally, the tubes were centrifuged for 10 minutes (20,300 g, $4\,^{\circ}\mathrm{C}$) to ensure the sample was precipitate free prior to injection. Fifty microliters was pipetted into a HPLC vial.

2.2.8.4 Sample Analysis

The pterin analysis was carried out using a Phenomenex Luna® 5 μm SCX, 50 x 4.6 mm column (California, USA) heated to $35\,^{\circ}\mathrm{C}$. The column separates positively charged compounds by ion exchange.

A 20 mM ammonium phosphate (pH 3) mobile phase was prepared (see **Section 2.1.3.3**). A 90% ammonium phosphate/ACN mixture was pumped through the column at 1 mL/minute, with 10 μL of each sample being injected onto the column. Neopterin was measured by a fluorescence detector (RF-20Axl, Shimadzu Corporation; Japan) using an excitation of 355 nm and emission of 438 nm. Neopterin typically had a retention time of 4.2 minutes which was confirmed using a neopterin standard. The concentration of neopterin in samples were calculated from the peak size of known standards (50 nM and 25 nM) of neopterin. The concentration of 7,8-NP can be calculated by finding the amount of total pterin in a sample and subtracting the value obtained for neopterin.

2.2.9 ELISA

The IL-1β enzyme-linked immunosorbent assay (ELISA) kit (Invitrogen; New York, USA) was performed according to the manufacturer's instructions. This sandwich assay relies on the target molecule binding to the primary antibody which is present on

the ELISA plate. The addition of the secondary antibody forms the "sandwich" around the target molecule. The presence of the target molecule is quantified by the addition of a luminescent reagent.

A standard curve of IL-1β was prepared by serial dilution from the standard provided. One hundred microliters of each diluted standard was pipetted in the 96-well plate provided. The same volume of non-diluted supernatant from samples was also pipetted into the plate. The standards and samples were then incubated for two hours at room temperature. After this incubation period, the wells were aspirated and the plate was thoroughly washed. Next, the secondary antibody (100 μL) was added to each well and the plate was incubated for one hour. Again, after the incubation period the solution was aspirated and the plate was washed. Finally, 100 μL of the chemiluminescent reagent was added. The plate was read after 30 minutes incubation in the dark. The luminescence was measured on SpectraMax M5 microplate reader (Molecular Devices; California, USA) using a 1000 msec integration time and a five-parameter algorithm to fit the standard curve.

2.2.10 Statistical Analysis

Prism 6.0 (GraphPad Software; California, USA) was used to graph and statistically analyze data. Significance is indicated as follows: $p \leq 0.05$ - *, $p \leq 0.01$ - **, $p \leq 0.001$ - ***, $p \leq 0.0001$. Results in this thesis are presenting data from a single experiment that is representative of three separate experiments unless stated otherwise. All experiments were performed in triplicate (unless otherwise stated). The mean and standard error of the mean (SEM) were calculated from the triplicate data.

3

Culture of Foreign Body Giant Cells

The aim of this chapter is to explore the potential of giant cells as an *in vitro* model of the foreign body response occurring in atherosclerotic plaques due to cholesterol crystals. The experiments in this chapter will analyze whether or not giant cells can be successfully cultured and used as an experimental system. Human monocyte-derived macrophages (HMDMs) are an example of a well documented, established culture system (the history of the discovery and use of macrophages is reviewed in Gordon (2007)). As HMDMs are the progenitor of the giant cell lineage they will act as a comparison throughout this chapter against which giant cell culture can be standardized.

3.1 Introduction

By the late 19th century it was already known that giant cells form by the fusion of individual monocyte or macrophage cells around foreign-bodies as opposed to cell division (Metchnikoff, 1884). There is a strong histological record documenting the

occurrence of giant cells in inflammatory conditions. Unfortunately, whilst *in vivo* and *ex vivo* procedures are well documented, very few *in vitro* methods of culturing giant cells exist. Deriving giant cells from a cell line would produce a highly replicable system. However, previous research has found that monocyte-like cell lines U937 and THP-1 are unable to form giant cells even after 15 days of stimulation with cytokines (Jay et al., 2010). Hence, monocytes isolated from human blood are used in this research.

To complicate matters a number of different factors, commonly referred to as fusion molecules, have been shown to induce fusion. These include but are not limited to: RANKL, M-CSF, interleukin-3 (IL-3), and IFN-γ (Helming and Gordon (2009) provide an extensive review of fusion molecules). Different fusion factors result in varying phenotypes of giant cells (refer to **Section 2.2.4.3**). It is important for this work that the phenotype induced is the foreign-body giant cell as the aim is to model the foreign-body response to cholesterol crystals. IIL-4 and α-TocH were selected as fusion molecules for the experiments in this chapter as they have been shown to induce this phenotype (McNally and Anderson, 2003).

Previous studies have used sub-optimal concentrations for the specific purpose of inducing further fusion with other fusogenic molecules (McNally and Anderson, 1995). In this chapter optimal concentrations of both IL-4 and α-TocH are sought by experimental testing. For the purposes of this thesis, the optimal concentration is determined by the highest number of giant cells formed above the baseline using the smallest quantity of the fusion mediators. This is in part to maintain an economically feasible cell culture system.

Having established an optimal concentration of fusogenic factors, it is important to select a method for obtaining cell viability. No studies of giant cell viability have been

published so two methods measuring different aspects of cell viability were chosen to be tested. MTT reduction and trypan blue exclusion assays are commonly used to assess cell viability. The MTT reduction assay uses the metabolic activity of the cells to determine viability, whereas trypan blue exclusion relies on the fact that intact, healthy cells will exclude the dye but dead or compromised cells will be permeable and stain brightly blue. This chapter will explore the validity of these methods in respect to the measurement of giant cell viability.

Finally, it has been hypothesized that giant cells are capable ingesting cholesterol crystals by endocytosis *in vivo*. However, this has not been tested *in vitro*. This chapter will examine the ability of giant cells to absorb cholesterol crystals compared to HMDM cells. It will also examine the effect of the cholesterol crystals on cell viability using the methods established earlier.

3.2 Results

3.2.1 Identifying Giant Cells

In order for giant cells to be a viable option for cell culture experimentation, they need to be easily distinguished from normal HMDMs. It has been suggested that giant cells can be identified by their cytoplasmic spreading and lamellipodia formation (MacLauchlan et al., 2009).

To test this, human monocytes were cultured for an initial 4 days in RPMI 1640 with 10% HS (as described in **Section 2.2.4.3**). On the fifth day the cells were transferred into SFM and 10 ng/mL of IL-4 and 50 μM α-TocH were added. The cells were then cultured for a further 6 days. The cells were were stained with oil red

O (see **Section 2.2.5**), as it has been shown previously that giant cells contain large lipid droplets (Kosteli et al., 2010). They were then photographed using an inverted light microscope. **Figure 3.1a** shows that staining giant cells with oil red O makes them clearly visible. Giant cells stain heavily for lipid deposits whereas neighboring macrophages do not. This technique allows the giant cells to be quantified. However, a major draw back of this technique is that the cells must be fixed before staining which prevents any further experiments being carried out on the cells.

In fact, most techniques that would allow giant cells to be easily visible in cell culture require the cells to be fixed or cause permanent changes to the cell. It was investigated whether giant cells could be distinguished and quantified without the aid of any dyes, stains, or tags. Fortunately, giant cells possess a distinct morphology from HMDMs. Unstained cells can be identified as shown in **Figure 3.1b** by their distinctive shape, granularity and size. The average size of the giant cell after 10 days in culture is 79.97 μm $\pm$ 4.973 (N=6) compared to 23.5 μm $\pm$ 1.024 (N=6) for HMDM cells (see **Figure 3.2**). As giant cells are significantly larger than macrophages, they can be differentiated from HMDMs based on their size.

As further cytoplasmic spreading takes place giant cells become more difficult to identify (**Figure 3.3a**). After two weeks in culture many cells have lost their macrophage-like morphology and have become exceptionally thin. This thinness makes the cells difficult to identify using bright phase or IMC microscopy as the edges of the cell blend in with the background of the image. Often a giant cell can be most easily identified by an apparent gap surrounded by monocytes. Another microscopy technique, dark phase microscopy, improves the ability to distinguish giant cells from one another but gives poor image clarity (see **Figure 3.3b**). Dark phase microscopy allows the visualization of unstained transparent cells by causing a phase shift which

(a) Oil red O stained giant cell

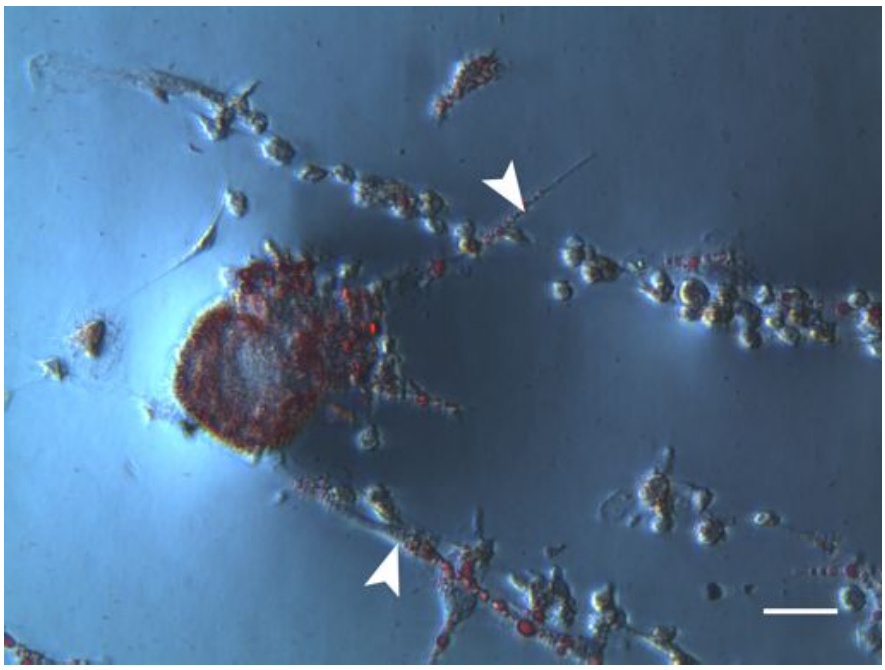

(b) Unstained giant cell

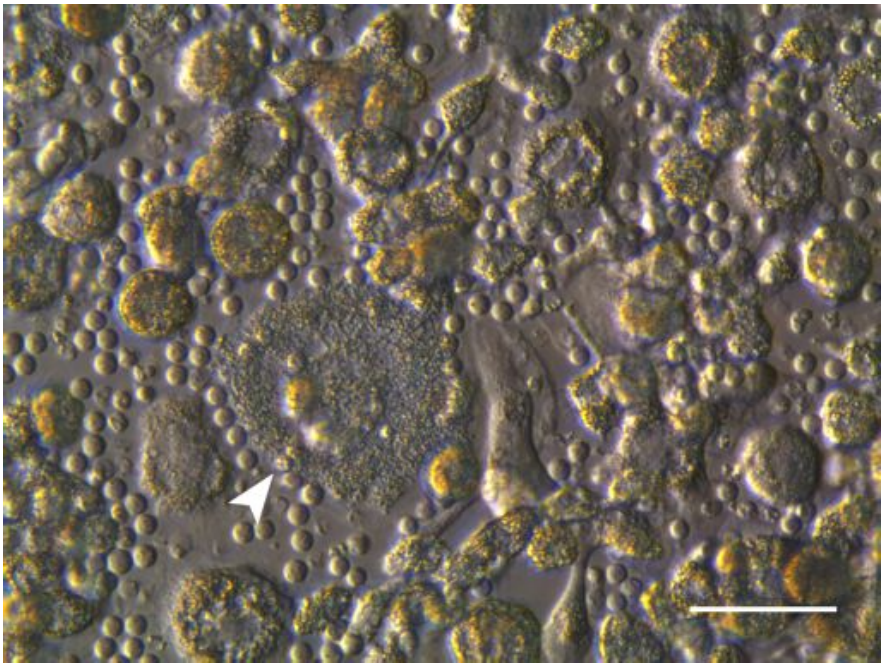

Figure 3.1: Foreign body giant cells in culture. **(a)** The giant cell stained with oil red O is showing lamellipodia formation (indicated by arrowheads) Image was taken at 20x magnification. **(b)** The unstained giant cell, as indicated by the arrowhead, is showing cytoplasmic spreading. Image was taken on an inverted microscope at 40x magnification using IMC. Scale bars represent 50 μm.

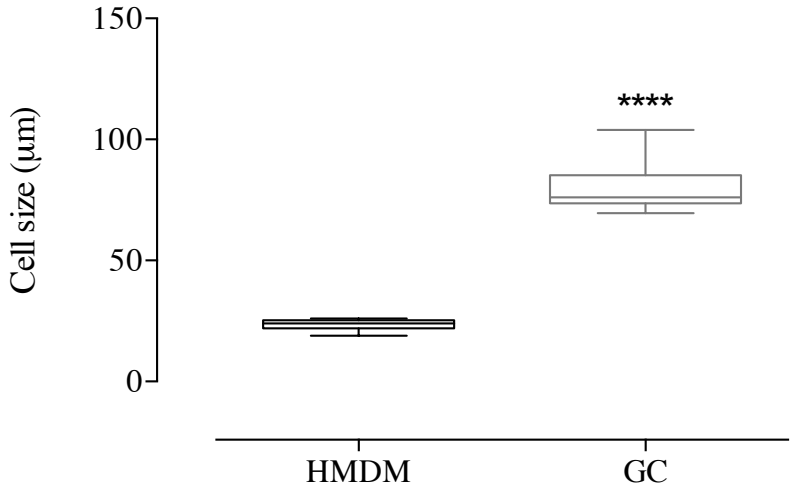

Figure 3.2: Comparison of HMDM and giant cell (GC) size - Cells were cultured for 10 days before having their size measured. The size was calculated using ImageJ software to analyze the diameter of each cell. An average of cell size in two fields of view was calculated per well. Data are from a single experiment that is representative of three independent experiments. Data shown is ± SEM of triplicate measurements. Significance is indicated as follows: $p \leq 0.05$ - *, $p \leq 0.01$ - **, $p \leq 0.001$ - ***, $p \leq 0.0001$.

results in differences in brightness between the background and the object that is being identified. Dark phase microscopy is only appropriate when there is a single layer of cells, which is not always the case in HMDM and giant cell culture.

It seems giant cells can be identified with ease during their early stages of development prior to any significant cytoplasmic spreading. The identification of giant cells after more than two weeks is more complex and most likely would require some type of staining such as with oil red O.

(a) Light microscopy

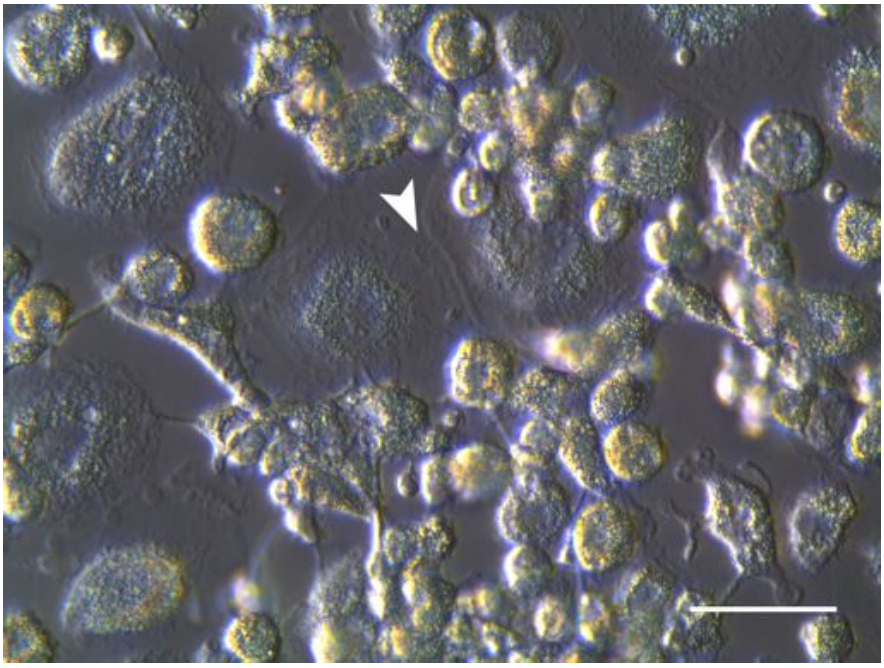

(b) Dark phase microscopy

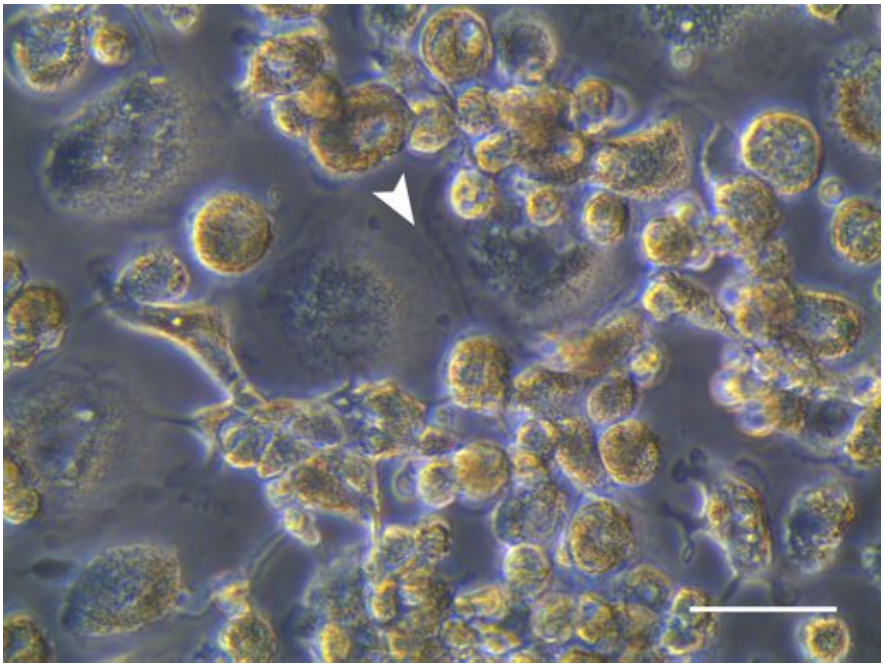

Figure 3.3: Cytoplasmic spreading of foreign body giant cells. **(a)** The boundaries (indicated by the arrowhead) of foreign body giant cells are difficult to distinguish even at high magnification. **(b)** Dark phase microscopy highlights the area and boundaries of giant cells. Images were taken on an inverted microscope at 40x magnification. The scale bar on each image represents 50 μm.

3.2.2 Optimal Interleukin-4 and α-Tocopherol Concentrations to Induce Giant Cell Fusion

Macrophage fusion is difficult to quantify and highly variable from culture to culture. In order to find the optimum concentrations of IL-4 and α-TocH, cells were treated with either IL-4 or α-TocH at a range of concentrations for 7 days. After this time the effect of treatment was examined by microscopy (see **Figure 3.4**). The degree of fusion was determined by calculating the percentage of giant cells present compared to the total number of cells in the particular field of view. As the average size of an HMDM was determined earlier as being 23.5 μm, any cell over 40 μm was designated as a giant cell.

Untreated HMDMs cultured in SFM without the addition of α-TocH or IL-4 showed a baseline fusion of 3.5% (**Table 3.1**). The addition of 10 ng/mL IL-4 resulted in a 1.5 fold increase in fusion over untreated cells. Cells given 15 ng/mL showed a 1.8 fold increase, and those given 20 ng/mL showed a 2 fold increase. Whilst IL-4 alone is capable of inducing a low level of fusion, the rates seen here are not ideal. These results are counter to the available literature which suggests these concentrations of IL-4 should induce much higher rates of fusion.

It has also been proposed that α-TocH can induce giant cell formation by causing PS flipping (Helming et al., 2009; Klein et al., 2006). Cells treated with 25 μM α-TocH showed a 1.9 fold increase in fusion over the control. Treatment with 50 μM and 75 μM resulted in a 3.8 and 4.1 fold increase respectively. Neither IL-4 nor α-TocH alone induced significant amounts of fusion so cells were treated with a combination of both (see **Figure 3.5**). The results of the previous experiment had shown no significant difference between IL-4 concentrations so the experiment was repeated with both 10

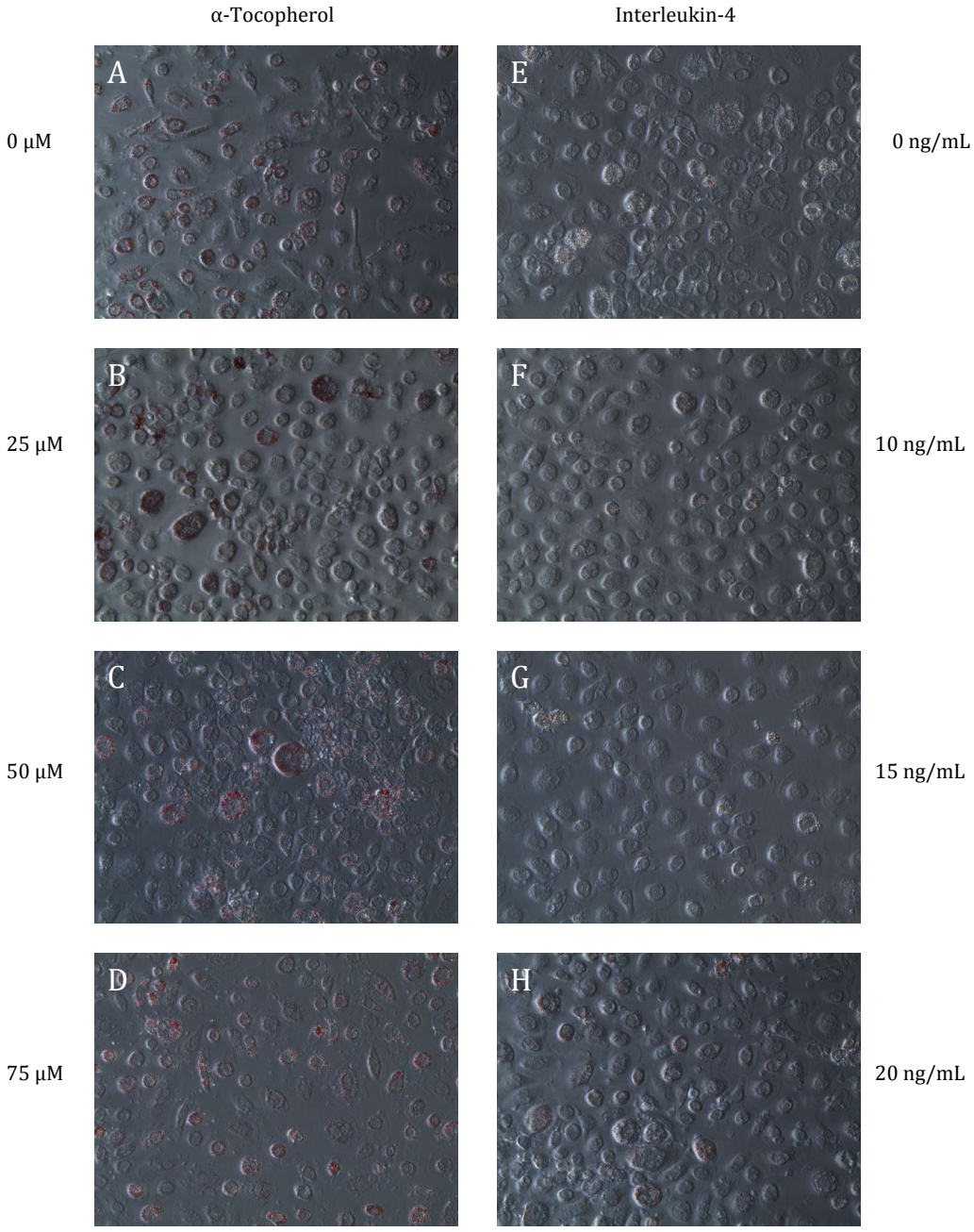

Figure 3.4: Effect of α-tocopherol and IL-4 on giant cell culture - On day 5 of cell culture, α-TocH or IL-4 was added to fresh cell culture media in increasing concentrations. All cells were stained with oil red O to aid in the identification of giant cells. Images are representative of triplicate wells per experimental treatment. The images were taken on an inverted light microscope at 20x magnification.

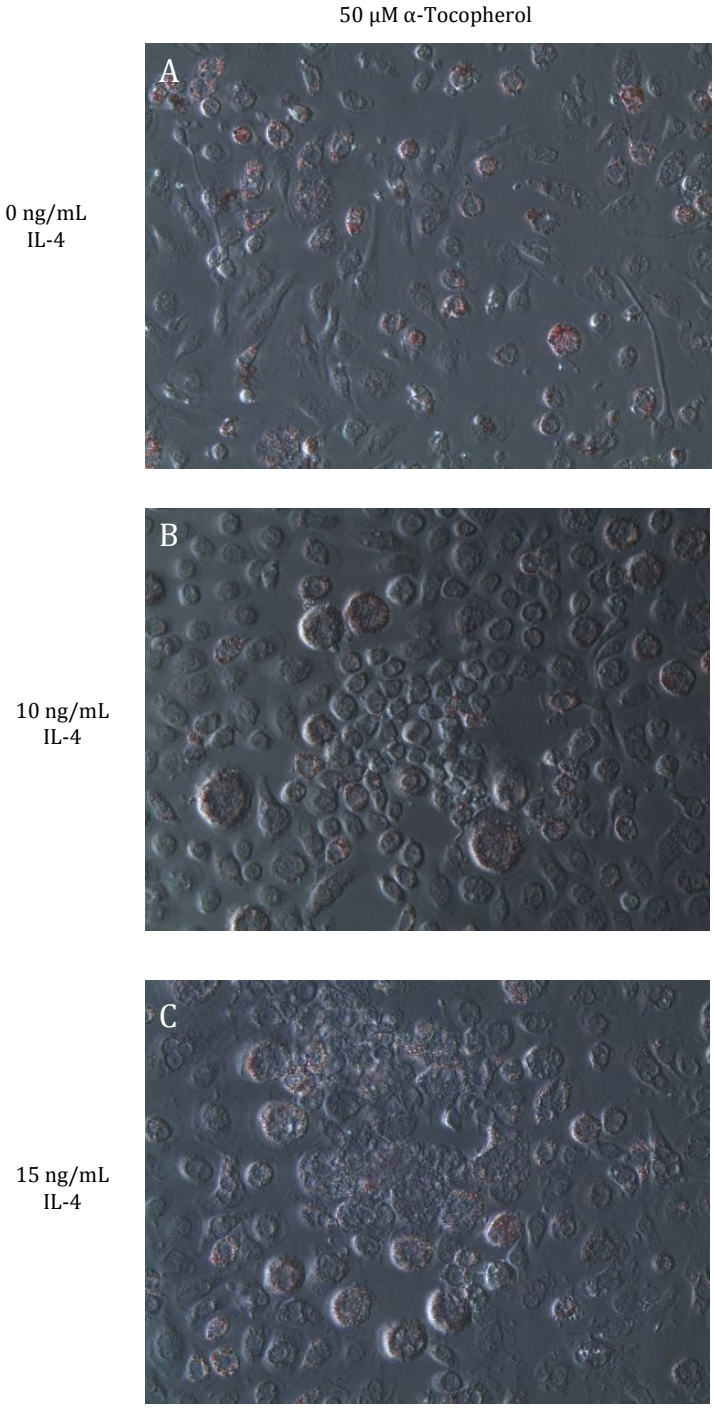

Figure 3.5: Effect of IL-4 on giant cell fusion - All cells were seeded at a concentration of 5 x 10^6 cells/mL and cultured in SFM for 7 days after the addition of the treatment. Control cells were treated with 50 μM α-TocH only. The images were taken on an inverted light microscope at 20x magnification.

and 15 ng/mL of IL-4.

As increasing the concentration of α-TocH from 50 μM to 75 μM showed very little improvement in macrophage fusion the experiment was performed in the presence of 50 μM α-TocH. Increasing the concentration of IL-4 from 10 ng/mL to 15 ng/mL boosted cell fusion by 8.3%. The addition of 50 μM α-TocH and 15 ng/mL IL-4 improved fusion by 25.6% over the cell only control. All experiments from this point onwards were carried out using the optimal concentrations of 15 ng/mL IL-4 and 50 μM α-TocH.

Table 3.1: Maximum percentage of giant cell formation after treatment with α-tocopherol and interleukin-4.

Concentration	**0 μM α-TocH**	**25 μM**	**50 μM**	**75 μM**
0 ng/mL IL-4	3.5%	6.7%	13.3%	14.2%
10 ng/mL	5.4%	-	20.8%	-
15 ng/mL	6.2%	-	29.1%	-
20 ng/mL	7.1%	-	-	-

3.2.3 Measurement of Giant Cell Viability

A thorough literature search has failed to yield any evidence of giant cells being tested for viability. Either this has never been attempted or has never been published. To study the viability of giant cells two common measures of cell viability were used. MTT reduction is a metabolism based assay whereas trypan blue is an exclusion based assay using membrane integrity as its measure. The viability assays were performed on healthy HMDMs and giant cells after two weeks in cell culture.

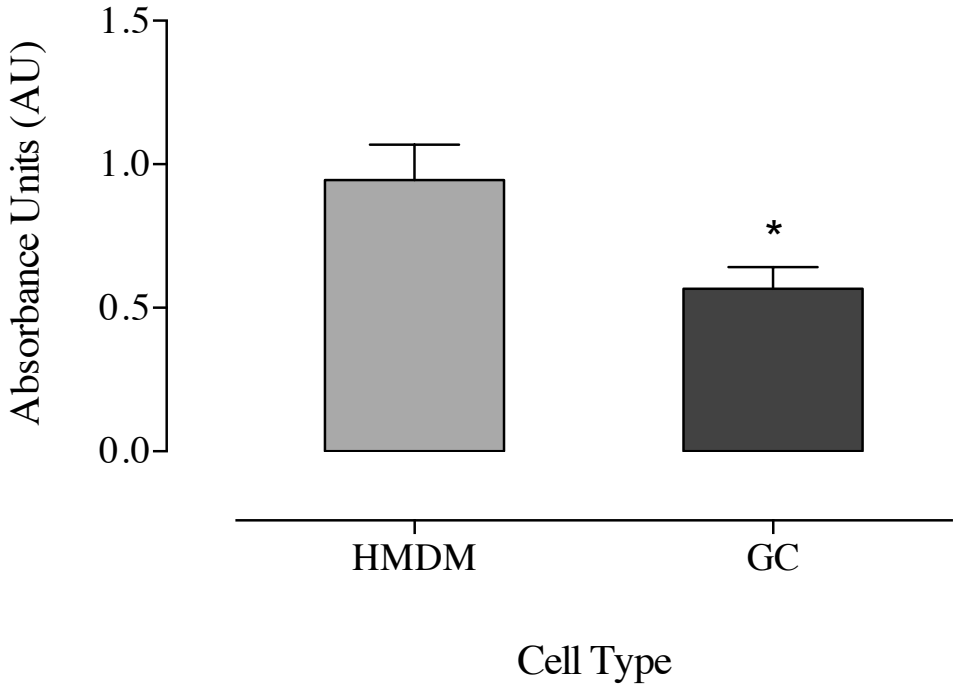

Figure 3.6: Viability of HMDMs and GCs as measured by MTT reduction assay - HMDMs and GCs seeded at 5 x 10^6 cells/mL were incubated for 12 days in RPMI 1640 and SFM respectively. The cells were incubated with MTT for 2 hours prior to absorbance being read. The data in the graph is from four independent experiments performed in triplicate. Data shown is the mean of the means ± SEM. Significance is indicated as follows: $p \leq 0.05$ - *, $p \leq 0.01$ - **, $p \leq 0.001$ - ***, $p \leq 0.0001$.

The cells were incubated with MTT for 2 hours before the cell viability was analyzed by spectroscopy. **Figure 3.6** shows that giant cells have an average absorbance of 0.56 $\pm$ 0.08 AU (N=12) compared to 0.94 $\pm$ 0.12 AU (N=12) for HMDM cells. Untreated cells are expected to fall between 0.75 and 1.25 AU, so that absorbance measurements are made in the linear part of the curve. Seeding 5 x 10^6 cells produced the correct amount of formazan in the HMDM cells but not in the giant cells. This suggests that either fewer cells are present in the giant cell cultures or the giant cells are less capable of metabolizing MTT than HMDMs. If the lack of formazan production was due to a lower number of cells present, then allowing the culture to incubated for longer with the MTT reagent should increase the production of formazan.

To test the ability of giant cells to metabolize MTT, cells were incubated for 2 hours and 24 hours and then photographed. **Figure 3.7a** shows very little production of formazan crystals after 2 hours in the giant cell culture compared to control HMDM cells (**Figure 3.7b**). Even after 24 hours the giant cells still failed to produce formazan crystals (**Figure 3.7c**).

In comparison, cells stained with trypan blue showed close to 98% viability (**Figure 3.8**). There was very little difference between replicates of HMDM cells. There was some variation between replicates of giant cells but the range was much smaller than seen with MTT. Using the trypan blue, there was no significant difference in the average cells per field of view between HMDMs and giant cells (**Figure 3.9**).

These results suggest that MTT is not an appropriate tool for measuring giant cell viability, but trypan blue appears to give a fairly accurate measure of viability. Experiments from this point on involving giant cells and cell viability will use trypan blue.

(a) GCs after 2 hour incubation with MTT

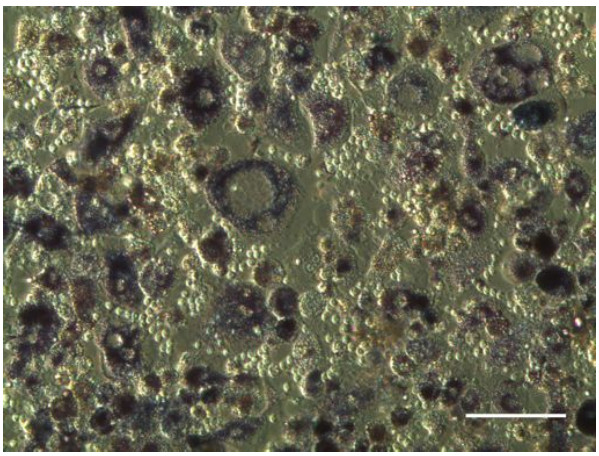

(b) HMDMs after 2 hour incubation with MTT

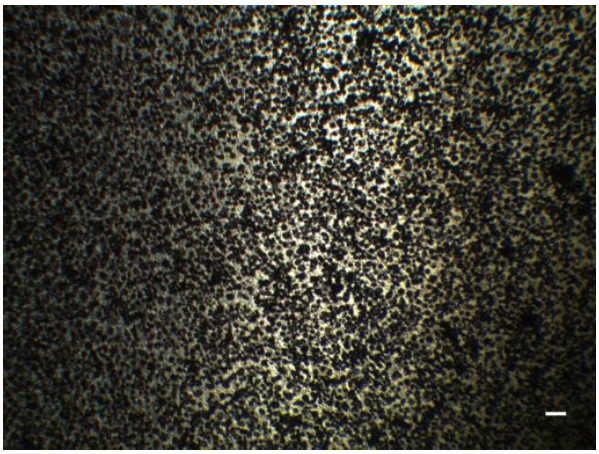

(c) GCs after 24 hour incubation with MTT

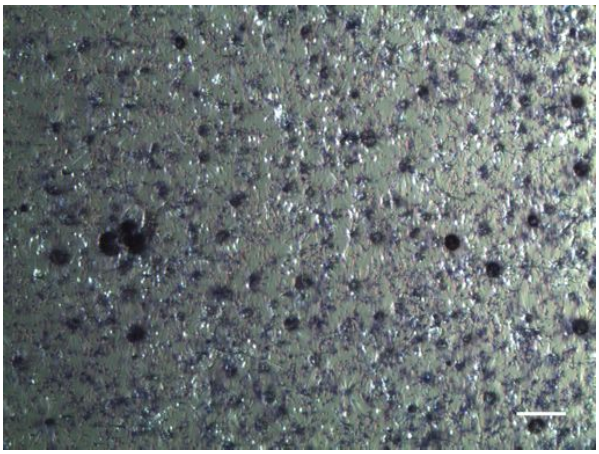

Figure 3.7: Giant cells are unable to produce significant quantities of formazan crystals. HMDMs and GCs seeded at 5 x 10^6 cells/mL were incubated for 12 days in RPMI 1640 and SFM respectively. The cells were incubated with MTT for either 2 or 24 hours. Images were taken on a light microscope. Scale bars represent 100 μm.

(a) Viability of GCs and HMDMs measured by trypan blue exclusion assay

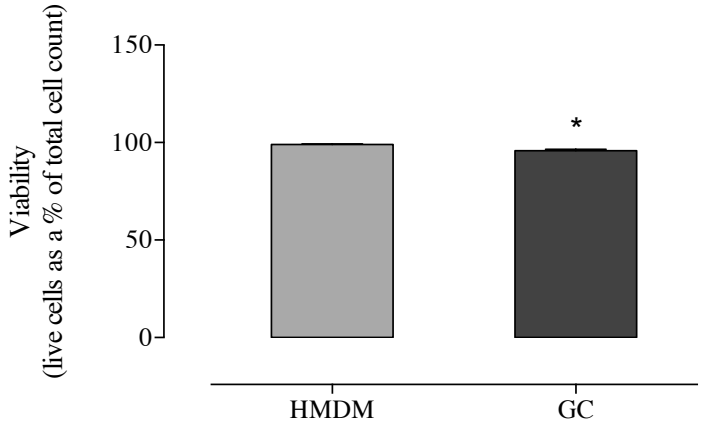

(b) Intraexperimental variation

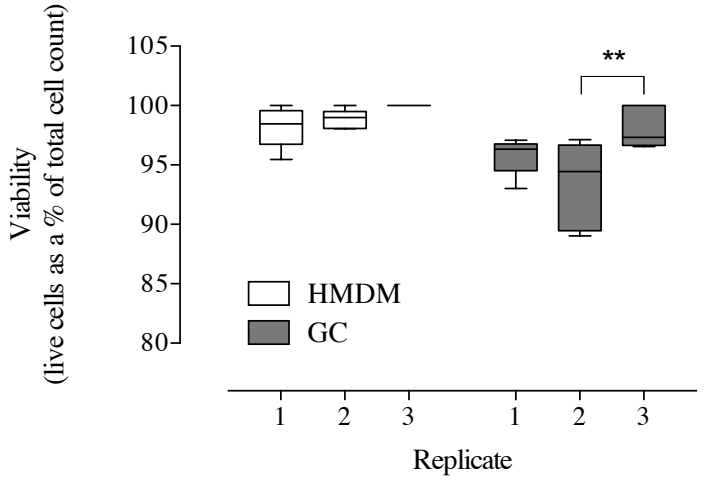

Figure 3.8: Cell viability as measured by trypan blue exclusion assay. HMDMs and GCs seeded at 5 x 10^6 cells/mL were incubated for 12 days in RPMI 1640 and SFM respectively. HMDM and GCs had trypan blue added before being counted on an inverted light microscope with a magnification of 20x. Data are of 5 random images per well. Each treatment was performed in triplicate. Data is from a single experiment that is representative of 3 independent experiments. Data shown is the mean ± SEM of triplicate measurements. Significance is indicated as follows: $p \leq 0.05$ - *, $p \leq 0.01$ - **, $p \leq 0.001$ - ***, $p \leq 0.0001$.

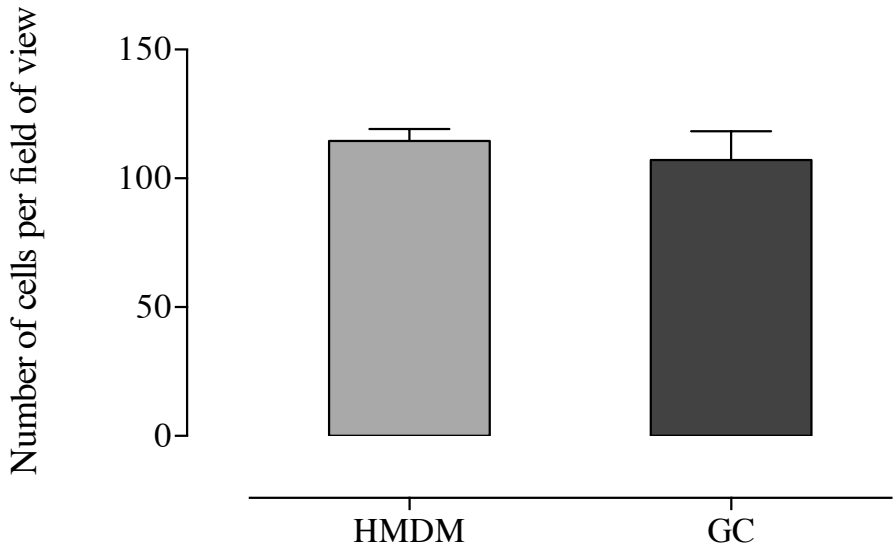

Figure 3.9: Comparison of cell count between HMDMs and GCs - HMDMs and GCs seeded at 5 x 10^6 cells/mL were incubated for 12 days in RPMI 1640 and SFM respectively. HMDM and GCs had trypan blue added before being counted on an inverted light microscope with a magnification of 20x. Data are representative of 5 random images per well. Each treatment was performed in triplicate. Data is from a single experiment that is representative of 3 independent experiments. Data shown is the mean $\pm$ SEM of triplicate measurements. Significance is indicated as follows: $p \leq 0.05$ - *, $p \leq 0.01$ - **, $p \leq 0.001$ - ***, $p \leq 0.0001$.

3.2.4 Formation of Cholesterol Crystals

Foreign body giant cells are thought to form around cholesterol crystals in order to absorb them (Bayliss, 1976; Samokhin et al., 2010). *In vivo*, cholesterol crystals naturally form in areas of extracellular lipid deposits (Bocan et al., 1986). However, nucleation of cholesterol crystals has also been achieved *in vitro* using lipid-laden macrophage foam cells (Tangirala et al., 1994). For experiments in this chapter, cholesterol crystals were produced through the addition of cholesterol to hot ethanol and allowing the mixture to cool (see **section 2.2.6**). Initially the crystals were too large to transfer via a 1000 μL pipette, so the mixture was sonicated to break the crystals into a more manageable size. This had the additional benefit of making the crystals a comparable size to the macrophages.

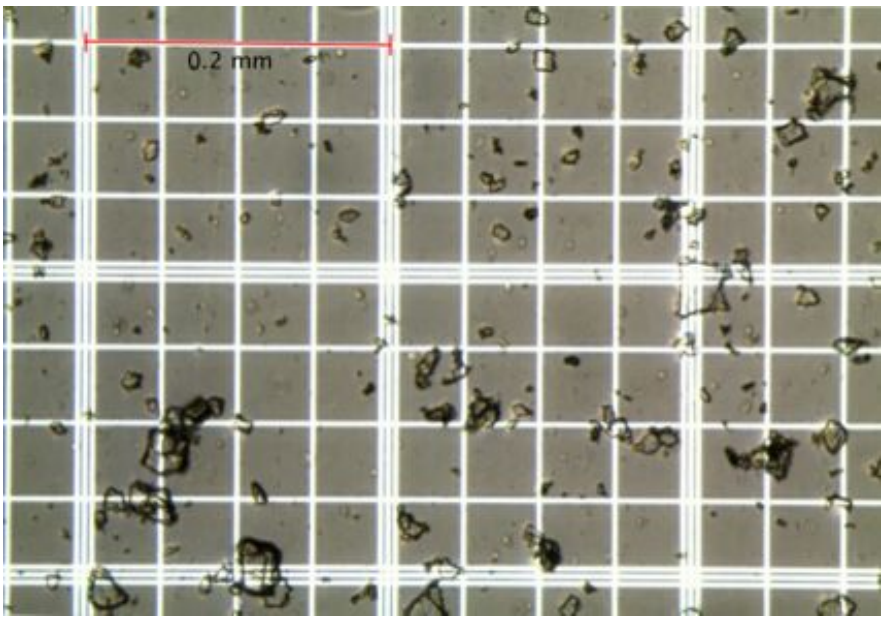

Figure 3.10: Cholesterol crystals - Cholesterol crystals have been sonicated to produce smaller fragments no larger than 50 μm in diameter.

3.2.5 Absorption of Cholesterol Crystals by Cells

It is thought that giant cells are able to actively absorb cholesterol crystals as a means of removing a foreign body. Cholesterol crystals *in vivo* can grow up to 200 μm in size (Moolenaar and Lamers, 1996). Crystals of less than 10 μm can be easily phagocytized by macrophages as they are much smaller than the macrophage itself. To model inefficient cholesterol reabsorption, the majority of crystals had a diameter above 20 μm but no larger than 50 μm. It was not possible to create a uniform cholesterol crystal size with the techniques available, however this diversity in size reflects the *in vivo* development of crystals.

Both HMDMs and giant cells were incubated with 5.0 mg/mL of cholesterol crystals for 7 days to test their ability to absorb the crystals (see **Figure 3.11**). This concentration of cholesterol crystals was chosen as it completely covered the well. HMDMs after 7 days showed some clearance of the cholesterol crystals as can be seen in **Figure 3.11a**. The amount of clearance occurring is difficult to quantify, but using Image J software to highlight the remaining crystals, it was estimated to be around 50%. The same technique applied to giant cells shows cholesterol crystal clearance of approximately 21%. It appears that giant cells cannot metabolize as many cholesterol crystals as HMDMs. This result is in agreement with microscopy and histological data (Friedmann and Graham, 1979). Both giant cells and HMDMs were incubated with cholesterol crystals for a further 7 days to test whether any further crystal absorption occurred (data not shown). It was found that no further absorption occurred.

Incubating cells with cholesterol crystals had little effect on their viability according to measurements made using trypan blue exclusion staining (see **Figure 3.12a**). The viability of giant cells compared to HMDMs was significantly different,

(a) HMDM with cholesterol crystals

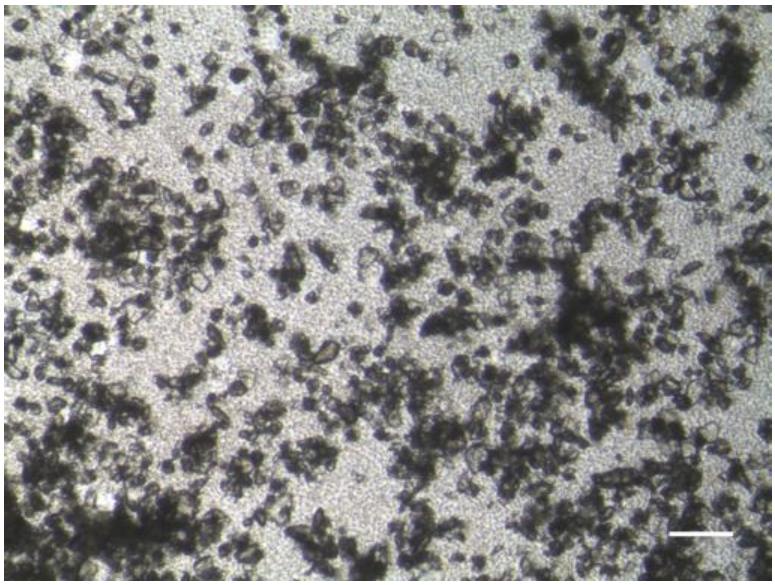

(b) Giant cells with cholesterol crystals

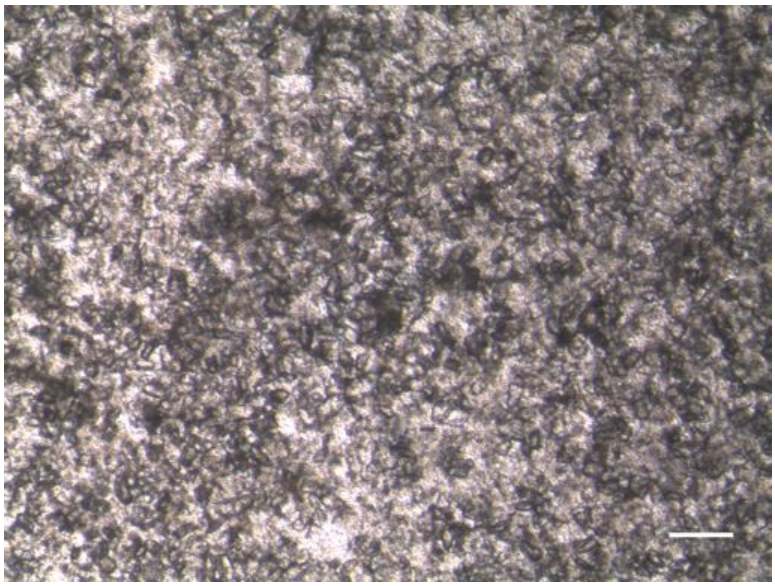

Figure 3.11: Absorption of cholesterol crystals HMDM and GCs - A) HMDMs showing significant absorption of cholesterol crystals after 7 days. B) GCs showing little absorption of cholesterol crystals after 7 days. Images were taken on an inverted microscope at 10x magnification. Scale bar represents 100 μM.

with giant cells having a mean viability of 90.81% ± 1.977 (N=15) compared to 98.46% ± 0.4065 (N=14) for HMDMs. Whilst the difference between HMDMs and giant cells is statistically significant, in terms of a biological system this is a very small percentage cell death.

Viability obtained using trypan blue exclusion staining is calculated by measuring the proportion of live cells in five fields of view in three separate wells for each treatment. It would be expected that each well, or replicate, would produce a similar result to the other two replicates. As expected, HMDM replicates showed very little variation from one another. Giant cell replicates showed much higher intraexperimental variation (see **Figure 3.12b**). Replicate 3 differed significantly from both replicate 1 and 2. Replicate 3 had a mean of 84.04% ± 4.413 (N=5) compared to means of 92.42% ± 1.328 and 95.98% ± 1.001 (N=5) for replicate 1 and 2, respectively. Observing the giant cell culture revealed that the coverage and number of cells present was much less uniform than the HMDM culture. It is also possible that the presence of cholesterol crystals are introducing some of the variability as **Figure 3.8b**, where trypan blue staining was completed in the absence of cholesterol crystals, showed less variability. These factors appear to be influencing the results of the viability assay.

From these results it appears that cholesterol crystals are largely non-toxic to cells *in vitro*. It also appears that the ability of cells to absorb cholesterol crystals is reduced when macrophages are transformed into giant cells.

(a) Effect of cholesterol crystals on viability of HMDM and GCs measured by Trypan blue exclusion assay

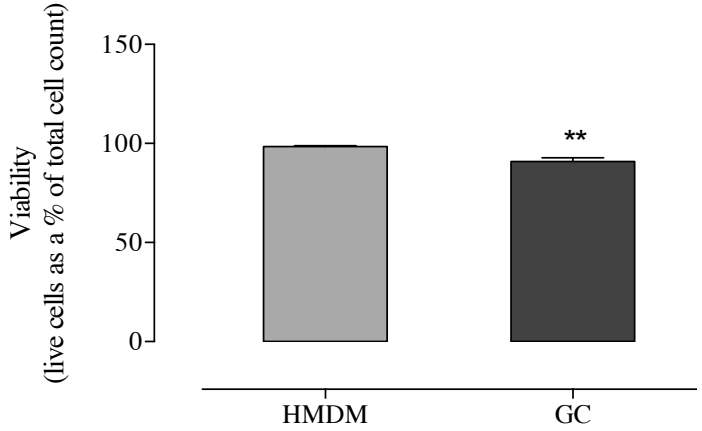

(b) Differences in cell viability between replicates

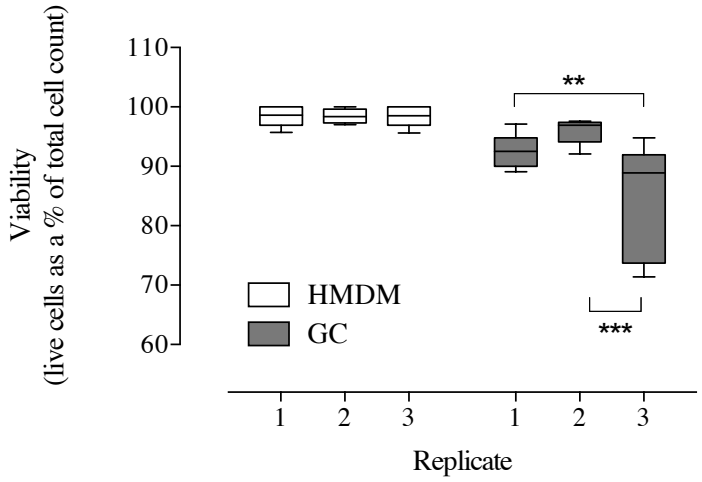

Figure 3.12: Cells remain viable after treatment with cholesterol crystals. HMDMs and GCs seeded at 5 x 10^6 cells/mL were incubated for 12 days in RPMI 1640 and SFM respectively. Cholesterol crystals (1.0 mg/mL in serum free RPMI 1640) were added to the culture on day 13 and the cells were incubated for a further 24 hours. Cell viability was measured by direct addition of trypan blue to the wells. Data are representative of 5 random images per well. Each treatment was performed in triplicate. Data is from a single experiment that is representative of 3 independent experiments. Data shown is the mean $\pm$ SEM. Significance is indicated as follows: $p \leq 0.05$ - *, $p \leq 0.01$ - **, $p \leq 0.001$ - ***, $p \leq 0.0001$.

4

Pterin Production in Monocytes and HMDMs in Response to Cholesterol Crystals

The aim of this chapter is to investigate the effect of cholesterol crystals on neopterin and total pterin production in monocyte and monocyte-derived cells. The experiments in this chapter will explore the effect of cholesterol crystals in the presence and absence of IFN-γ. It will also investigate the production of IL-1β in monocytes and whether pterins have an impact on this production.

4.1 Introduction

There remains some debate as to whether cholesterol crystals are an inflammatory stimulus. Recent research has shown that cholesterol crystals activate the NLP3 inflammasome in a concentration-dependent manner (Duewell et al., 2010). This

chapter will explore the inflammatory nature of cholesterol crystals using a common measure of inflammation, that is, neopterin. Currently, no studies have investigated whether cholesterol crystals are able to induce the production of 7,8-NP and neopterin in monocyte-derived cells. By using IFN-γ, which is known to stimulate pterin production, as a positive control, the ability of cholesterol crystals to modulate the production of pterins can be studied. In **Chapter 3** it was shown that HMDMs and giant cells had different capabilities regarding the absorption of cholesterol crystals. Absorption of the cholesterol crystal appears to be a key element in activating inflammation. As this ability differs between cell phenotypes, it is has yet to be established whether cholesterol crystals can cause different inflammatory responses in different cell types. This chapter will examine the effect of cholesterol crystals on monocytes, HMDMs and mixed culture. Finally, it is known that cholesterol crystals induce IL-1β production through activation of the inflammasome. However, it is not known whether the presence of 7,8-NP has an effect on this production.

4.2 Results

4.2.1 Effect of Cholesterol Crystal Concentration on Pterin Production in HMDMs

HMDMs (1 x 10^6 cells/mL) were incubated with cholesterol crystals for 24 hours to investigate whether there was an effect of cholesterol crystal concentration on the production of intracellular and extracellular pterins. Neopterin is highly fluorescent which means it can be directly measured by HPLC. 7,8-NP, however, does not have the same fluorescent property. The level of 7,8-NP is measured indirectly by oxidizing

the 7,8-NP in the sample to neopterin. After oxidation, the sample contains both the original neopterin as well as the neopterin oxidized from 7,8-NP so it is termed total pterin. The concentration of 7,8-NP in the sample can then be inferred by calculating the difference between neopterin and total pterin.

Cholesterol crystals were observed to have little effect on neopterin production in HMDMs (**Figure 4.1a**). Only 10 mg/mL of cholesterol crystals induced a small rise in intracellular neopterin (0.65 $\pm$ 0.099 pmol per 1 x 10^6 cells compared to 0.60 $\pm$ 0.037 in the control), however, this rise was not statistically or biologically significant. Cholesterol crystals did cause a statistically significant reduction in total pterin at 0.5, 5 and 10 mg/mL. This reduction was not seen at 1 mg/mL of cholesterol crystals.

The presence of cholesterol crystals resulted in less intracellular 7,8-NP production compared to the cell only control (**Figure 4.1b**). It appears that the reduction in intracellular 7,8-NP is significantly correlated with cholesterol crystal concentration (R^2=0.82, p=0.034). This dose-dependent reduction in 7,8-NP occurs with concentrations up to 1 mg/mL of cholesterol crystals in the extracellular fraction (see **Figure 4.2**). At concentrations above 5 mg/mL the amount of 7,8-NP produced appears to plateau. Due to this semi-biphasic response, the cholesterol crystal concentration does not explain the variation in extracellular 7,8-NP levels with R^2=0.001, p=0.956. It was suggested that cholesterol crystals may have a direct interaction with extracellular neopterin or 7,8-NP. Cholesterol crystals were incubated with neopterin and 7,8-NP in a cell free environment in order to establish whether cholesterol crystals could modify pterin levels by direct interaction in the absence of cells. It was confirmed that cholesterol crystals had no impact on neopterin or 7,8-NP concentrations in a cell free environment (data not shown).

From the results indicated in **Figures 4.1 & 4.2**, 5 mg/mL of cholesterol crystals

was selected for use in all further experiments. Incubating cells with 5 mg/mL produced minimal intraexperimental variation and had a consistent effect on both the intracellular and extracellular production of pterins. Other experiments found that this concentration also gave the least variability in terms of cell viability (data not shown). The levels of pterins produced in these experiments were at the limits of detection for the HPLC, so future experiments were carried out with a higher concentration of cells (5 x 10^6 cells/mL) which produces a stronger signal on the HPLC chromatograph. It was interesting that there was less neopterin and total pterin produced by cells incubated with cholesterol crystals. The cholesterol crystals appear to be having a inhibitory effect on pterin levels. To further investigate this, cells were incubated with both cholesterol crystals and IFN-γ, to stimulate GTPCH-1, the enzyme that converts GTP to the precursor of 7,8-NP and neopterin (**Section 4.2.2**).

(a) Intracellular neopterin and total pterin production after 24 hours in HMDMs

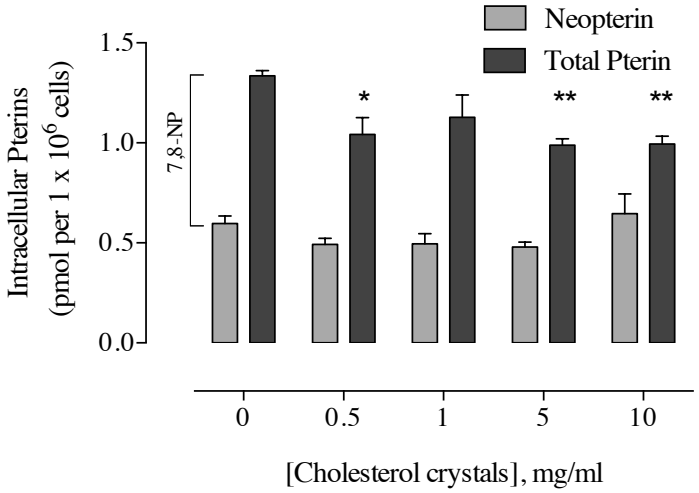

(b) Intracellular 7,8-NP production after 24 hours in HMDMs

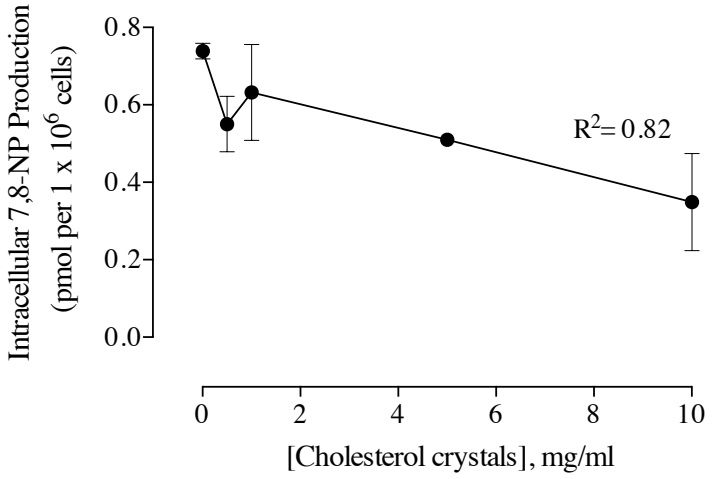

Figure 4.1: Effect of cholesterol crystal concentration on intracellular pterin production in HMDMs. HMDMs (1 x 10^6 cells/mL) were incubated for 24 hours with increasing concentrations of cholesterol crystals. Neopterin and total pterin were measured by HPLC analysis. The graphs are of data from a single experiment that is representative of three separate experiments. Data are mean values ± SEM of triplicate measurements. Statistical significance is calculated compared to control values. Significance is indicated as follows: $p \leq 0.05$ - *, $p \leq 0.01$ - **, $p \leq 0.001$ - ***, $p \leq 0.0001$.

(a) Extracellular neopterin and total pterin production after 24 hours in HMDMs

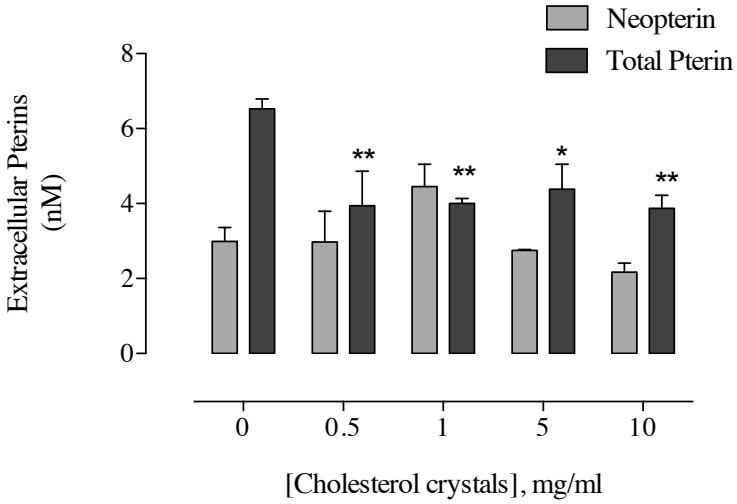

(b) Extracellular 7,8-NP production after 24 hours in HMDMs

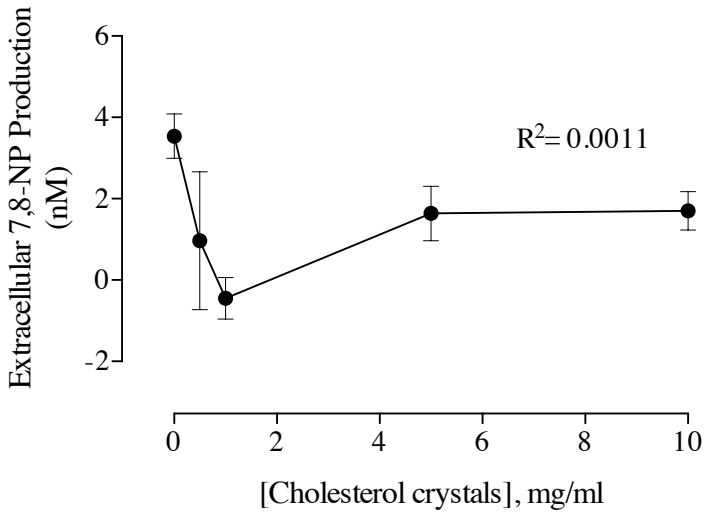

Figure 4.2: Effect of cholesterol crystal concentration on extracellular pterin production in HMDMs. HMDMs (1 x 10^6 cells/mL) were incubated for 24 hours with increasing concentrations of cholesterol crystals. Neopterin and total pterin was measured by HPLC analysis. The graphs are of data from a single experiment that is representative of three separate experiments. Data are mean values ± SEM of triplicate measurements. Statistical significance is calculated compared to control values. Significance is indicated as follows: $p \leq 0.05$ - *, $p \leq 0.01$ - **, $p \leq 0.001$ - ***, $p \leq 0.0001$.

4.2.2 Pterin Production After 24 hours of Incubation with Cholesterol Crystals

It is hypothesized that cholesterol crystals may be able to induce pterin production in macrophages, as it is thought that cholesterol crystal are an inflammatory stimulus, and that macrophages are involved in the clearance of these crystals. Compared to other processes occurring in the body, pterin production is rather slow as it is modulated at the gene expression level (Katusic et al., 1998). It was decided that pterin production would be analyzed after 24 hours as studies by Huber (1984) have shown that HMDMs begin to produce 7,8-NP and neopterin after this time.

4.2.2.1 HMDMs

From previous experiments (**Figure 3.12**), it was already known that cholesterol crystals are non-toxic to cells. To investigate the potential toxicity of IFN-γ a cell viability assay was used which quantified the proportion of live cells prior to sample preparation for HPLC. This was carried out to make sure cell death due to any of the treatments was not confounding the results. Prestoblue, a resazurin-based cell permeable solution, was chosen as the reagent for the cell viability assay for all pterin experiments as it has several advantages over MTT and trypan blue. Not only is prestoblue a much faster assay procedure than MTT, but also the assay leaves cells viable for further experimentation, unlike both MTT and trypan blue. The prestoblue does not interfere with the HPLC as it fluoresces at an excitation of 544 nm and emission of 590 nm whereas neopterin is excited at 353 nm and emits at 438 nm (Demel et al., 2001). HMDMs were incubated with the treatments for 24 hours, after which remaining cell viability was measured. Cell viability is presented as

a percentage viability remaining compared to control HMDMs in RPMI 1640 only which are adjusted to 100%. **Figure 4.3** reveals that there is no viability loss associated with any of the treatments. Cells treated with cholesterol crystals (CHC), either alone or in the presence of IFN-γ, show a slight increase in viability compared to the control. The viability of HMDMs treated with both IFN-γ and cholesterol crystals is 124.6% $\pm$ 3.4, approximately 25% higher than the control. HMDMs treated with cholesterol crystals alone have 110.0% $\pm$ 10.7 viability, but this 10% increase was not significant.

Table 4.1: Experimental set up for HMDM pterin measurement

	Control	IFN-γ	IFN-γ + CHC	CHC
10,000 U/mL IFN-γ	0 μL	10 μL	10 μL	0 μL
10 mg/mL CHC	0 μL	0 μL	500 μL	500 μL
RPMI 1640	1000 μL	990 μL	490 μL	500 μL
Total	1000 μL	1000 μL	1000 μL	1000 μL

Having established that all of the treatments were non-toxic to HMDMs, pterin production was measured. All pterin experiments with HMDMs in this chapter follow the experimental set up detailed in **Table 4.1**. In these experiments, HMDM cells, incubated in RPMI 1640 only, are the negative control. HMDMs stimulated with IFN-γ only act as the positive control. IFN-γ is known to induce 7,8-NP production in a dose-dependent manner by upregulating GTPCH-1 mRNA, the enzyme that converts GTP to 7,8-NP-PPP as discussed in **Section 1.8**. It has previously been shown that 100 U/mL of IFN-γ is sufficient to induce 7,8-NP production in monocyte-derived cells (Wirleitner et al., 2002). Interestingly, HMDMs incubated with 100 U/mL IFN-γ

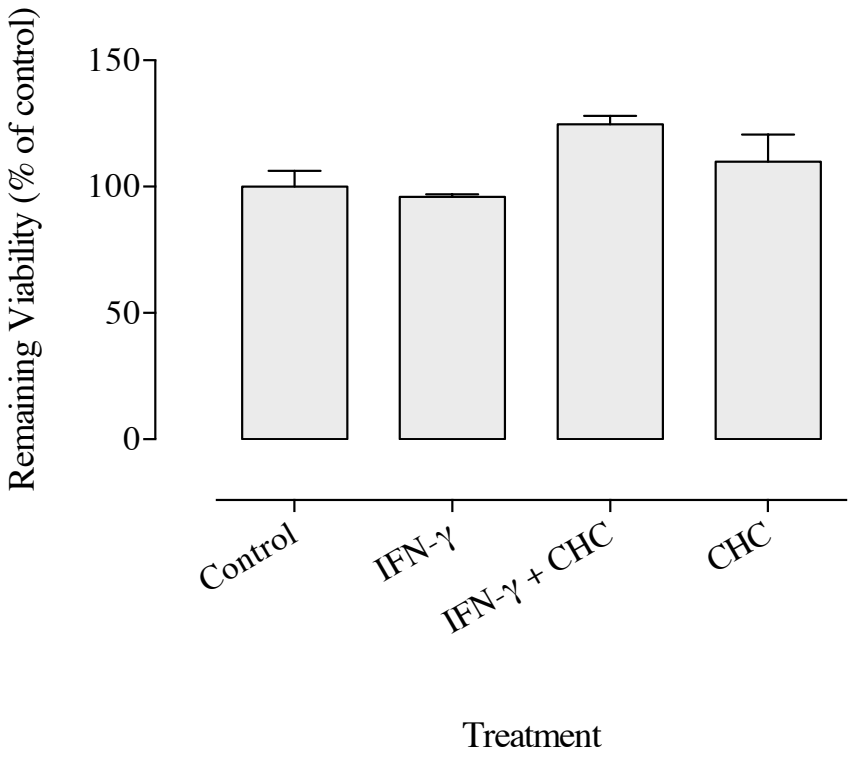

Figure 4.3: HMDM cell viability after 24 hours - HMDMs (5 x 10^6 cells/mL) were incubated at 37 °C in RPMI 1640 with 5 mg/mL of cholesterol crystals and 100 U/mL IFN-γ for 24 hours. Controls were conducted in the absence of cholesterol crystals and IFN-γ. HMDMs were analyzed for remaining cell viability using PrestoBlue. The graphs are of data from a single experiment that is representative of three separate experiments. Data are mean values $\pm$ SEM of triplicate measurements. Statistical significance is calculated compared to control values. Significance is indicated as follows: $p \leq 0.05$ - *, $p \leq 0.01$ - **, $p \leq 0.001$ - ***, $p \leq 0.0001$.

failed to show any significant neopterin or 7,8-NP production above the levels shown by the control either intracellularly or extracellularly (**Figure 4.4**). The intracellular control produced 1.5 pmol per 5 x 10^6 cells of 7,8-NP whereas cells treated with IFN-γ only produced 0.1 pmol per 5 x 10^6 cells. This is somewhat unusual at the IFN-γ treatment would be expected to have the same level of 7,8-NP, if not more, than the amount in the control. As the amount of total pterin produced is the same in both treatments, it appears that the 7,8-NP produced in the IFN-γ treatment has been oxidized to neopterin. In the supernatant, HMDMs incubated with IFN-γ produced 16.5 nM of 7,8-NP compared to 14.6 nM in the control. This slight increase in 7,8-NP production is not statistically significant. In essence, the addition of 100 U/mL IFN-γ had no effect on pterin production in HMDM cells over 24 hours. However, HMDMs treated with both IFN-γ and cholesterol crystals showed higher intracellular production of 7,8-NP (10.3 pmol per 5 x 10^6 cells compared to 1.5 pmol per 5 x 10^6 cells in the control). HMDMs incubated with only cholesterol crystals also produced more 7,8-NP than the control (9.5 pmol). It appears that the introduction of cholesterol crystals either by itself or in the presence of IFN-γ has elicited an inflammatory response from HMDM cells. Whilst treatments containing cholesterol crystals showed higher 7,8-NP production, neopterin levels in these samples were lower than the control (8.2 pmol per 5 x 10^6 cells in the control, 2.8 pmol for cells incubated with a combination of IFN-γ and cholesterol crystals, and 5.7 pmol per 5 x 10^6 cells for cells incubated with cholesterol crystals alone). Cholesterol crystals appear to not only modulate the balance of 7,8-NP/neopterin, which suggests an oxidative stress, but also increase the total level of pterin production in the cell, indicating inflammation.

The extracellular fraction has a very similar pattern of neopterin and 7,8-NP production to the intracellular fraction. One notable difference is that neopterin levels

in the cholesterol crystal containing samples are higher than in the control (34.3 nM in the IFN-γ and cholesterol crystal sample, and 29.5 nM in the cholesterol crystal sample compared to 9.5 nM in the control sample). HMDMs treated with cholesterol crystals produced the most 7,8-NP (27.1 nM) whereas the control cells produced the least (14.6 nM). Cells treated with IFN-γ and a combination of IFN-γ and cholesterol crystals produced 16.5 nM cells and 24.5 nM, respectively.

It is clear from these results that 100 U/mL of IFN-γ is not enough to induce significant 7,8-NP or neopterin production in HMDM cells over 24 hours.

(a) Intracellular NP and Total Pterin in HMDMs after 24 hours

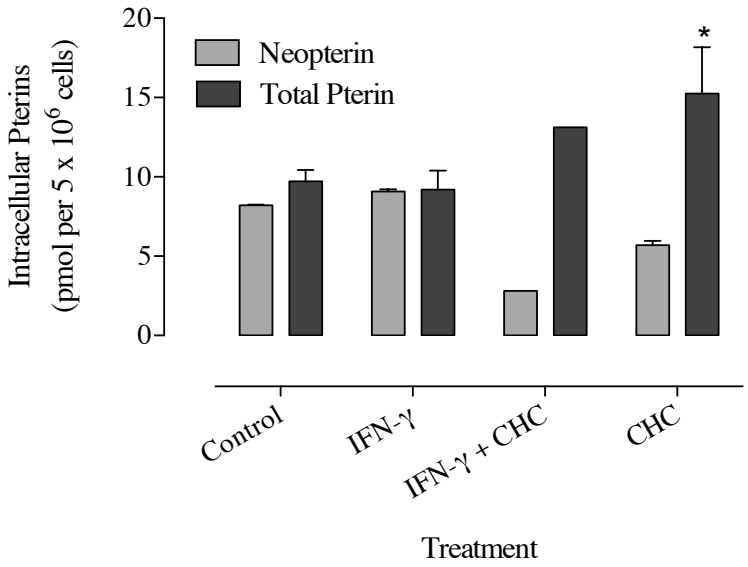

(b) Extracellular NP and Total Pterin in HMDMs after 24 hours

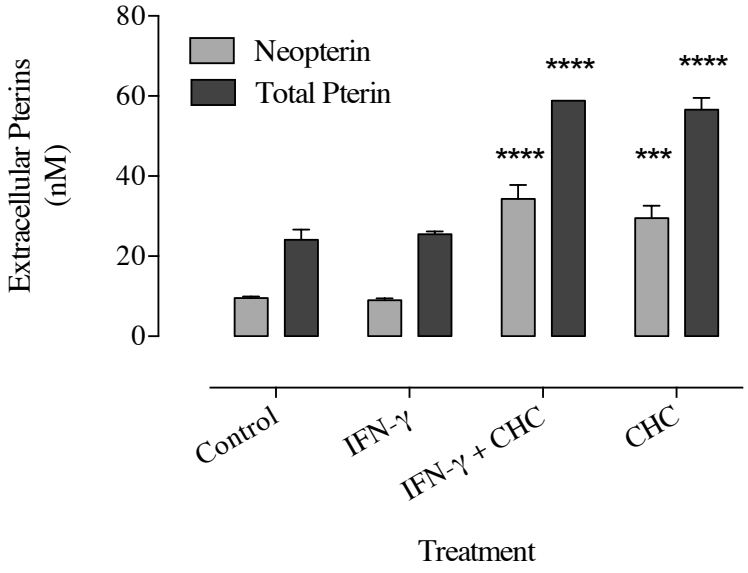

Figure 4.4: Neopterin and Total Pterin measurements in HMDMs after 24 hours. HMDMs (5 x 10^6 cells/mL) were incubated at 37 °C in RPMI 1640 with 5 mg/mL of cholesterol crystals and 100 U/mL IFN-γ for 24 hours. Controls were conducted in the absence of cholesterol crystals and IFN-γ. HMDMs were analyzed for neopterin and total pterin (7,8-NP and neopterin) production by HPLC analysis. The graphs are of data from a single experiment that is representative of three separate experiments. Data are mean values $\pm$ SEM of triplicate measurements. Statistical significance is calculated compared to control values. Significance is indicated as follows: $p \leq 0.05$ - *, $p \leq 0.01$ - **, $p \leq 0.001$ - ***, $p \leq 0.0001$.

4.2.2.2 Monocytes

It is hypothesized that cholesterol crystals may modulate pterin production in monocytes as monocytes are the initial cells that infiltrate the site of inflammation. For the same reasons as outlined in **Section 4.2.2.1**, a viability assay was conducted prior to HPLC analysis. The prestoblue viability assay (**Figure 4.5**) showed that there was no viability loss due to experimental conditions or the cholesterol crystals. Again one of the treatments shows a slight rise in viability. Monocytes treated with IFN-γ have 122.7% $\pm$ 4.77 viability compared to the control (100% $\pm$ 8.38). The other treatments resulted in a 5 to 10% increase in viability over controls, which was not significant.

The experimental set up for all pterin experiments using monocytes is outlined below in **Table 4.2**. Monocytes were incubated with the treatments for 24 hours before neopterin and total pterin levels were measured both in the supernatant and cellular fractions. Intracellularly, monocytes failed to produce any detectable levels of 7,8-NP in the control (**Figure 4.6**). All pterin produced in the intracellular control was in the form of neopterin (3.5 pmol per 5 x 10^6 cells). Monocytes treated with cholesterol crystals also failed to induce 7,8-NP production. It appears that cholesterol crystals have had no effect on monocytes as neither 7,8-NP nor neopterin production is significantly different from the control. By comparison, cells incubated with IFN-γ alone produced 4.96 pmol per 5 x 10^6 cells of 7,8-NP and cells with IFN-γ plus cholesterol crystals produced 8.25 pmol per 5 x 10^6 cells. It appears that cholesterol crystals have a small intracellular effect on monocytes that occurs only in the presence of IFN-γ. IFN-γ and cholesterol crystals appear to act synergistically, producing both more 7,8-NP and neopterin than shown by either treatment alone. From the intracellular results, it also seems that monocytes are more sensitive to IFN-γ than

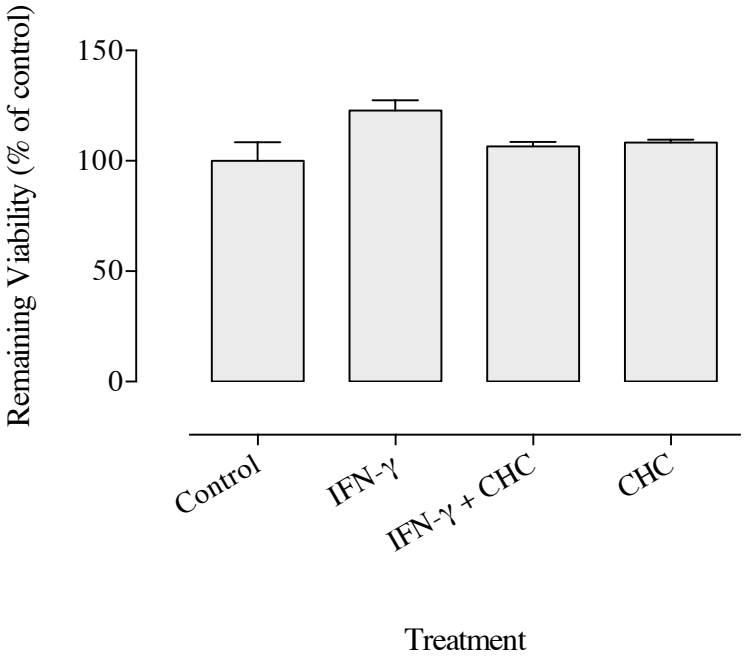

Figure 4.5: Monocyte cell viability after 24 hours - Monocytes were incubated at 37 °C in RPMI 1640 with 5 mg/mL of cholesterol crystals and 100 U/mL IFN-γ for 24 hours. Controls were conducted in the absence of cholesterol crystals and IFN-γ. Monocytes were analyzed for remaining cell viability using PrestoBlue. The graphs are of data from a single experiment that is representative of three separate experiments. Data are mean values $\pm$ SEM of triplicate measurements. Statistical significance is calculated compared to control values. Significance is indicated as follows: $p \leq 0.05$ - *, $p \leq 0.01$ - **, $p \leq 0.001$ - ***, $p \leq 0.0001$.

Table 4.2: Experimental set up for monocyte pterin measurement

	Control	IFN-γ	IFN-γ + CHC	CHC
10,000 U/mL IFN-γ	0 μL	10 μL	10 μL	0 μL
10 mg/mL CHC	0 μL	0 μL	500 μL	500 μL
10 x 10^6 cells /mL	500 μL	500 μL	500 μL	500 μL
RPMI 1640	510 μL	500 μL	0 μL	10 μL
Total	1010 μL	1010 μL	1010 μL	1010 μL

HMDMs, as there is a small increase in 7,8-NP production upon stimulation with IFN-γ that is not seen with HMDM cells.

All treatments resulted in significant 7,8-NP production in the extracellular fraction. This suggests that the intracellular and extracellular processes that are occurring operate quite differently from one another. Cholesterol crystals alone produced the highest amount of 7,8-NP at 49.5 nM, followed by IFN-γ with cholesterol crystals (36.0 nM). It seems plausible that the cell may benefit from maintaining different levels of neopterin and 7,8-NP inside the cell to outside the cell when cholesterol crystals are present. Treatment with IFN-γ resulted in 20.6 nM 7,8-NP which is significantly higher than the 3.9 nM produced by the control. This is not as high as expected in cells stimulated with IFN-γ. There was no significant difference in neopterin levels in the intracellular fraction, however, in the extracellular fraction both treatments containing cholesterol crystals produced significantly more neopterin than the control. Incubating monocytes with IFN-γ and cholesterol crystals produced the most neopterin (43.25 $\pm$ 1.25 nM). Cells treated with cholesterol crystals only

produced 32.89 $\pm$ 0.92 nM. This is more than twice that found in the control (12.00 $\pm$ 3.10 nM). It appears that cholesterol crystals are capable of inducing pterin production in monocytes as hypothesized, and that this induction can be increased in the presence of IFN-γ.

(a) Intracellular NP and Total Pterin in monocytes after 24 hours

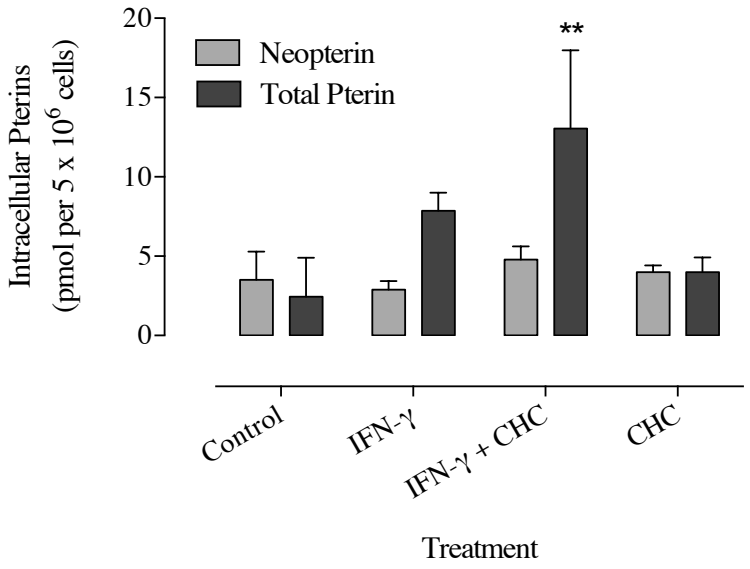

(b) Extracellular NP and Total Pterin in monocytes after 24 hours

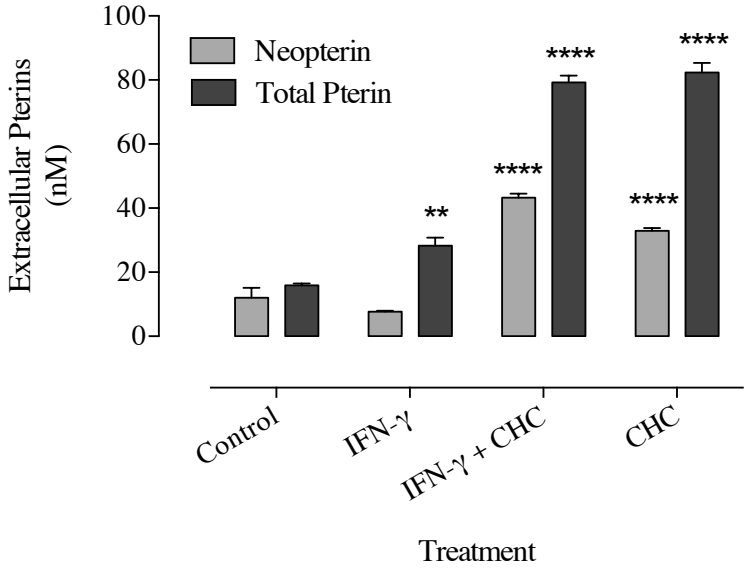

Figure 4.6: Neopterin and Total Pterin measurements in monocytes after 24 hours - Monocytes (5 x 10^6 cells/mL) were incubated at 37 °C in RPMI 1640 with 5 mg/mL of cholesterol crystals and 100 U/mL IFN-γ for 24 hours. Controls were conducted in the absence of cholesterol crystals and IFN-γ. Monocytes were analyzed for neopterin and total pterin (7,8-NP and neopterin) production by HPLC analysis. The graphs are of data from a single experiment that is representative of three separate experiments. Data are mean values $\pm$ SEM of triplicate measurements. Statistical significance is calculated compared to control values. Significance is indicated as follows: $p \leq 0.05$ - *, $p \leq 0.01$ - **, $p \leq 0.001$ - ***, $p \leq 0.0001$.

As stated earlier, 100 U/mL of IFN-γ did not induce the expected rise in 7,8-NP and neopterin levels in either monocytes or HMDMs. To counteract this, the concentration of IFN-γ was increased to 250 U/mL. Experiments at the new concentration of 250 U/mL were only carried out on monocytes as results from Firth et al. (2008) showed that raising the concentration of IFN-γ to 500 U/mL had little effect on 7,8-NP production in HMDMs. **Figure 4.7** shows the range and average neopterin and total pterin production of monocytes after 24 hours across 5 separate experiments. The results from these experiments show that increasing the concentration of IFN-γ to 250 U/mL successfully induced the production of 7,8-NP in monocytes. It was noted during these experiments that whilst the trend of neopterin and total pterin production was the same, the actual amount of pterin produced were quite variable. Control cells had very consistent neopterin production which ranged between 13.2 and 19.4 nM for the 5 experiments. The total pterin produced in the control was slightly more variable (22.4 - 86.3 nM, median= 32.0 nM). Neopterin for all of the treatments ranged significantly. This suggests that the variation is not an innate artifact due to the cells, but is probably due to the experimental treatments or donor specific variables. Cells treated with IFN-γ produced anywhere between 92 and 382 nM of neopterin. After incubation with IFN-γ and cholesterol crystals, a range of 27 to 220 nM of neopterin was produced. Cells incubated with cholesterol crystals only had a smaller range of 13.68 to 45.96 nM of neopterin. It appears that the response to IFN-γ induces the most variation which may be due to modulation in signal transduction in different batches of cells.

Figure 4.8 shows the 7,8-NP concentrations produced across the five replicate experiments. From observation, it seemed that cells that had a higher baseline production of 7,8-NP where the ones that produced higher levels in the treatments,

almost as if they were already primed. This may partially explain why the amount of 7,8-NP is relatively variable across the experiments. Cells treated with cholesterol crystals and IFN-γ produced the largest range of 7,8-NP concentrations (30 - 232 nM) where as control cells produced the smallest (9.2 - 69.2 nM). Monocytes incubated with either cholesterol crystals alone or IFN-γ alone were also highly variable (14 - 156 nM and 127 - 315 nM respectively). While this variation between experiments is interesting to note, the fact that the overarch trends of 7,8-NP production are consistent suggests that this variation may be due to the use of primary cells from different donors, which may respond to treatments differently. As controls across all of the experiments are consistent, it would suggest that this is a real cellular effect and not an experimental artifact.

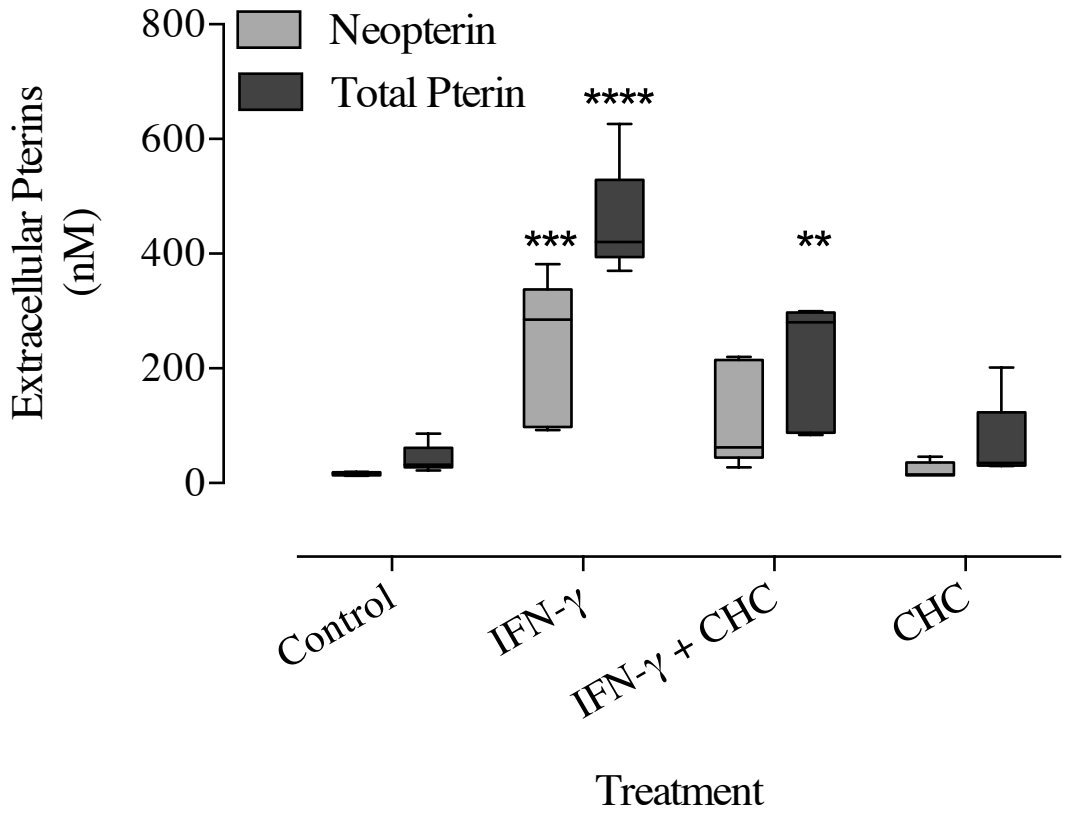

Figure 4.7: Range and average extracellular pterin production - Monocytes (5 x 10^6 cells/mL) were incubated at 37 °C in RPMI 1640 with 5 mg/mL of cholesterol crystals and 250 U/mL IFN-γ for 24 hours. Controls were conducted in the absence of cholesterol crystals and IFN-γ. Monocytes were analyzed for neopterin and total pterin (7,8-NP and neopterin) production by HPLC analysis. The graph is of data from five independent experiments. Data are the mean and range from the five experiments. Statistical significance is calculated compared to control values. Significance is indicated as follows: $p \leq 0.05$ - *, $p \leq 0.01$ - **, $p \leq 0.001$ - ***, $p \leq 0.0001$.

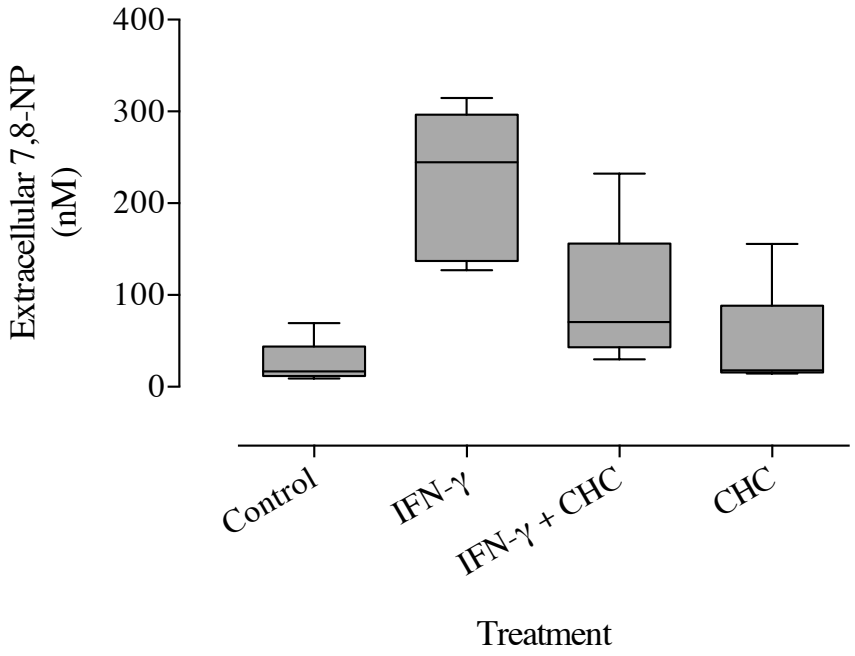

Figure 4.8: Average 7,8-NP production - Monocytes (5 x 10^6 cells/mL) were incubated at 37 °C in RPMI 1640 with 5 mg/mL of cholesterol crystals and 250 U/mL IFN-γ for 24 hours. Controls were conducted in the absence of cholesterol crystals and IFN-γ. Monocytes were analyzed for neopterin and total pterin (7,8-NP and neopterin) production by HPLC analysis. The graph is of data from five independent experiments. Data are the mean and range from the five experiments. Statistical significance is calculated compared to control values. Significance is indicated as follows: $p \leq 0.05$ - *, $p \leq 0.01$ - **, $p \leq 0.001$ - ***, $p \leq 0.0001$.

4.2.3 Pterin Production after 48 hours of Incubation with Cholesterol Crystals

4.2.3.1 Monocytes

Literature results have suggested that monocytes produce their maximal pterin levels after 48 hours (Bitterlich et al., 1988). To investigate whether the IFN-γ and cholesterol crystals have the same effect on the production of 7,8-NP and neopterin with a longer incubation, monocytes were left in the treatments for a further 24 hours. Monocytes showed significantly higher production of both neopterin and total pterin after 48 hours (**Figure 4.9**). In previous results (**Figure 4.6**), it was shown that monocytes produced no detectable levels of 7,8-NP in the intracellular control. However, after 48 hours in culture monocytes produced 12.1 pmol per 5 x 10^6 cells in the control. It appears that achieving detectable levels of 7,8-NP is a slower process than initially thought. Similarly, after 24 hours there was no detectable 7,8-NP produced by cells treated with cholesterol crystals. After 48 hours these cells produced 10.9 pmol per 5 x 10^6 cells of 7,8-NP which is similar to the amount produced by the control. This appears to confirm that on their own cholesterol crystals have no effect on intracellular 7,8-NP production. The increase to 250 U/mL of IFN-γ along with the extra 24 hours of incubation has resulted in an increase in 7,8-NP from 5.0 to 18.3 and 8.3 to 19.3 pmol per 5 x 10^6 cells, in cells treated with IFN-γ and a combination of IFN-γ and cholesterol crystals respectively. After 24 hours of incubation, only the total pterin concentration in cells treated with both IFN-γ and cholesterol crystals was statistically significant different from the control value. With the additional incubation time and increase in IFN-γ concentration total pterin levels in the two treatments containing IFN-γ are now significantly different from the control. In the two treatments contain

cholesterol crystals, the concentration of neopterin produced is significantly different from the control. It appears that the cholesterol crystals are able to induce an oxidative stress which results in the oxidation of 7,8-NP to neopterin. The effect of the additional incubation is even more pronounced in the extracellular fraction. After 48 hours all treatments were significantly different from the control. Treatment of monocytes with IFN-γ produced the highest amount of neopterin (328.7 $\pm$ 10.2 nM). However, the highest production of 7,8-NP was found in cells treated with IFN-γ and cholesterol crystals (169.2 nM) (**Figure 4.9**). The additional incubation time has no influenced the way in which the treatments effect pterin production. It does appear that the rate of pterin production significantly increases between 24 and 48 hours. This effect of time on pterin production will be explored in more detail in **Section 4.2.4**.

(a) Intracellular NP and Total Pterin

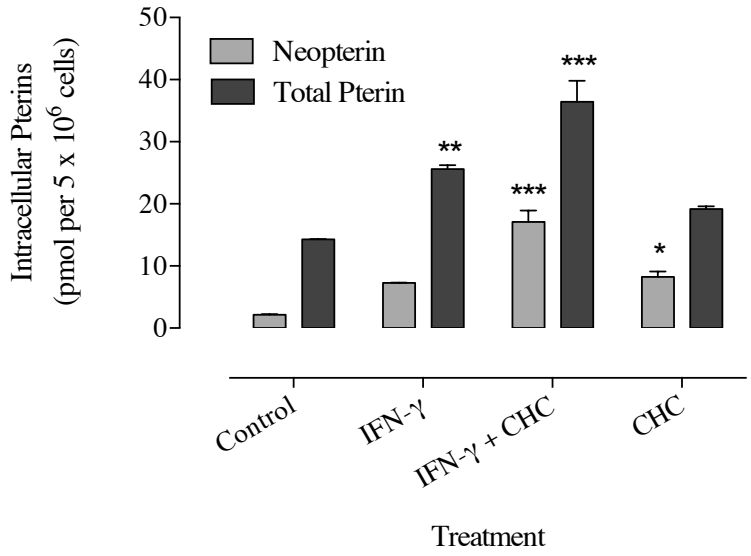

(b) Extracellular NP and Total Pterin

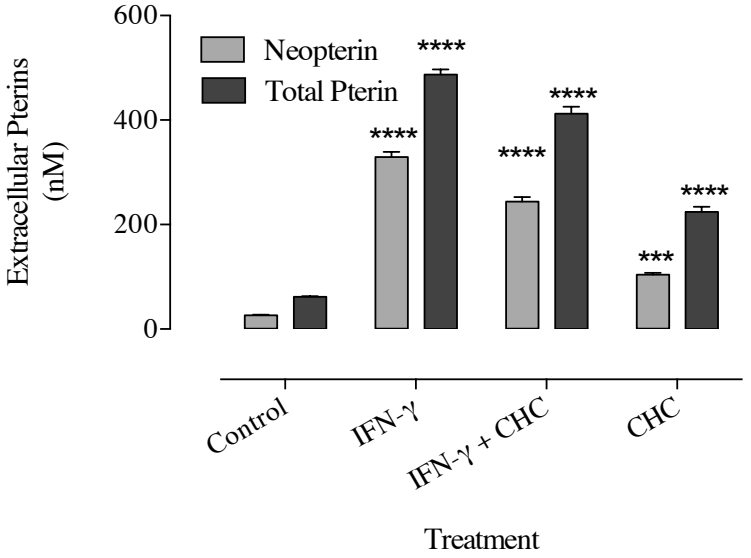

Figure 4.9: Neopterin and Total Pterin measurements in monocytes after 48 hours - Monocytes were incubated at 37 °C in RPMI 1640 with 5 mg/mL of cholesterol crystals and 250 U/mL IFN-γ for 24 hours. Controls were conducted in the absence of cholesterol crystals and IFN-γ. Monocytes were analyzed for neopterin and total pterin (7,8-NP and neopterin) production by HPLC analysis. The graphs are of data from a single experiment that is representative of three separate experiments. Data are mean values $\pm$ SEM of triplicate measurements. Statistical significance is calculated compared to control values. Significance is indicated as follows: $p \leq 0.05$ - *, $p \leq 0.01$ - **, $p \leq 0.001$ - ***, $p \leq 0.0001$.

4.2.3.2 Mixed Lymphocyte Culture

In vivo there is a milieu of cytokines, immune cells and other factors. Using a simple purified monocyte culture removes these other factors to give a clean system. The benefit to using a clean system is that there are less confounding factors influencing the results. Unfortunately by using a purified monocyte system, some of the more complex interactions that would normally occur *in vivo* can be missed. To address some of these issues a mixed lymphocyte culture can be used instead of pure monocytes. A mixed lymphocyte culture contains monocytes as well as T cells and B cells. To investigate whether the presence of T cells, which are known to produce IFN-γ, modulate the production of pterins in cells treated with IFN-γ and cholesterol crystals, a mixed lymphocyte culture was used. The mixed lymphocyte culture was produced in parallel, using blood from the same donor bag, with the monocyte culture in **Section 4.2.3.1** and the experiments were carried out at the same time so that the results could be directly compared. The mixed lymphocyte culture resulted in even high levels of neopterin and 7,8-NP production than monocytes after 48 hours. Mixed lymphocyte culture control cells produced 3 times as much neopterin as monocytes after 48 hours (6.3 $\pm$ 0.15 pmol per 5 x 10^6 cells compared to 2.2 $\pm$ 0.08). The effect was not as strong in the IFN-γ and combined IFN-γ and cholesterol crystal treatments where a 1.3 and 1.7 fold increase respectively in neopterin was seen. Intriguingly, cells treated with cholesterol crystals only showed no change in neopterin production (8.7 $\pm$ 1.29 pmol per 5 x 10^6 cells for mixed culture compared to 8.2 $\pm$ 0.89 for monocytes). In the mixed culture, cells incubated with cholesterol crystals only showed an identical response to the control cells both intracellularly and extracellularly. Treatment with both IFN-γ and cholesterol crystals resulted in the strongest intracellular response, in terms of

neopterin and 7,8-NP production. These cells had nearly equal concentrations of neopterin and 7,8-NP present (30.94 and 34.19 pmol per 5 x 10^6 cells respectively). In the extracellular component, IFN-γ alone (NP= 482 nM, 7,8-NP= 266 nM), resulted in a slightly stronger response than IFN-γ and cholesterol crystals (NP= 391 nM, 7,8-NP= 247 nM).

These results suggest the presence of T-cells increases the amount of 7,8-NP produced across both the controls and the treatments. It also appears that the cholesterol crystal induced oxidation of 7,8-NP to neopterin is not enhanced by the presence of T-cells, as the amount of neopterin produced intracellularly is consistent in both monocytes and mixed lymphocyte culture. This suggests that this oxidation is limited, and is not effected by the amount of 7,8-NP present.

(a) Intracellular NP and Total Pterin in mixed lymphocyte culture after 48 hours

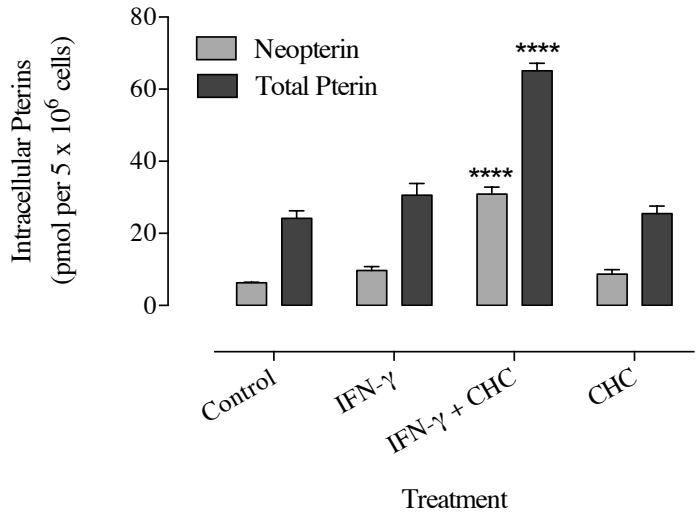

(b) Extracellular NP and Total Pterin in mixed lymphocyte culture after 48 hours

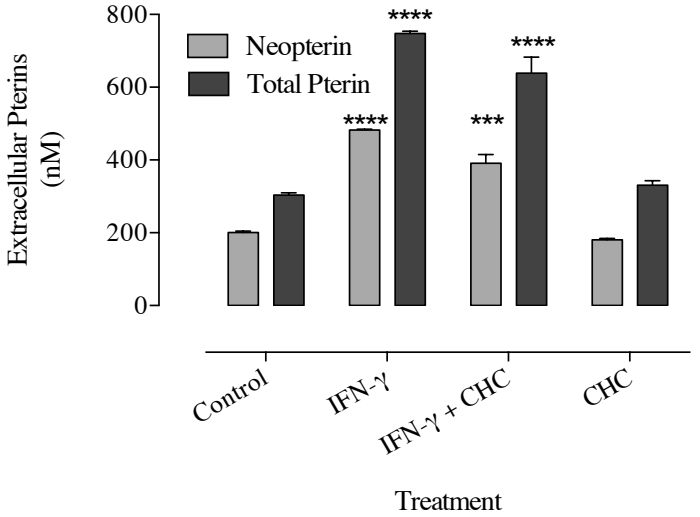

Figure 4.10: Neopterin and Total Pterin measurements in mixed culture after 48 hours - Mixed lymphocyte culture cells (5 x 10^6 cells/mL) were incubated at 37 °C in RPMI 1640 with 5 mg/mL of cholesterol crystals and 250 U/mL IFN-γ for 48 hours. Controls were conducted in the absence of cholesterol crystals and IFN-γ. Mixed culture cells were analyzed for neopterin and total pterin (7,8-NP and neopterin) production by HPLC analysis. The graphs are of data from a single experiment that is representative of three separate experiments. Data are mean values $\pm$ SEM of triplicate measurements. Statistical significance is calculated compared to control values. Significance is indicated as follows: $p \leq 0.05$ - *, $p \leq 0.01$ - **, $p \leq 0.001$ - ***, $p \leq 0.0001$.

4.2.4 Timecourse of 7,8-NP Production

From the results of previous experiments, it seemed that the length of incubation of monocytes with the treatments appeared to be having a significant effect on the amount of neopterin and 7,8-NP produced. To investigate this effect further, monocytes were incubated with IFN-γ and cholesterol crystals for up to 96 hours, with neopterin and total pterin measured at time points across this incubation. Control cells show a steady level of baseline production of 7,8-NP over the 96 hour period. The rate of 7,8-NP production in the control cells is 0.2 nM/hr. It appears that the addition of IFN-γ produces a strong early effect, within the first 24 hours, on 7,8-NP production. For the first 24 hours, cells treated with IFN-γ produce 7,8-NP at 4.25 nM/hr. After 24 hours this slows to 1.04 nM/hr for the remaining 72 hours. Monocytes incubated with both IFN-γ and cholesterol crystals initially have a slower rate of 7,8-NP production compared to their IFN-γ only counterpart. For the first 48 hours 7,8-NP is produced at 1.4 nM/hr, higher than baseline levels but much lower than IFN-γ only cells. However, during the next 48 hours 7,8-NP production is strongly induced at a rate of 5.4 nM/hr. Cells treated with cholesterol crystals have a rate of 7,8-NP similar to the control cells (0.33 nM/hr) which is consistent across the whole 96 hour period.

Although there appeared to be no sign of the 7,8-NP production slowing in the IFN-γ and cholesterol crystal treatment, the experiment was not taken any further as cell death would have begun to occur. It appears that the period of incubation does effect the pterin production in monocytes. Cholesterol crystals appear to be able to inhibit the production of 7,8-NP due to IFN-γ stimulation. However, this inhibition only occurs for the first 48 hours, after which significant 7,8-NP production takes place in these cells.

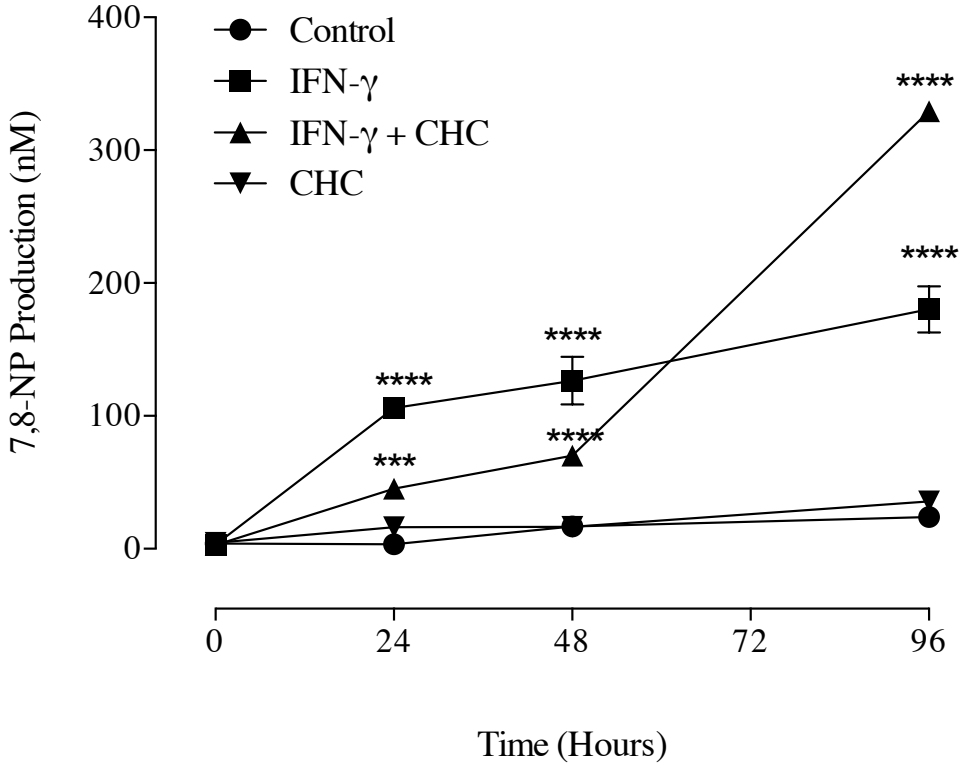

Figure 4.11: Monocyte 7,8 NP production over 96 hours - Monocytes were incubated at 37 °C in RPMI 1640 with 5 mg/mL of cholesterol crystals and 250 U/mL IFN-γ for up to 96 hours. Control cells were measured in the absence of cholesterol crystals and IFN-γ. The graphs are of data from a single experiment that is representative of three separate experiments. Data are mean values $\pm$ SEM of triplicate measurements. Statistical significance is calculated compared to control values. Significance is indicated as follows: $p \leq 0.05$ - *, $p \leq 0.01$ - **, $p \leq 0.001$ - ***, $p \leq 0.0001$.

4.2.5 Modulation of Pterin Production in Monocytes by 7,8-NP

Many of the previous experiments seem to suggest that cholesterol crystals cause an oxidative stress which results in the oxidation of 7,8-NP to neopterin. To test this, monocytes were incubated with exogenous 7,8-NP for 48 hours. The addition of 200 μM of 7,8-NP resulted in the presence of significant amounts of 7,8-NP in supernatant of cells treated with IFN-γ and in the cell only control (**Figure 4.12**). There was very little 7,8-NP found in the supernatant of cell in treatments containing cholesterol crystals. Monocytes incubated with IFN-γ and cholesterol crystals had 0.096 μM of 7,8-NP present in the supernatant while monocytes treated with cholesterol crystals only had 0.601 μM of 7,8-NP. Compared to the 5.469 μM of 7,8-NP in the control, these values are insignificant. The cell free control showed that the presence of cholesterol crystals alone does not cause the total loss of 7,8-NP. The presence of cholesterol crystals did cause the oxidation of some of the 7,8-NP to neopterin. This oxidation was also seen in the cell free 7,8-NP only control (data not shown), which suggests that during the 48 hour incubation some of the 7,8-NP spontaneously oxidizes to neopterin. Interestingly, monocytes treated with both cholesterol crystals and IFN-γ produced the least amount of neopterin (0.034 μM over control) compared to the other treatments (0.071 μM over control for cholesterol crystals only and 0.102 μM over control for IFN-γ only).

It appears that in the presence of monocytes and cholesterol crystals, 7,8-NP is not oxidized to neopterin but instead may be converted to 7,8-dihydroxanthopterin (7,8-DXP) or its derivative xanthopterin (XP). Cholesterol crystals may be able to induce a small amount of oxidation of 7,8-NP to neopterin, as seen in previous experiments, but on a larger scale it appears that this does not occur.

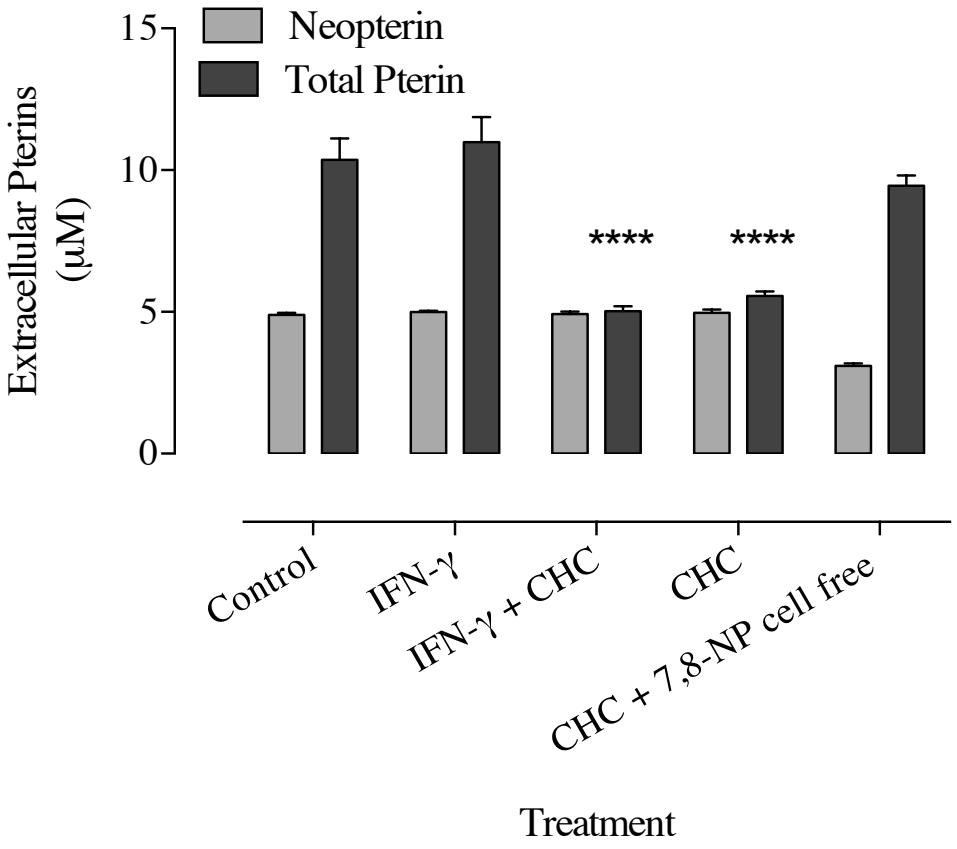

Figure 4.12: Pterin production in monocytes after addition of extracellular 7,8-NP - Monocytes (5 x 10^6 cells/mL) were incubated at 37 °C in RPMI 1640 with 5.0 mg/mL of cholesterol crystals and 250 U/mL IFN-γ for 48 hours. 7,8-NP (200 μM) was added to all treatments prior to incubation. Controls were conducted in the absence of cholesterol crystals and IFN-γ. The graphs are of data from a single experiment that is representative of three separate experiments. Data are mean values $\pm$ SEM of triplicate measurements. Statistical significance is calculated compared to control values. Significance is indicated as follows: $p \leq 0.05$ - *, $p \leq 0.01$ - **, $p \leq 0.001$ - ***, $p \leq 0.0001$.

4.2.6 Production of IL-1β by Monocytes

It has been found that cholesterol crystals cause the upregulation of IL-1β via the activation of the NLRP3 inflammasome (Duewell et al., 2010). It is unknown whether pterins have a role in modulating inflammasome activation and expression of IL-1β as 7,8-NP has been shown to be involved in the downregulation of proteins such as CD36 (Gieseg et al., 2010). To investigate the effect of 7,8-NP on IL-1β production in monocytes, the supernatant from cells was assayed by ELISA.

Treating cells with cholesterol crystals increased IL-1β production after 24 hours as expected (**Figure 4.13a**). This effect was heightened by the combination of IFN-γ and cholesterol crystals. The addition of 7,8-NP had no effect on IL-1β levels in samples without cholesterol crystals. In samples with cholesterol crystals there is a slight increase in IL-1β levels, however this difference is not statistically significant when compared to the amount of IL-1β produced by cells in the absence of 7,8-NP. This production of IL-1β is significantly different from the control which indicates that the combination of cholesterol crystals and 7,8-NP can modulate IL-1β production in monocytes.

After 48 hours, the effect of 7,8-NP on IL-1β production is reversed (**Figure 4.13b**). Cells which had 7,8-NP present show a lower amount of IL-1β than cells without. This difference between the presence and absence of 7,8-NP is statistically significant in the cholesterol only treatment. The combination of IFN-γ and cholesterol crystals results in the highest concentration of IL-1β (2.3 ng/mL in the 7,8-NP free sample compared to 0.74 ng/mL in the control). The treatment of cells with cholesterol crystals only produced significant amounts of IL-1β when compared to the control. This was slightly lower than the IFN-γ and cholesterol treatment at 2.1 ng/mL.

It appears that 7,8-NP does have an effect on IL-1β production that is time sensitive. The ability of 7,8-NP to modulate IL-1β levels may be part of a feedback loop, as IL-1β has been shown to upregulate 7,8-NP production.

(a) IL-1β production after 24 hours

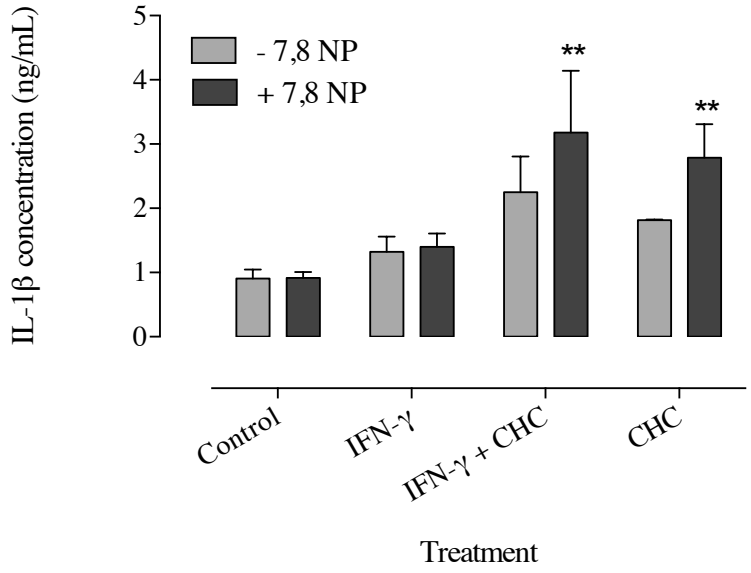

(b) IL-1β production after 48 hours

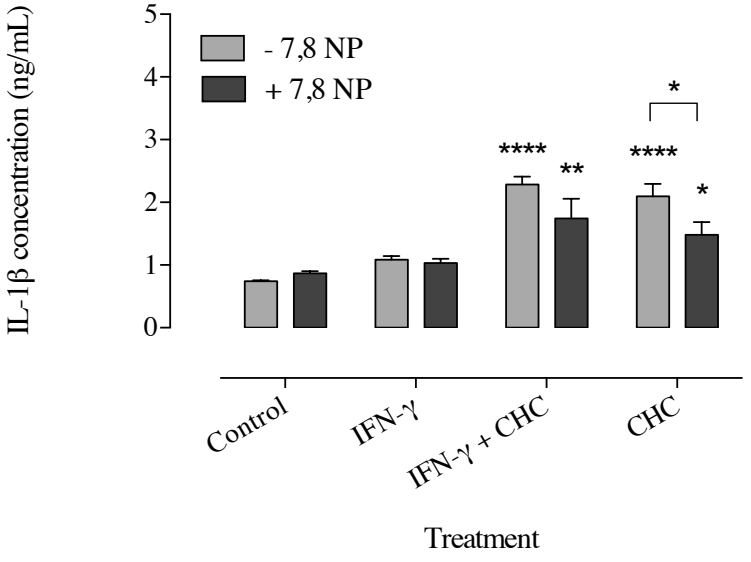

Figure 4.13: Production of IL-1β by monocytes- Monocytes (5 x 10^6 cells/mL) were incubated at 37 °C in RPMI 1640 with 5 mg/mL of cholesterol crystals and 250 U/mL IFN-γ for 48 hours. In the treatments containing 7,8-NP, 200 μM was added prior to incubation. Controls were conducted in the absence of cholesterol crystals and IFN-γ. The graphs are of data from a single experiment that is representative of two separate experiments. Data are mean values $\pm$ SEM of triplicate measurements. Statistical significance is calculated compared to control values. Significance indicated by a bracket is calculated between samples in the absence and presence of 7,8-NP. Significance is indicated as follows: $p \leq 0.05$ - *, $p \leq 0.01$ - **, $p \leq 0.001$ - ***, $p \leq 0.0001$.

5

Discussion

5.1 Limitations of Giant Cell Culture for Experimental Purposes

McNally and Anderson (1995, 2003), among others, have shown that FBGC can be cultured *in vitro* using IL-4 and α-TocH. However, a clear distinction must be made between the ability to culture cells and the development of a model system for experimental purposes. It is known that when using primary cells, up to 20% of the experimental variation can be accounted for by inter-donor differences (personal communication). Even taking this known source of variation into account, giant cell cultures were much more variable in nature than HMDM cultures.

Macrophage cell culture is a technique that has been refined over many decades and is commonly used by many laboratories. It is much simpler and better understood than giant cell culture. Successful macrophage culture has two main requirements. The requirements are attachment of monocytes to the culture surface and differentiation

from monocytes into macrophages. These two processes can be easily controlled through the use of specialized adherent tissue culture plates and a bolus introduction of a differentiation promoting growth factor, such as GM-CSF, at the time of plating.

In contrast, much less is known about the processes that govern giant cell formation. Giant cell culture is only performed by a small number of research groups and is a relatively recent development.

5.1.1 Giant Cell Culture and Quantification

It was intended that the giant cells would be cultured in as similar a manner to macrophages as possible to limit the number of factors that could influence differences between the cell types. It was hoped that by maintaining analogous culture conditions it would enable direct comparison of the function and pterin production of these two cell types. This put constraints on techniques that could be used. HMDM cell cultures are carried out in Nunc brand plates designed for the culture of adherent cells using a proprietary surface technology made from modified resins. A recent paper has highlighted the importance of the variety of cell culture plate used. McNally and Anderson (2011) found that giant cells grow best on plates containing RGD peptides which are composed of L-arginine, glycine and L-aspartic acid. RGD peptides are a recognition sequence used by integrins, the proteins used in cellular adhesion (Ruoslahti, 1996). Plates that contain RGD peptides are able to mimic the conditions commonly associated with a foreign body *in vivo*. This may explain why it was often observed that giant cells would form on Nunc cell culture plates, but failed to adhere completely. This failure to adhere meant that during wash steps during techniques such as staining, the giant cells would often detach from the plate.

Brodbeck et al. (2005) found that mixed lymphocyte culture, a combination of monocytes, B cells and T cells, significantly improves the rate of macrophage adhesion and fusion. A mixed lymphocyte culture, as part of the giant cell culture, was maintained by direct plating into 12 well plates in the presence of 10% human serum. Direct plating in the presence of serum prevents the death of the T and B cells that usually occurs in the absence of serum. However, Brodbeck et al. (2005) initially plated cells in 20% serum and then subsequently increased to 40% serum. It appears that this may explain the low adhesion of giant cells observed even in the presence of mixed lymphocytes.

It appears that the addition of IL-4 aids in the formation of FBGC by activating the JAK/STAT pathway which leads to the binding of cell to a surface (Varin and Gordon, 2009). This activation leads to the upregulation of DC-STAMP and E-cadherin (Mantovani et al., 2007; Moreno et al., 2007). HMDMs treated with IL-4 showed higher than baseline rates of fusion (**Figure 3.4**), however, they did not appear to produce many lamellipodia. Macrophages treated with α-TocH did produce lamellipodia and had a higher percentage of fusion than cells with IL-4. Not only is α-TocH able to induce PS flipping, it is also able to stabilize the lipid bilayer in a non-asymmetrical arrangement through interactions with arachidonyl and linenoyl residues within membrane phospholipids (Azzi et al., 2004; Diplock, 1983; Lucy, 1972). Usually, PS exposure would result in an apoptotic response. For example, in monocyte-like THP-1 cells PS exposure in response to oxLDL coincides with caspase activation (Baird et al., 2004). Cell death was not observed in the giant cell cultures (data not shown), which suggests that the cells were expressing the necessary signals to prevent efferocytosis, that is apoptotic cell removal, by another cell. These same signals that prevent clearance lead to the fusion of macrophages.

5.1.2 Fusion

The area of giant cell research is highly focused on the fusion mechanisms of these cells, as many of the processes leading to fusion are still unknown. In that context it is not surprising that very few groups have attempted to culture giant cells to model a disease condition. This thesis attempted to culture and quantify giant cells in a way that they could be used to model the foreign body response. From the results in this thesis (**Table 3.1**), it appears that α-TocH is more potent than IL-4 in inducing giant cell formation. This result differs from that found by McNally and Anderson (1995). It appears that RGD peptides, mimicking the presence of a foreign body, and IL-4 in concert are able to potently induce FBGC formation. This would suggest the key step in facilitating FBGC formation is the ability to form lamellipodia than reach out to other macrophages. α-TocH is then able to mediate cell-cell recognition through the bind of PS to the CD36 receptor, which in the presence of other signals (e.g. CD47), leads to cell fusion. In light of what is known about the mechanism of giant cell fusion, it makes sense that the highest rates of fusion were achieved in the presence of both IL-4 and α-TocH (**Figure 3.5**). Whilst it was possible to form giant cells, the actual rate of fusion even with high concentrations of fusion factors was relatively low. The maximum rate of fusion achieved in this thesis was 29.1%. Rates of fusion reported in the literature are quite variable. Helming et al. (2009) reported approximately 20% fusion in the presence of IL-4 and GMCSF. However, under similar conditions using IL-4 and GMSCF, McNally and Anderson (1995) reported 75% fusion. Vignery (2008) obtained 50% fusion after 18 days of culture with M-CSF and RANKL. Perhaps one reason the rates of fusion achieved in **Table 3.1** were so low was that they were measured using a different technique to some of the other studies. Most studies

solely aim to quantify macrophage fusion, so use techniques such as nuclei staining (MacLauchlan et al., 2009) or colocalization of fluorescent tags (Jay et al., 2010). As the cells were intended to be used for further work, staining the nuclei, which involves fixing the cells, was not a viable technique. Instead the percentage fusion is quantified by the number of giant cells present in the culture compared to the total number of macrophages and giant cells present. The seminal paper on macrophage fusion induced by IL-4 used a similar technique of counting the percentage of multinucleated giant cells formed and reported a fusion rate of 13% after 5 days (McInnes and Rennick, 1988).

Previous studies (Hicks, unpublished) suggested using giant cells for experiments from day eight onwards. However, very few giant cells had formed at this point, and often did not display typical giant cell phenotypic features, such as cytoplasmic spreading. One benefit to using early giant cells is that since they maintain much of their macrophage-like morphology, they are very easy to visualize (**Figure 3.1**). If giant cells are used at a later stage of development they have lost most of their macrophage like features. As cytoplasmic spreading occurs, the cells become increasingly thin. This makes the cells particularly difficult to detect on the plate (**Figure 3.3**).

5.1.3 Cell Viability

McInnes and Rennick (1988) measured the effect of IL-4 on the viability of non-adherent cells in mice bone marrow macrophage cultures, but did not measure the viability of the adherent giant cells which formed in the same cultures. The adherent nature of the giant cells limits the options of viability assays available to use. When

using non-adherent cells, it is possible to take a small sample of cells from the treatment to test viability. In adherent cultures, the viability assay must be carried out directly in the well, which generally prevents any further use of that well.

Healthy giant cells were unable to produce enough of the MTT formazan crystal to be accurately detected by spectroscopy (**Figure 3.6**). Giant cells have been shown to have lower succinate dehydrogenase activity than normal macrophages (Papadimitriou and Wyche, 1976) which will affect their ability to reduce MTT and produce formazan crystals. Trypan blue staining provided a relatively accurate measure of giant cell viability (**Figure 3.8**). Unfortunately, trypan blue exclusion is one of the more time consuming methods of measuring viability, particularly in adherent cells. Trypan blue staining was most successful at measuring giant cell viability during the first week of culture. After this time, the cytoplasmic spreading took place, which made healthy giant cells much more prone to staining with trypan blue (data not shown). Sone et al. (1981) found that the giant cell membrane is more ruffled and convoluted than HMDMs which means that trypan blue become trapped between the folds of the membrane. This gives the appearance of trypan blue staining, however, the stain has not actually penetrated the membrane.

With the techniques available, it appears that giant cells cannot be cultured in the same manner as monocytes or macrophages. This makes a direct comparison between the cell types problematic. Part of the problem is that this model does not reflect in vivo conditions. Giant cells in the body only form when a stimulus is present. However, here we were attempting to induce giant cell formation in the absence of a foreign body.

5.1.4 Absorption of Cholesterol Crystals

Small cholesterol crystals (< 10 μm) can be absorbed by macrophages, but large cholesterol crystals induce a foreign body response (Warren and Yales, 1976). It appears that mature giant cells are less able absorb cholesterol crystals than HMDMs (**Figure 3.10**). The absorption of foreign objects is a complex process which requires specific receptors to mediate the recognition and uptake of the object. From this experiment, it appears that cholesterol crystal absorption does not occur due to giant cell formation, rather that giant cell formation occurs in response to the presence of cholesterol crystals. It would make sense that mature giant cells that do not contain cholesterol crystals lose the ability to absorb cholesterol crystals, as it has been suggested that once the cholesterol crystal has been resolved, the giant cell is also removed (Luttikhuizen et al., 2006). Giant cells are the end stage of differentiation in the monocyte lineage (Cohen et al., 1988) and appear to have lost many of the features that characterize monocytes and macrophages. The timing of giant cell culture is very important as the age of the monocytes will dramatically impact the ability of the cells to fuse (Möst et al., 1997). Typically, giant cell formation occurs in the presence of a foreign body and requires specific mechanisms to occur.

Whilst is it possible to force cells into the foreign body giant cell phenotype, it is difficult to know whether these cells behave in the same way as those that have formed in the presence of a stimulus. Monocytes incubated with cholesterol crystals for seven days began to show features typical of giant cells such as lamellipodia (data not shown). For that reason, studying the effect of cholesterol crystals on pterin production in macrophages and monocytes is in some ways more relevant in terms of modelling the FBR.

5.2 Modification of Pterin Production by Cholesterol Crystals in Monocyte-derived Cells

5.2.1 Modification of Pterin Production by Cholesterol Crystals

The effect of cholesterol crystals on pterin production has not been studied before, which means there is no benchmark or expected response to compare with. Cholesterol crystals appeared to have a dose-dependent effect on 7,8-NP production in macrophages (**Figure 4.1**). Interestingly, this effect was only seen in the intracellular fraction. This could potentially be explained by the fact that cholesterol crystals seem to only cause inflammation through activation of the inflammasome (Freigang et al., 2011). Perhaps it is the uptake of the cholesterol crystals that sets off intracellular processes such as the production of IL-1β which may lead to the induction of 7,8-NP.

Cholesterol crystals stimulate significant 7,8-NP production in macrophages (**Figure 4.4**), however, when this is compared to neopterin production in monocytes (**Figure 4.8**) this production is quite small.

One problem of working with primary cells is differences due to donor variation (**figure 4.7**). Neopterin and 7,8-NP production was measured in batches of monocytes from different donors. Batches with a high baseline 7,8-NP production in the controls produced much higher quantities of 7,8-NP when stimulated (**Figure 4.8**).

5.2.2 Pterin Production in Monocyte-derived Cells

It was surprising to find that monocytes were much more sensitive to modulation of 7,8-NP production by both IFN-γ and cholesterol crystals than macrophages. It was assumed that macrophages, as more mature cells would produce higher quantities

of neopterin and 7,8-NP. This suggests a role for monocytes in the initiation of inflammation. It is unknown why monocytes produce so much more 7,8-NP than macrophages. It is interesting that this difference is apparent at 24 hours, a point where macrophages have reached their maximum neopterin and 7,8-NP production, but monocytes have not.

It was found that the presence of cholesterol crystals causes an inhibition of pterin production in monocytes and mixed lymphocyte culture cells (**Figures 4.9 & 4.10**). It was surprising to find that cholesterol crystals alone are able to induce a small amount of neopterin and 7,8-NP as generally IFN-γ is thought to be the main stimulus of GTPCH-1 activity. Plüss et al. (1996) were able to show that IL-1β causes a dose-dependent increase in GTPCH-1 mRNA in mesangial cells, a type of smooth muscle cell found around blood vessels. The presence of cholesterol crystals seemed to mediate the effect of IFN-γ. Cells treated with both IFN-γ and cholesterol crystals were unable to produce the same amount of neopterin or 7,8-NP as cells treated with IFN-γ alone. As monocytes incubated for 48 hours were able to produce more 7,8-NP than cells incubated for 24 hours, this effect appeared to be time-dependent. To further explore this a 96 hour timecourse was carried out.

The 96 hour timecourse (**Figure 4.11**) confirmed that the inhibition of 7,8-NP production in monocytes was not a total inhibition. Rather the presence of cholesterol crystals caused a delay or lag phase for the first 48 hours. However, after this time point monocytes produced more 7,8-NP than seen in cells treated with IFN-γ. This increase in 7,8-NP is very significant as it has been found that 7,8-NP acts as an antioxidant once it reaches μM levels (Gieseg et al., 1995). Recent studies within the Free Radical Biochemistry laboratory at the University of Canterbury have found that IFN-γ was able to stimulate 7,8-NP production in cells within excised plaque sections (personal

communication). This suggests that recently recruited monocytes may have a key role in providing antioxidant protection within the atherosclerotic plaque.

5.2.3 Modulation of Pterin Production by the Addition of 7,8-NP

In order to explore why cholesterol crystals appeared to inhibit 7,8-NP production within the first 48 hours, cells were incubated with 200 μM of exogenous 7,8-NP (**Figure 4.12**). In the presence of cholesterol crystals, by 48 hours all of the exogenous 7,8-NP had been removed. Most unusual was that it was not oxidized to neopterin, as had occurred in some of the previous experiments. It was thought that this could be a direct interaction of cholesterol crystals with the 7,8-NP, however, this loss of 7,8-NP failed to occur in the absence of cells. It is highly unlikely that this amount of 7,8-NP could have been taken up by the cells, which suggests that this is most likely an extracellular process. Also, as the 7,8-NP is not phosphorylated it could not proceed down the BH_4 pathway. Furthermore, 7,8-NP is known to be involved with the folate biosynthesis pathway, however this pathway is not present in human cells. It is most likely that the exogenous 7,8-NP has been converted to 7,8-DXP or its derivative XP which cannot be directly detected at these concentrations by HPLC. The presence of ROS can induce this conversion of 7,8-NP to 7,8-DXP and XP (Biondi et al., 2012; Gieseg et al., 2008).

5.2.4 IL-1β Production in Monocytes and Modulation by 7,8-NP

Inflammasome activation by cholesterol crystals has been shown to induce IL-1β production Rajamäki et al. (2010). As expected, cells incubated with cholesterol crystals produced more IL-1β than the control (**Figure 4.13a**). Incubating with both

IFN-γ and cholesterol crystals had a synergistic effect on IL-1β production. This was further enhanced by the presence of 7,8-NP. The addition of 7,8-NP had no effect on IL-1β in the absence of cholesterol crystals.

By 48 hours (**Figure 4.13b**) the effect of 7,8-NP on IL-1β is reversed, with less IL-1β found in the presence of cholesterol crystals and 7,8-NP.

Bauernfeind et al. (2009) found that priming of monocytes was a requirement for inflammasome activation by crystalline material. They found that monocytes deficient in interleukin-1 receptor-associated kinase 4 (IRAK4), a protein kinase downstream of TLR4 and myeloid differentiation primary response protein 88 (MyD88) were unable to induce caspase-1 activation. The results in this thesis seem to support the possibility of a single stimulus causing inflammasome activation, as increased IL-1β levels were seen in cells given only cholesterol crystals. To confirm this hypothesis, it would need to be proven that the IL-1β production was only due to inflammasome activation.

It is known that the activation of IL-1β can cause a fever (Duff, 1985). Body temperature can often reach close to $40\,^{\circ}\mathrm{C}$ during a fever (Pettigrew et al., 1974). This may play a role in the resolution of cholesterol crystals as it has been shown that cholesterol crystals will re-solubilize at this temperature (Geng et al., 2003). Cholesterol embolization is often accompanied by a fever (Saric and Kronzon, 2011).

5.3 Mechanisms of Cholesterol Crystal Induced Modification of Pterin Production

Cholesterol crystals appear to induce inflammasome activation, seen as an increase in IL-1β levels, and potentially produce ROS in monocytes. As well as being implicated

in these roles, cholesterol crystals also appeared to modulate pterin production. It is unknown how cholesterol crystals are able to influence pterin production. In most cells the conversion of GTP to 7,8-NP-PPP is the rate limiting step in the BH_4 pathway. It has been found that the addition of IFN-γ causes up to a 40 fold increase in GTPCH-1 activity (Werner et al., 1990).

Monocytes and macrophages produce higher levels of neopterin and 7,8-NP than other cells as the are deficient in the enzyme PTPS. This deficiency prevents the flow of 7,8-NP-PPP down the BH_4 synthesis pathway. It has been found that blood derived cells are able to produce the mRNA transcript for PTPS, however, a number of the transcripts are truncated due to the skipping of exon 3 (Leitner et al., 2003). These truncated transcripts are unable to produce functioning PTPS. Not all of the mRNA transcripts encounter this problem so a low level of functioning PTPS is produced. The presence of IL-1β induces the transcription of PTPS, so purely by shear volume, it is likely that more functioning PTPS is produced (Franscini et al., 2003).

5.4 Role of Cholesterol Crystals and Foreign Body Giant Cells in Atherosclerosis

Cholesterol crystals have been shown to induce inflammation and can be particularly dangerous when present in atherosclerotic plaques. Cholesterol crystals may cause erosion of the fibrous cap and rupture of the necrotic core in plaques (Abela, 2010; Michel et al., 2011). If the plaque ruptures, hemorrhage can occur. Cholesterol crystals exposed to the blood form emboli which can block blood flow (Flory, 1945; Moolenaar and Lamers, 1996). Katz et al. (1982) found that there was a very low

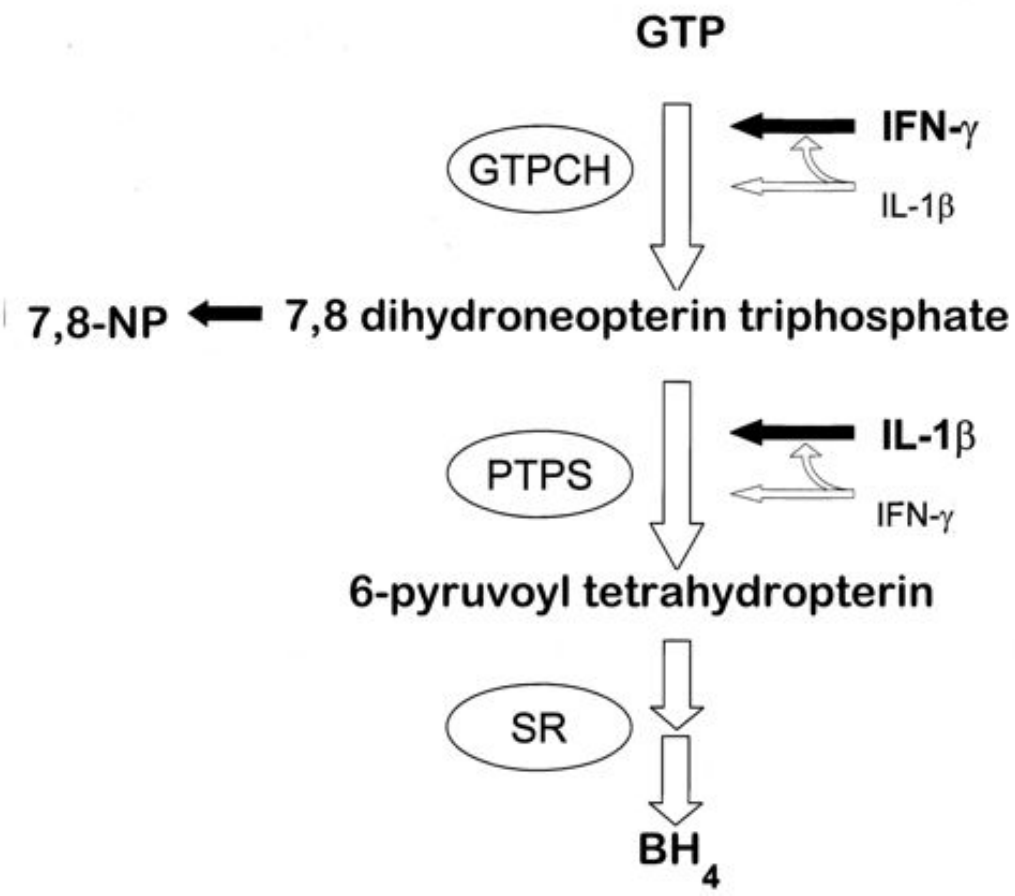

Figure 5.1: Modulation of pterin production by IL-1β - The enzymatic conversion of GTP to 7,8-NP-PPP is strongly induced by IFN-γ and to a lesser extent by IL-1β. IL-1β causes the upregulation of the enzyme PTPS that converts 7,8-NP-PPP to 6-pyruvoyl tetrahydropterin. IFN-γ is able to upregulate PTPS as well, but not to the same extent as IL-1β .Adapted from Franscini et al. (2003)

turnover of cholesterol crystals in plaques by studying the lipid composition. Small (1988) confirmed this result using a primate model. Both Katz et al. (1982) and Small (1988) suggest that this low turnover may prevent plaque regression.

The presence of multinucleated cells in human atherosclerotic plaques has been confirmed by both transmission electron and scanning microscopy of samples taken from post-mortem subjects (Tokunaga et al., 1989). FBGC are thought to form in plaques in order to resolve cholesterol crystals. It has been found that giant cells release matrix metalloproteinase-9 (MMP-9) which is involved in matrix degradation (Boyle, 2005; Rittner et al., 1999). This is thought to add to plaque instability and inflammation through remodelling of the fibrous cap (Zhu et al., 2007).

5.5 Future Research

The role of cholesterol crystals and the FBR is a largely unresearched area. In particular, there has been very little study into pterin production as a result of cholesterol crystals. Continuing from the work in this thesis, further study on how cholesterol crystals modify pterin production, would develop the understanding of the role of cholesterol crystals in atherosclerotic plaques. It would be especially informative to study how cholesterol crystals caused the total loss of exogenous 7,8-NP. Clearly, this process is cell mediated and does not involve the oxidation of the 7,8-NP to neopterin.

Another area which has yet to be fully explored is the type of inflammatory response that cholesterol crystals induce. It would be interesting to know if cholesterol crystals add to the atherosclerotic burden through the stimulation of the production of ROS. Shen and Blair (2006) found that cholesterol crystals interfere with flow

cytometry, the technique commonly used to quantify oxidative stress. However, ROS production could be measured by a dihydroethidium (DHE) stain which can be quantified by fluorescence microscopy.

Furthermore, additional study may confirm the production of BH_4 in monocytes due to cholesterol crystals. According to the currently known mechanisms, BH_4 production is likely to be increased in the presence of cholesterol crystals. Often BH_4 is indirectly measured through an assay which quantifies NO production as BH_4 is a NOS cofactor. However, it has been shown that IL-1β can directly increase NO production through NF-κB transcriptional regulation of NOS (Kwon et al., 1995). This would need to be considered when designing an experiment to measure BH_4 production.

5.6 Summary

Foreign body giant cells play an important role in the resolution of the foreign body response *in vivo*. The resolution of cholesterol crystals has the potential to lessen inflammation in the atherosclerotic plaque and aid in limiting disease progression. For this reason, understanding the modulation of inflammatory processes such as the production of pterins in monocyte derived cells by cholesterol crystals is important. Cholesterol crystals also provide a potential target in atherosclerotic plaques for newly developed imaging technology and may be able to act as an indirect measure of the level of disease progression.

References

Abela, G. S. (2010). Cholesterol crystals piercing the arterial plaque and intima trigger local and systemic inflammation. *Journal of Clinical Lipidology*, 4(3):156–164.

Anderson, J. M., Rodriguez, A., and Chang, D. (2008). Foreign body reaction to biomaterials. *Seminars in Immunology*, 20(2):86–100.

Aterman, K., Remmele, W., and Smith, M. (1988). Karl Touton and his 'xanthelasmatic giant cell'. A selective review of multinucleated giant cells. *American Journal of Dermatopathology*, 10(3):257–269.

Azzi, A., Gysin, R., Kempna, P., Adelina, M., Negis, Y., Villacorta, L., Visarius, T., and Zingg, J.-M. (2004). Vitamin E Mediates Cell Signaling and Regulation of Gene Expression. *Annals of the New York Academy of Sciences*, 1031(1):86–95.

Babic, I., Schallhorn, A., Lindberg, F., and Jirik, F. (2000). SHPS-1 induces aggregation of Ba/F3 pro-B cells via an interaction with CD47. *Journal of Immunology*, 164(7):3652–3658.

Baird, S., Reid, L., Hampton, M., and Gieseg, S. (2005). OxLDL induced cell death is inhibited by the macrophage synthesised pterin, 7,8-dihydroneopterin, in U937 cells but not THP-1 cells. *Biochimica et Biophysica Acta - Molecular Cell Research*, 1745(3):361–369.

Baird, S. K., Hampton, M. B., and Gieseg, S. P. (2004). Oxidized LDL triggers

phosphatidylserine exposure in human monocyte cell lines by both caspase-dependent and -independent mechanisms. *FEBS Letters*, 578(1-2):169–174.

Ballestrem, C., Wehrle-Haller, B., Hinz, B., and Imhof, B. A. (2000). Actin-dependent lamellipodia formation and microtubule-dependent tail retraction control-directed cell migration. *Molecular Biology of the Cell*, 11(9):2999–3012.

Bauernfeind, F. G., Horvath, G., Stutz, A., Alnemri, E. S., MacDonald, K., Speert, D., Fernandes-Alnemri, T., Wu, J., Monks, B. G., Fitzgerald, K. A., Hornung, V., and Latz, E. (2009). Cutting edge: NF-κB activating pattern recognition and cytokine receptors license NLRP3 inflammasome activation by regulating NLRP3 expression. *The Journal of Immunology*, 183(2):787–791.

Bayliss, O. B. (1976). The giant cell in cholesterol resorption. *British Journal of Experimental Pathology*, 57(5):610–618.

Bellingan, G., Caldwell, H., Howie, S., Dransfield, I., and Haslett, C. (1996). In vivo fate of the inflammatory macrophage during the resolution of inflammation: Inflammatory macrophages do not die locally, but emigrate to the draining lymph nodes. *Journal of Immunology*, 157(6):2577–2585.

Bhadani, P., Sah, S., Sen, R., and Singh, R. (2006). Diagnostic value of fine needle aspiration cytology in gouty tophi: A report of 7 cases. *Acta Cytologica*, 50(1):101–104.

Biondi, R., Ambrosio, G., De Pascali, F., Tritto, I., Capodicasa, E., Druhan, L., Hemann, C., and Zweier, J. (2012). HPLC analysis of tetrahydrobiopterin and its pteridine derivatives using sequential electrochemical and fluorimetric detection: Application to tetrahydrobiopterin autoxidation and chemical oxidation. *Archives of Biochemistry and Biophysics*, 520(1):7–16.

Bitterlich, G., Szabo, G., Werner, E., Larcher, C., Fuchs, D., Hausen, A., Reibnegger, G., Schulz, T., Troppmair, J., Wachter, H., and Dierich, M. (1988). Selective induction of mononuclear phagocytes to produce neopterin by interferons. *Immunobiology*, 176(3):228–235.

Bjorkerud, S. and Bondjers, G. (1973). Arterial repair and atherosclerosis after mechanical injury. Part V. Tissue response after induction of a large superficial transverse injury. *Atherosclerosis*, 18(2):235–255.

Bobryshev, Y. V. (2006). Monocyte recruitment and foam cell formation in atherosclerosis. *Micron*, 37(3):208–222.

Bocan, T. M., Schifani, T. A., and Guyton, J. R. (1986). Ultrastructure of the human aortic fibrolipid lesion. Formation of the atherosclerotic lipid-rich core. *American Journal of Pathology*, 123(3):413–424.

Botticelli, A., Criscuolo, M., and Di Gregorio, C. (1989). Multinucleated giant cells in aids encephalopathy: an immunohistochemical study. *The Italian Journal of Neurological Sciences*, 10(3):301–305.

Boyle, J. J. (2005). Macrophage activation in atherosclerosis: pathogenesis and pharmacology of plaque rupture. *Current Vascular Pharmacology*, 3(1):63–68.

Bradley, E. and Oursler, M. (2008). Osteoclast culture and resorption assays. *Methods in Molecular Biology*, 455:19–35.

Brigelius-Flohé, R. (2009). Vitamin E: the shrew waiting to be tamed. *Free Radic Biol Med*, 46(5):543–554.

Brodbeck, W. G. and Anderson, J. M. (2009). Giant cell formation and function. *Current Opinion in Hematology*, 16(1):53–57.

REFERENCES

Brodbeck, W. G., MacEwan, M., Colton, E., Meyerson, H., and Anderson, J. M. (2005). Lymphocytes and the foreign body response: Lymphocyte enhancement of macrophage adhesion and fusion. *Journal of Biomedical Materials Research Part A*, 74A(2):222–229.

Chen, E. H. and Olson, E. N. (2005). Unveiling the mechanisms of cell-cell fusion. *Science*, 308(5720):369–373.

Cohen, M., Grossman, E., and Thompson, S. (1988). Features of central giant cell granuloma of the jaws xenografted in nude mice. *Oral Surgery, Oral Medicine, Oral Pathology*, 66(2):209–217.

Colville-Nash, P. and Gilroy, D. (2001). Potential adverse effects of cyclooxygenase-2 inhibition: Evidence from animal models of inflammation. *BioDrugs*, 15(1):1–9.

De Nardo, D. and Latz, E. (2011). NLRP3 inflammasomes link inflammation and metabolic disease. *Trends in Immunology*, 32(8):373–379.

Demel, U., Foldes-Papp, Z., Fuchs, D., and Tilz, G. P. (2001). Characterization of pteridines: a new approach by fluorescence correlation spectroscopy and analysis of assay sensitivity. *Pteridines*, 12(4):147–154.

Diplock, A. (1983). The role of vitamin E in biological membranes. *Ciba Foundation Symposium*, 101:45–55.

Dos Santos, M., Pegoraro, M., Sandrini, F., and Macuco, E. (2008). Risk factors for the development of atherosclerosis in childhood and adolescence [fatores de risco no desenvolvimento da aterosclerose na infância e adolescência]. *Arquivos Brasileiros de Cardiologia*, 90(4):276–283.

Drummond, C., Savdie, E., and Kossard, S. (2001). Sarcoidosis with prominent giant cells. *Australasian Journal of Dermatology*, 42(4):290–293.

Duewell, P., Kono, H., Rayner, K. J., Sirois, C. M., Vladimer, G., Bauernfeind, F. G., Abela, G. S., Franchi, L., Nuñez, G., Schnurr, M., Espevik, T., Lien, E., Fitzgerald, K. A., Rock, K. L., Moore, K. J., Wright, S. D., Hornung, V., and Latz, E. (2010). NLRP3 inflammasomes are required for atherogenesis and activated by cholesterol crystals. *Nature*, 464(7293):1357–1361.

Duff, G. (1985). Interleukin-1 and fever. *British Journal of Rheumatology*, 24(SUPPL. 1):12–14.

Enelow, R., Sullivan, G., Carper, H., and Mandell, G. (1992). Induction of multinucleated giant cell formation from in vitro culture of human monocytes with interleukin-3 and interferon-gamma: comparison with other stimulating factors. *American Journal of Respiratory Cell and Molecular Biology*, 6(1):57–62.

Fadok, V. A., Bratton, D. L., Frasch, S. C., Warner, M. L., and Henson, P. M. (1998). The role of phosphatidylserine in recognition of apoptotic cells by phagocytes. *Cell Death and Differentiation*, 5(7):551–562.

Firth, C. A., Crone, E. M., Flavall, E. A., Roake, J. A., and Gieseg, S. P. (2008). Macrophage mediated protein hydroperoxide formation and lipid oxidation in low density lipoprotein are inhibited by the inflammation marker 7,8-dihydroneopterin. *Biochimica et Biophysica Acta*, 1783(6):1095–1101.

Flavall, E. A., Crone, E. M., Moore, G. A., and Gieseg, S. P. (2008). Dissociation of neopterin and 7,8-dihydroneopterin from plasma components before HPLC analysis. *Journal of Chromatography. B, Analytical Technologies in the Biomedical and Life Sciences*, 863(1):167–171.

Flory, C. M. (1945). Arterial occlusions produced by emboli from eroded aortic atheromatous plaques. *American Journal of Pathology*, 21(3):549–565.

Franchi, L. and Nuñez, G. (2008). The Nlrp3 inflammasome is critical for aluminium hydroxide-mediated IL-1 secretion but dispensable for adjuvant activity. *European Journal of Immunology*, 38(8):2085–2089.

Franscini, N., Blau, N., Walter, R., Schaffner, A., and Schoedon, G. (2003). Critical role of interleukin-1beta for transcriptional regulation of endothelial 6-pyruvoyltetrahydropterin synthase. *Arteriosclerosis, Thrombosis, and Vascular Biology*, 23(11):e50–53.

Freigang, S., Ampenberger, F., Spohn, G., Heer, S., Shamshiev, A. T., Kisielow, J., Hersberger, M., Yamamoto, M., Bachmann, M. F., and Kopf, M. (2011). Nrf2 is essential for cholesterol crystal-induced inflammasome activation and exacerbation of atherosclerosis. *European Journal of Immunology*, 41(7):2040–2051.

Friedmann, I. and Graham, M. (1979). The ultrastructure of cholesterol granuloma of the middle ear: an electron microscope study. *Journal of Laryngology and Otology*, 93(5):433–442.

Fuchs, D., Weiss, G., and Wachter, H. (1993). Neopterin, biochemistry and clinical use as a marker for cellular immune reactions. *International Archives of Allergy and Immunology*, 101(1):1–6.

Galea, J., Armstrong, J., Gadsdon, P., Holden, H., Francis, S., and Holt, C. (1996). Interleukin-1 in coronary arteries of patients with ischemic heart disease. *Arteriosclerosis, Thrombosis, and Vascular Biology*, 16(8):1000–1006.

Geng, Y.-J., Phillips, J. E., Mason, R. P., and Casscells, S. W. (2003). Cholesterol crystallization and macrophage apoptosis: implication for atherosclerotic plaque instability and rupture. *Biochemical Pharmacology*, 66(8):1485–1492.

Gieseg, S., Crone, E., Flavall, E., and Amit, Z. (2008). Potential to inhibit growth of atherosclerotic plaque development through modulation of macrophage

neopterin/7,8-dihydroneopterin synthesis. *British Journal of Pharmacology*, 153(4):627–635.

Gieseg, S., Reibnegger, G., Wachter, H., and Esterbauer, H. (1995). 7,8 Dihydroneopterin inhibits low density lipoprotein oxidation in vitro. Evidence that this macrophage secreted pteridine is an anti-oxidant. *Free Radical Research*, 23(2):123–136.

Gieseg, S., Whybrow, J., Glubb, D., and Rait, C. (2001). Protection of U937 cells from free radical damage by the macrophage synthesized antioxidant 7,8-dihydroneopterin. *Free Radical Research*, 35(3):311–318.

Gieseg, S. P., Amit, Z., Yang, Y.-T., Shchepetkina, A., and Katouah, H. (2010). Oxidant production, oxLDL uptake, and CD36 levels in human monocyte–derived macrophages are downregulated by the macrophage-generated antioxidant 7,8-dihydroneopterin. *Antioxidants and Redox Signaling*, 13(10):1525–1534.

Gooch, J., Christy, B., and Yee, D. (2002). STAT6 mediates interleukin-4 growth inhibition in human breast cancer cells. *Neoplasia*, 4(4):324–331.

Gordon, S. (2007). The macrophage: Past, present and future. *European Journal of Immunology*, 37(S1):S9–S17.

Grahames, C., Michel, A., Chessell, I., and Humphrey, P. (1999). Pharmacological characterization of ATP- and LPS-induced IL-1β release in human monocytes. *British Journal of Pharmacology*, 127(8):1915–1921.

Habecker, B., Klein, M., Sundgren, N., Li, W., and Woodward, W. (2002). Developmental regulation of neurotransmitter phenotype through tetrahydrobiopterin. *Journal of Neuroscience*, 22(21):9445–9452.

REFERENCES

Han, X., Sterling, H., Chen, Y., Saginario, C., Brown, E. J., Frazier, W. A., Lindberg, F. P., and Vignery, A. (2000). CD47, a ligand for the macrophage fusion receptor, participates in macrophage multinucleation. *Journal of Biological Chemistry*, 275(48):37984–37992.

Hansson, G. K. and Libby, P. (2006). The immune response in atherosclerosis: a double-edged sword. *Nature Reviews Immunology*, 6(7):508–519.

Helming, L. and Gordon, S. (2009). Molecular mediators of macrophage fusion. *Trends in Cell Biology*, 19(10):514–522.

Helming, L., Winter, J., and Gordon, S. (2009). The scavenger receptor CD36 plays a role in cytokine-induced macrophage fusion. *Journal of Cell Science*, 122(Pt 4):453–459.

Hornung, V., Bauernfeind, F., Halle, A., Samstad, E. O., Kono, H., Rock, K. L., Fitzgerald, K. A., and Latz, E. (2008). Silica crystals and aluminum salts activate the NALP3 inflammasome through phagosomal destabilization. *Nature Immunology*, 9(8):847–856.

Hu, W. J., Eaton, J. W., Ugarova, T. P., and Tang, L. (2001). Molecular basis of biomaterial-mediated foreign body reactions. *Blood*, 98(4):1231–1238.

Huber, C. (1984). Immune response-associated production of neopterin. Release from macrophages primarily under control of interferon-gamma. *Journal of Experimental Medicine*, 160(1):310–316.

Janney, C., Hurt, M., and Santa Cruz, D. (1991). Deep juvenile xanthogranuloma: Subcutaneous and intramuscular forms. *American Journal of Surgical Pathology*, 15(2):150–159.

Jaworski, Z., Duck, B., and Sekaly, G. (1981). Kinetics of osteoclasts and their nuclei in evolving secondary haversian systems. *Journal of Anatomy*, 133(3):397–405.

Jay, S. M., Skokos, E., Laiwalla, F., Krady, M.-M., and Kyriakides, T. R. (2007). Foreign body giant cell formation is preceded by lamellipodia formation and can be attenuated by inhibition of Rac1 activation. *American Journal of Pathology*, 171(2):632–640.

Jay, S. M., Skokos, E. A., Zeng, J., Knox, K., and Kyriakides, T. R. (2010). Macrophage fusion leading to foreign body giant cell formation persists under phagocytic stimulation by microspheres in vitro and in vivo in mouse models. *Journal of Biomedical Materials Research Part A*, 93(1):189–199.

Joyner, C., Quinn, J., Triffitt, J., Owen, M., and Athanasou, N. (1992). Phenotypic characterisation of mononuclear and multinucleated cells of giant cell tumour of bone. *Bone and Mineral*, 16(1):37–48.

Katusic, Z. S., Stelter, A., and Milstien, S. (1998). Cytokines stimulate GTP cyclohydrolase I gene expression in cultured human umbilical vein endothelial cells. *Arteriosclerosis, Thrombosis, and Vascular Biology*, 18(1):27–32.

Katz, S., Small, D., Smith, F., Dell, R., and Goodman, D. (1982). Cholesterol turnover in lipid phases of human atherosclerotic plaque. *The Journal of Lipid Research*, 23(5):733–737.

Klein, A., Deckert, V., Schneider, M., Dutrillaux, F., Hammann, A., Athias, A., Le Guern, N., Pais de Barros, J.-P., Desrumaux, C., Masson, D., Jiang, X.-C., and Lagrost, L. (2006). Alpha-tocopherol modulates phosphatidylserine externalization in erythrocytes: relevance in phospholipid transfer protein-deficient mice. *Arteriosclerosis, Thrombosis, and Vascular Biology*, 26(9):2160–2167.

Kosteli, A., Sugaru, E., Haemmerle, G., Martin, J. F., Lei, J., Zechner, R., and Ferrante Jr, A. W. (2010). Weight loss and lipolysis promote a dynamic immune response in murine adipose tissue. *The Journal of clinical investigation*, 120(10):3466.

REFERENCES

Kreja, L., Liedert, A., Schmidt, C., Claes, L., and Ignatius, A. (2007). Influence of receptor activator of nuclear factor (NF)-κB ligand (RANKL), macrophage-colony stimulating factor (M-CSF) and fetal calf serum on human osteoclast formation and activity. *Journal of Molecular Histology*, 38(4):341–345.

Kwon, G., Corbett, J., Rodi, C., Sullivan, P., and McDaniel, M. (1995). Interleukin-1β-induced nitric oxide synthase expression by rat pancreatic β-cells: Evidence for the involvement of nuclear factor κB in the signaling mechanism. *Endocrinology*, 136(11):4790–4795.

Kyriakides, T. R. and Bornstein, P. (2003). Matricellular proteins as modulators of wound healing and the foreign body response. *Thrombosis and Haemostasis*, 90(6):986–992.

Lay, G., Poquet, Y., Salek-Peyron, P., Puissegur, M.-P., Botanch, C., Bon, H., Levillain, F., Duteyrat, J.-L., Emile, J.-F., and Altare, F. (2007). Langhans giant cells from M. tuberculosis-induced human granulomas cannot mediate mycobacterial uptake. *The Journal of Pathology*, 211(1):76–85.

Leitner, K., Meyer, M., Leimbacher, W., Peterbauer, A., Hofer, S., Heufler, C., Müller, A., Heller, R., Werner, E., Thöny, B., and Werner-Felmayer, G. (2003). Low tetrahydrobiopterin biosynthetic capacity of human monocytes is caused by exon skipping in 6-pyruvoyl tetrahydropterin synthase. *Biochemical Journal*, 373(3):681–688.

Lemaire, I., Falzoni, S., Leduc, N., Zhang, B., Pellegatti, P., Adinolfi, E., Chiozzi, P., and Di Virgilio, F. (2006). Involvement of the purinergic $P2X_7$ receptor in the formation of multinucleated giant cells. *Journal of Immunology*, 177(10):7257–7265.

Li, A. G., Quinn, M. J., Siddiqui, Y., Wood, M. D., Federiuk, I. F., Duman, H. M., and Ward, W. K. (2007). Elevation of transforming growth factor beta (TGFβ) and its downstream mediators in subcutaneous foreign body capsule tissue. *Journal of Biomedical Materials Research Part A*, 82(2):498–508.

Liu, Z., Noguchi, M., Hiwatashi, N., and Toyota, T. (1996). Monocyte aggregation and multinucleated giant-cell formation in vitro in Crohn's disease: The effect of cell adhesion molecules. *Scandinavian Journal of Gastroenterology*, 31(7):706–710.

Low, Q., Drugea, I., Duffner, L., Quinn, D., Cook, D., Rollins, B., Kovacs, E., and DiPietro, L. (2001). Wound healing in MIP-1α-/- and MCP-1-/- mice. *American Journal of Pathology*, 159(2):457–463.

Lucy, J. (1972). Functional and structural aspects of biological membranes: a suggested structural role for vitamin E in the control of membrane permeability and stability. *Annals of the New York Academy of Sciences*, 203:4–11.

Luttikhuizen, D. T., Harmsen, M. C., and van Luyn, M. J. A. (2006). Cellular and molecular dynamics in the foreign body reaction. *Tissue Engineering*, 12(7):1955–1970.

Ly, K.-H., Régent, A., Tamby, M. C., and Mouthon, L. (2010). Pathogenesis of giant cell arteritis: More than just an inflammatory condition? *Autoimmunity Reviews*, 9(10):635–645.

MacLauchlan, S., Skokos, E. A., Meznarich, N., Zhu, D. H., Raoof, S., Shipley, J. M., Senior, R. M., Bornstein, P., and Kyriakides, T. R. (2009). Macrophage fusion, giant cell formation, and the foreign body response require matrix metalloproteinase 9. *Journal of Leukocyte Biology*, 85(4):617–626.

Maier, W., Cosentino, F., Lütolf, R., Fleisch, M., Seiler, C., Hess, O., Meier, B., and Lüscher, T. (2000). Tetrahydrobiopterin improves endothelial function in patients with coronary artery disease. *Journal of Cardiovascular Pharmacology*, 35(2):173–178.

Malik, A., Hoque, R., Ouyang, X., Ghani, A., Hong, E., Khan, K., Moore, L., Ng, G., Munro, F., and Flavell, R. (2011). Inflammasome components Asc and caspase-1 mediate biomaterial-induced inflammation and foreign body response. *Proceedings of the National Academy of Sciences*, 108(50):20095–20100.

Mantovani, A., Sica, A., and Locati, M. (2007). Macrophage fusion induced by IL-4 alternative activation is a multistage process involving multiple target molecules. *European Journal of Immunology*, 37(1):33–42.

Martinez, F. and Helming, L. (2009). Alternative activation of macrophages: an immunologic functional perspective. *Annual Review of Immunology*, 27:451–483.

Martinon, F., Mayor, A., and Tschopp, J. (2009). The inflammasomes: guardians of the body. *Annual Review of Immunology*, 27:229–265.

McInnes, A. and Rennick, D. (1988). Interleukin 4 induces cultured monocytes/macrophages to form giant multinucleated cells. *Journal of Experimental Medicine*, 167(2):598–611.

McNally, A. K. and Anderson, J. M. (1995). Interleukin-4 induces foreign body giant cells from human monocytes/macrophages. Differential lymphokine regulation of macrophage fusion leads to morphological variants of multinucleated giant cells. *American Journal of Pathology*, 147(5):1487–1499.

McNally, A. K. and Anderson, J. M. (2003). Foreign body-type multinucleated giant cell formation is potently induced by alpha-tocopherol and prevented by the diacylglycerol kinase inhibitor R59022. *American Journal of Pathology*, 163(3):1147–1156.

McNally, A. K. and Anderson, J. M. (2005). Multinucleated giant cell formation exhibits features of phagocytosis with participation of the endoplasmic reticulum. *Experimental and Molecular Pathology*, 79(2):126–135.

McNally, A. K. and Anderson, J. M. (2011). Macrophage fusion and multinucleated giant cells of inflammation. *Advances in Experimental Medicine and Biology*, 713:97–111.

McVean, D. E., Patrick, R. L., and Witchett, C. E. (1965). An aqueous oil red o fixative stain

for histological preparations. *Technical Bulletin of the Registry of Medical Technologists*, 35:33–35.

Metchnikoff, E. (1884). Researches on the intracellular digestion of invertebrates. *Quarterly Journal of Microscopical Science*, 24:89–111.

Michel, J.-B., Virmani, R., Arbustini, E., and Pasterkamp, G. (2011). Intraplaque haemorrhages as the trigger of plaque vulnerability. *European Heart Journal*, 32(16):1977–85.

Miller, C., Boulter, N., Fuller, S., Zakrzewski, A., Lees, M., Saunders, B., Wiley, J., and Smith, N. (2011). The role of the $P2X_7$ receptor in infectious diseases. *PLoS Pathogens*, 7(11).

Miyamoto, H., Katsuyama, E., Miyauchi, Y., Hoshi, H., Miyamoto, K., Sato, Y., Kobayashi, T., Iwasaki, R., Yoshida, S., Mori, T., Kanagawa, H., Fujie, A., Hao, W., Morioka, H., Matsumoto, M., Toyama, Y., and Miyamoto, T. (2012). An essential role for STAT6-STAT1 protein signaling in promoting macrophage cell-cell fusion. *Journal of Biological Chemistry*, 287(39):32479–32484.

Moldeus, P., Hogberg, J., and Orrenius, S. (1978). Isolation and use of liver cells. *Method in Enzymology*, 52(C):60–71.

Moolenaar, W. and Lamers, C. B. (1996). Cholesterol crystal embolisation to the alimentary tract. *Gut*, 38(2):196–200.

Moreno, J. L., Mikhailenko, I., Tondravi, M. M., and Keegan, A. D. (2007). IL-4 promotes the formation of multinucleated giant cells from macrophage precursors by a STAT6-dependent, homotypic mechanism: contribution of E-cadherin. *Journal of Leukocyte Biology*, 82(6):1542–1553.

Mosmann, T. (1983). Rapid colorimetric assay for cellular growth and survival: Application to proliferation and cytotoxicity assays. *Journal of Immunological Methods*, 65(1-2):55–63.

REFERENCES

Möst, J., Spötl, L., Mayr, G., Gasser, A., Sarti, A., and Dierich, M. P. (1997). Formation of multinucleated giant cells in vitro is dependent on the stage of monocyte to macrophage maturation. *Blood*, 89(2):662–671.

Murch, A., Grounds, M., Marshall, C., and Papadimitriou, J. (1982). Direct evidence that inflammatory multinucleate giant cells form by fusion. *Journal of Pathology*, 137(3):177–180.

Murray, P. J. (2007). The JAK-STAT signaling pathway: input and output integration. *Journal of Immunology*, 178(5):2623–2629.

Nair, P. N., Sjögren, U., and Sundqvist, G. (1998). Cholesterol crystals as an etiological factor in non-resolving chronic inflammation: an experimental study in guinea pigs. *European Journal of Oral Sciences*, 106(2 Pt 1):644–650.

Okamoto, H., Mizuno, K., and Horio, T. (2003a). Langhans-type and foreign-body-type multinucleated giant cells in cutaneous lesions of sarcoidosis. *Acta Dermato-Venereologica*, 83(3):171–174.

Okamoto, H., Mizuno, K., and Horio, T. (2003b). Monocyte-derived multinucleated giant cells and sarcoidosis. *Journal of Dermatological Science*, 31(2):119–128.

Papadimitriou, J. M. and Wyche, P. A. (1976). A biochemical profile of glass-adherent cell populations containing multinucleated foreign body giant cells. *The Journal of Pathology*, 119(4):239–254.

Pétrilli, V., Papin, S., Dostert, C., Mayor, A., Martinon, F., and Tschopp, J. (2007). Activation of the NALP3 inflammasome is triggered by low intracellular potassium concentration. *Cell Death and Differentiation*, 14(9):1583–1589.

Pettigrew, R., Galt, J., Ludgate, C., Horn, D., and Smith, A. (1974). Circulatory and biochemical effects of whole body hyperthermia. *British Journal of Surgery*, 61(9):727–730.

Plüss, C., Werner, E. R., Blau, N., Wachter, H., and Pfeilschifter, J. (1996). Interleukin 1 beta and cAMP trigger the expression of GTP cyclohydrolase I in rat renal mesangial cells. *Biochemical Journal*, 318(Pt 2):665–671.

Prieditis, H. and Adamson, I. (1996). Alveolar macrophage kinetics and multinucleated giant cell formation after lung injury. *Journal of Leukocyte Biology*, 59(4):534–538.

Pritchard, J., Foley, P., and Wong, H. (2003). Langerhans and Langhans: what's misleading in a name? *The Lancet*, 362(9387):922.

Provenzano, E., Barter, S., Wright, P., Forouhi, P., Allibone, R., and Ellis, I. (2010). Erdheim-chester disease presenting as bilateral clinically malignant breast masses. *American Journal of Surgical Pathology*, 34(4):584–588.

Quinn, M. T. and Schepetkin, I. A. (2009). Role of NADPH oxidase in formation and function of multinucleated giant cells. *Journal of Innate Immunology*, 1(6):509–526.

Rajamäki, K., Lappalainen, J., Öörni, K., Välimäki, E., Matikainen, S., Kovanen, P. T., and Eklund, K. K. (2010). Cholesterol crystals activate the NLRP3 inflammasome in human macrophages: a novel link between cholesterol metabolism and inflammation. *PLoS ONE*, 5(7):e11765.

Rittner, H. L., Kaiser, M., Brack, A., Szweda, L. I., Goronzy, J. J., and Weyand, C. M. (1999). Tissue-destructive macrophages in giant cell arteritis. *Circulation Research*, 84(9):1050–1058.

Roger, V., Go, A., Lloyd-Jones, D., Benjamin, E., Berry, J., Borden, W., Bravata, D., Dai, S., Ford, E., Fox, C., Fullerton, H., Gillespie, C., Hailpern, S., Heit, J., Howard, V., Kissela, B.,

Kittner, S., Lackland, D., Lichtman, J., Lisabeth, L., Makuc, D., Marcus, G., Marelli, A., Matchar, D., Moy, C., Mozaffarian, D., Mussolino, M., Nichol, G., Paynter, N., Soliman, E., Sorlie, P., Sotoodehnia, N., Turan, T., Virani, S., Wong, N., Woo, D., and Turner, M. (2012). Heart disease and stroke statistics-2012 update: A report from the American Heart Association. *Circulation*, 125(1):e2–e220.

Ruoslahti, E. (1996). RGD and other recognition sequences for integrins. *Annual Review of Cell and Developmental Biology*, 12:697–715.

Samokhin, A. O., Bühling, F., Theissig, F., and Brömme, D. (2010). ApoE-deficient mice on cholate-containing high-fat diet reveal a pathology similar to lung sarcoidosis. *American Journal of Pathology*, 176(3):1148–1156.

Saric, M. and Kronzon, I. (2011). Cholesterol embolization syndrome. *Current Opinion in Cardiology*, 26(6):472–479.

Schepetkin, A., Igor, A., Kiran, K., and Kwon, B. (2001). Macrophagal polykaryocytes in inflammation, tumor growth, and tissue remodeling. *Journal of Microbiology and Biotechnology*, 11(5):727–738.

Schindler, R., Clark, B., and Dinarello, C. (1990). Dissociation between interleukin-1β mRNA and protein synthesis in human peripheral blood mononuclear cells. *Journal of Biological Chemistry*, 265(18):10232–10237.

Seki, T., Sugie, N., Job, K., and Oh-ishi, T. (1996). The regulation of neopterin production by cytokines. *Pteridines*, 7(1):5–9.

Sethi, S., Beck, E., and Manojlovic, N. (1974). Giant cell formation after intraperitoneal application of crocidolite asbestos fibres in rats. Cover slip method. *Annals of Occupational Hygiene*, 17(1):53–56.

Sghiri, R., Feinberg, J., Thabet, F., Dellagi, K., Boukadida, J., Ben Abdelaziz, A., Casanova, J., and Barbouche, M. (2005). Gamma interferon is dispensable for neopterin production in vivo. *Clinical and Diagnostic Laboratory Immunology*, 12(12):1437–1441.

Shaskan, E., Brew, B., Rosenblum, M., Thompson, R., and Price, R. (1992). Increased neopterin levels in brains of patients with human immunodeficiency virus type 1 infection. *Journal of Neurochemistry*, 59(4):1541–1546.

Shen, M., Garcia, I., Maier, R. V., and Horbett, T. A. (2004). Effects of adsorbed proteins and surface chemistry on foreign body giant cell formation, tumor necrosis factor alpha release and procoagulant activity of monocytes. *Journal of Biomedical Materials Research Part A*, 70A(4):533–541.

Shen, M. and Horbett, T. A. (2001). The effects of surface chemistry and adsorbed proteins on monocyte/macrophage adhesion to chemically modified polystyrene surfaces. *Journal of Biomedical Materials Research*, 57(3):336–345.

Shen, P. and Blair, J. (2006). Cholesterol crystals causing falsely elevated automated cell count. *American Journal of Clinical Pathology*, 125(3):358–363.

Small, D. (1988). Progression and regression of atherosclerotic lesions. Insights from lipid physical biochemistry. *Arteriosclerosis*, 8(2):103–129.

Sone, S., Bucana, C., Hoyer, L., and Fidler, I. (1981). Kinetics and ultrastructural studies of the induction of rat alveolar macrophage fusion by mediators released from mitogen-stimulated lymphocytes. *American Journal of Pathology*, 103(2):234–246.

Strieter, R., Kunkel, S., Showell, H., Remick, D., Phan, S., Ward, P., and Marks, R. (1989). Endothelial cell gene expression of a neutrophil chemotactic factor by TNF-α, LPS, and IL-1β. *Science*, 243(4897):1467–1469.

Suhalim, J. L., Chung, C.-Y., Lilledahl, M. B., Lim, R. S., Levi, M., Tromberg, B. J., and Potma, E. O. (2012). Characterization of cholesterol crystals in atherosclerotic plaques using stimulated Raman scattering and second-harmonic generation microscopy. *Biophysical Journal*, 102(8):1988–1995.

Tangirala, R., Jerome, W., Jones, N., Small, D., Johnson, W., Glick, J., Mahlberg, F., and Rothblat, G. (1994). Formation of cholesterol monohydrate crystals in macrophage-derived foam cells. *The Journal of Lipid Research*, 35(1):93–104.

Tatzber, F., Rabl, H., Koriska, K., Erhart, U., Puhl, H., Waeg, G., Krebs, A., and Esterbauer, H. (1991). Elevated serum neopterin levels in atherosclerosis. *Atherosclerosis*, 89(2-3):203–208.

Thull, R. (2002). Physicochemical principles of tissue material interactions. *Biomolecular Engineering*, 19(2-6):43–50.

Tokunaga, O., Fan, J. L., and Watanabe, T. (1989). Atherosclerosis- and age-related multinucleated variant endothelial cells in primary culture from human aorta. *American Journal of Pathology*, 135(6):967.

Tschopp, J. and Schroder, K. (2010). NLRP3 inflammasome activation: the convergence of multiple signalling pathways on ROS production? *Nature Reviews Immunology*, 10(3):210–215.

van Putten, S. M., Wübben, M., Hennink, W. E., van Luyn, M., and Harmsen, M. (2009). The downmodulation of the foreign body reaction by cytomegalovirus encoded interleukin-10. *Biomaterials*, 30(5):730–735.

Varin, A. and Gordon, S. (2009). Alternative activation of macrophages: immune function and cellular biology. *Immunobiology*.

Vedre, A., Pathak, D. R., Crimp, M., Lum, C., Koochesfahani, M., and Abela, G. S. (2009). Physical factors that trigger cholesterol crystallization leading to plaque rupture. *Atherosclerosis*, 203(1):89–96.

Vignery, A. (2008). *Methods to fuse macrophages in vitro.*, volume 475 (Cell Fusion: Overviews and Methods) of *Methods in Molecular Biology*, chapter 22, pages 383–395. Humana Press.

Wang, X., Feuerstein, G., Gu, J.-L., Lysko, P., and Yue, T.-L. (1995). Interleukin-1β induces expression of adhesion molecules in human vascular smooth muscle cells and enhances adhesion of leukocytes to smooth muscle cells. *Atherosclerosis*, 115(1):89–98.

Warren, B. and Yales, O. (1976). The ultrastructure of the reaction of arterial walls to cholesterol crystals in atheroembolism. *British Journal of Experimental Pathology*, 57(1):67–77.

Watanabe, T., Hattori, F., and Tanaka, K. (1982). An experimental study on the origin of foam cells in glomerulonephritis. *Acta Pathologica Japonica*, 32(3):371–383.

Weiss, G., Murr, C., Zoller, H., Haun, M., Widner, B., Ludescher, C., and Fuchs, D. (1999). Modulation of neopterin formation and tryptophan degradation by Th1- and Th2-derived cytokines in human monocytic cells. *Clinical and Experimental Immunology*, 116(3):435–440.

Werner, E., Werner-Felmayer, G., Fuchs, D., Hausen, A., Reibnegger, G., Yim, J., Pfleiderer, W., and Wachter, H. (1990). Tetrahydrobiopterin biosynthetic activities in human macrophages, fibroblasts, THP-1, and T 24 cells. GTP-cyclohydrolase I is stimulated by interferon-, and 6-pyruvoyl tetrahydropterin synthase and sepiapterin reductase are constitutively present. *Journal of Biological Chemistry*, 265(6):3189–3192.

REFERENCES

Wirleitner, B., Reider, D., Ebner, S., Böck, G., Widner, B., Jaeger, M., Schennach, H., Romani, N., and Fuchs, D. (2002). Monocyte-derived dendritic cells release neopterin. *Journal of Leukocyte Biology*, 72(6):1148–1153.

Yang, C.-M., Chien, C.-S., Hsiao, L.-D., Luo, S.-F., and Wang, C.-C. (2002). Interleukin-1β-induced cyclooxygenase-2 expression is mediated through activation of p42/44 and p38 MAPKS, and NF-κB pathways in canine tracheal smooth muscle cells. *Cellular Signalling*, 14(11):899–911.

Yang, Y.-T. (2009). *Mechanism and inhibition of hypochlorous acid-mediated cell death in human monocyte-derived macrophages*. PhD thesis, University of Canterbury, Christchurch.

Zakharova, M. M., Nasonova, V. A., Konstantinova, A. F., Chudakov, V. S., and Gaĭnutdinov, R. V. (2009). An investigation of the optical properties of cholesterol crystals in human synovial fluid. *Crystallography Reports*, 54(3):509–512.

Zhou, R., Yazdi, A. S., Menu, P., and Tschopp, J. (2011). A role for mitochondria in NLRP3 inflammasome activation. *Nature*, 469(7329):221–225.

Zhu, X. W., Price, N. M., Gilman, R. H., Recarvarren, S., and Friedland, J. S. (2007). Multinucleate giant cells release functionally unopposed matrix metalloproteinase-9 in vitro and in vivo. *Journal of Infectious Disease*, 196(7):1076–1079.